Naval Research Laboratory
Washington, DC 20375-5320

AD-A271 981

NRL/FR/8105--93-9546

UVPI Imaging From The LACE Satellite:
The Starbird Rocket Plume

H. W. SMATHERS AND D. M. HORAN

LACE Program
Naval Center for Space Technology

J. G. CARDON, E. R. MALARET, AND L. PEREZ

Applied Coherent Technology Corp.
Herndon, Virginia

T. TRAN

Allied Signal Technical Services Corporation
Alexandria, Virginia

J. E. BRANDENBURG

Research Support Instruments
Alexandria, Virginia

R. R. STRUNCE, JR.

Star Technologies Corporation
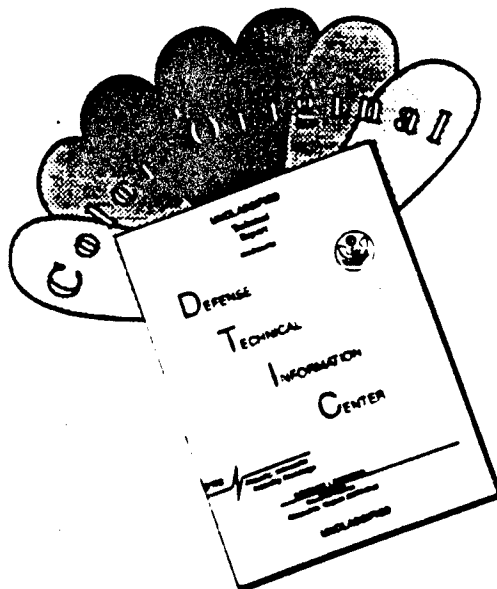*Great Falls, Virginia*

20000920038

August 18, 1993

93-26692

93 11 3   003

DISCLAIMER NOTICE

THIS DOCUMENT IS BEST QUALITY AVAILABLE. THE COPY FURNISHED TO DTIC CONTAINED A SIGNIFICANT NUMBER OF COLOR PAGES WHICH DO NOT REPRODUCE LEGIBLY ON BLACK AND WHITE MICROFICHE.

1. AGENCY USE ONLY (Leave Blank)	2. REPORT DATE August 18, 1993	3. REPORT TYPE AND DATES COVERED Interim	

4. TITLE AND SUBTITLE

UVPI Imaging From The LACE Satellite The Starbird Rocket Plume

5. FUNDING NUMBERS

PE - 63217C
PMA-N1305

6. AUTHOR(S)

H.W. Smathers, D.M. Horan, J.G. Cardon,* E.R. Malaret,* L. Perez,* T. Tran,**
J.E. Brandenburg,† and R.R. Strunce‡

7. PERFORMING ORGANIZATION NAME(S) AND ADDRESS(ES)

Naval Research Laboratory
Washington, DC 20375-5320

8. PERFORMING ORGANIZATION REPORT NUMBER

NRL/FR/8105–93-9546

9. SPONSORING/MONITORING AGENCY NAME(S) AND ADDRESS(ES)

Strategic Defense Initiative Organization
Washington, DC 20301-7100

10. SPONSORING/MONITORING AGENCY REPORT NUMBER

12a. DISTRIBUTION/AVAILABILITY STATEMENT

Approved for public release; distribution unlimited.

12b. DISTRIBUTION CODE

13. ABSTRACT (Maximum 200 words)

The Starbird rocket provides the second demonstration of the ability of the Ultraviolet Plume Instrument (UVPI) to observe missiles in flight above the atmosphere. The Starbird was launched from the Kennedy Space Center in Florida on 18 December 1990. The UVPI is a small, plume-tracking instrument flown on the Naval Research Laboratory's Low-power Atmospheric Compensation Experiment (LACE) satellite, launched in February 1990. The two cameras of the instrument, a tracker and a plume camera, use filters, image intensifiers, and CCD detectors to observe sources in the ultraviolet. The plume camera has a narrow field of view, 0.180° by 0.135°, and observes sources through any of the four filters with passbands of 195 to 295 nm, 200 to 300 nm, 235 to 350 nm, and 300 to 320 nm. The Starbird third and fourth stages, both of which used identical Orbus rocket motors, reached 90-km altitude and were successfully detected and tracked by the UVPI from a range of 596 to 483 km. The spectral radiance and intensities of the missile plumes were extracted from these images and made into contour plots. Spatial, temporal, and spectral characteristics of the plume are also provided.

14. SUBJECT TERMS

Starbird	Ultraviolet Plume Instrument (UVPI) LACE satellite
Spectral radiant	Spectral radiant intensities
Ultraviolet missile plume images	Orbus rocket motors

15. NUMBER OF PAGES

197

16. PRICE CODE

17. SECURITY CLASSIFICATION OF REPORT	18. SECURITY CLASSIFICATION OF THIS PAGE	19. SECURITY CLASSIFICATION OF ABSTRACT	20. LIMITATION OF ABSTRACT
UNCLASSIFIED	UNCLASSIFIED	UNCLASSIFIED	UL

CONTENTS

CONTENTS

FIGURES

FIGURES

TABLES

EXECUTIVE SUMMARY

The Starbird rocket provides the second demonstration of the ability of the Ultraviolet Plume Instrument (UVPI) [1] to observe missiles in flight above the atmosphere. The Starbird was launched from the Kennedy Space Center in Florida on 18 December 1990. The launch time and trajectory were selected to synchronize the flight with the LACE (Low-power Atmospheric Compensation Experiment) satellite pass and permit ground observations from the Malabar tracking site in Florida.

Missile tracking in the ultraviolet is advantageous because of extremely low Earth and solar backgrounds; extremely sensitive photodetectors, which do not require cryogenic cooling; and very high optical resolution, which is possible with optics of relatively modest size. The UVPI is a small, plume-tracking instrument flown on the Naval Research Laboratory's LACE satellite, launched on 14 February 1990.

The UVPI system aperture is only 10 cm in diameter. However, it can detect and image missile plumes at 500-km range. The two cameras of the instrument use narrowband filters, image intensifiers, and charge-coupled devices (CCD) to observe sources in the ultraviolet. The primary function of the tracker camera, viewing over a relatively wide field (1.98° by 2.60°) and broad spectrum (255 to 450 nm), is to locate and track a source for higher resolution observation by the plume camera. The plume camera has a narrow field of view (0.184° by 0.137°) and observes sources through any of four filters with passbands of 195 to 295 nm, 200 to 320 nm, 235 to 350 nm, and 300 to 320 nm. The wavelengths shorter than 310 nm are essentially invisible from the ground as the result of atmospheric absorption. The limiting resolution of the tracker camera is about 230 μradians (μrad), and that of the plume camera about 90 μrad; this is equivalent at 500-km range to 115 m and 45 m, respectively.

The first and second stages of the four-stage Starbird fired only at low altitude, below 40 km, and were not expected to be visible in the ultraviolet from space. The third and fourth stages, both of which used identical Orbus rocket motors, reached 90-km altitude and were successfully detected and tracked by the UVPI from a range of 596 to 483 km. The two Orbus motors, while identical in construction, differed markedly in performance. The fourth-stage performance was somewhat below the essentially nominal performance of the third stage. This less-than-nominal performance by the fourth stage caused the stage to undershoot its planned 105-km peak altitude and reach only 85 km. The less-than-nominal fourth-stage motor performance was seen in the total plume intensity detected by UVPI, which saw a somewhat lower total plume intensity for the fourth stage than was detected for the third stage.

The third-stage plume was successfully tracked for about 20 s, and 296 images of plume data (each 1/30th of a second) were acquired by using the four plume-camera filters. The weaker plume from the fourth stage was also tracked, and 297 images were acquired by using three plume-camera filters. For both stages, the image quality and tracking accuracy were of sufficient quality to permit the superposition of images for plume radiance determination. Image superposition to enhance the signal level is needed for accurate radiometry because of the small telescope aperture.

The spectral radiance and spectral radiant intensities of the missile plumes were extracted from these images. Absolute values are necessarily obtained on the basis of an assumed spectral shape, namely one derived from a physical model of the plume as a nearly transparent stream of sub-micron alumina particles at their melting point. This spectral shape is termed the reference spectrum. A comparison of the results for the four UVPI filters indicates that the reference spectral shape is not an inaccurate representation of the Starbird third- and fourth-stage plume spectra despite their

difference in performance. The spectra appeared to show an excess in the far UV ($\lambda < 300$ nm) relative to that expected from the reference spectrum. This apparent UV excess, relative to the reference spectrum, is in agreement with data gathered on the Strypi flight [2]. The Strypi data also showed an apparent excess in the far-UV relative to the reference spectrum. However, the Starbird data did not show an identifiable UV bright outer region of the plume, in contrast to the UV luminous outer region seen on the Strypi flight [2].

The time dependence of the plume central region radiant intensity within each filter interval showed no pronounced trends or variations for the third stage but showed a pronounced upward ramp for the fourth stage. Momentary, single-frame peaks exceeding the range of normal statistical variation were detected. Whether these can be correlated with missile engine events or other sensors remains to be seen.

The tracker camera, within its relatively limited resolution, obtained radiant intensity data in the 255 to 450-nm wavelengths. These data, taken with the plume camera data in the 195 to 350-nm range, support the conclusions that the central region spectrum is quite close to the reference model with some relative excess in the far UV and no apparent outer region of UV emission away from the UV-bright plume central region.

The Starbird third and forth stages both used identical Orbus motors. However, the fourth stage of the missile rose to a lower altitude than planned because performance was less than nominal. This less-than-nominal motor performance was reflected in the total plume intensities detected by UVPI and showed that UV plume intensities are correlated to actual motor performance rather than to motor design. Unlike the Strypi flight, no large persistent cloud trails were observed on the Starbird flight.

This base of Starbird UV radiometric data will be a foundation for further analysis to provide refined interpretations and evaluation. Comparison with models and with data from sensors on other platforms and with data from other test flights will also provide improved radiometric results and an enhanced phenomenological understanding of UV emission by solid rocket motors in the upper atmosphere.

UVPI IMAGING FROM THE LACE SATELLITE:
THE STARBIRD ROCKET PLUME

1.0 INTRODUCTION

1.1 Background

The Ultraviolet Plume Instrument (UVPI) carried aboard the Low-power Atmospheric Compensation Experiment (LACE) satellite launched in February 1990 was designed to collect rocket plume imagery in the ultraviolet (UV) band. A Starbird four-stage solid-fuel rocket was selected for one of a series of tests. The overall objective of the observation was to gather UV band data at moderate altitude, around 100 km, from space to enhance the current level of understanding of plume physics and chemistry, and to help answer questions about radiance, spatial extent, and temporal variability of plumes. A number of more specific objectives are listed in Section 1.3, which describes the Starbird mission plan.

1.2 UVPI Capability

The Ultraviolet Plume Instrument (UVPI) is carried aboard the Low-power Atmospheric Compensation Experiment (LACE) spacecraft. The UVPI's mission is to collect images of rocket plumes in the UV waveband and to collect background image data on the Earth, Earth's limb, and celestial objects. Background object imagery already collected with the UVPI includes the day and night Earth limb air glow, aurora, sunlit and moonlit clouds, solid Earth scenes with varying solar illumination, cities, and stars. A detailed description of UVPI can be found in the UVPI description and data methodology report [1] and in the Strypi plume report [2].

The UVPI sensor head assembly [3,4] contains two coaligned camera systems that are used in concert to acquire the object of interest, control UVPI, and acquire UVPI images and radiometric data. The two camera systems are the tracker camera and the plume camera, which are discussed briefly below. The two cameras share a fixed 10-cm diameter Cassegrain telescope that uses a gimbaled plane steering mirror to view a field of regard that is a 50-deg half angle cone around the nadir. In addition, UVPI contains a second plane mirror on the instrument door. The mirror can be set at an angle of approximately 45 deg relative to the nadir and used in conjunction with the steering mirror to view Earth's limb and stars near the limb. The configuration of the UVPI and the radiometric response of UVPI are discussed in Refs. 1 and 2; characteristics of the UVPI have been previously reported [4,5].

The tracker camera is an intensified charged-coupled device (CCD) camera, which is sensitive over a wide wavelength range extending from 255 to 450 nm. Figure 1 shows the overall response of the tracker camera as a function of wavelength, including the effects of the bandpass filter in the camera system, the photocathode response, and the other optical elements in detail. This camera has a relatively wide total field of view of 1.98 by 2.60 deg, and images over this full field of view can be recorded at a 5 Hz image rate. The tracker camera can also be operated in a mode where the transmitted field of view is restricted to the central 17 percent of the full field of view, and the image rate is increased to 30 Hz. The intensifier gain and the exposure time of the camera can be controlled to provide a radiometric dynamic range greater than 10^6.

The plume camera is also an intensified CCD camera operating in the ultraviolet. The plume-camera optical train contains a filter wheel with four selectable filters that have bandpasses within the

195 to 350 nm range. Figure 2 shows the overall response of the plume camera for each of these four filters. The plume camera has a total field of view of 0.184 by 0.137 deg with a correspondingly higher resolution than can be achieved by the tracker camera. Plume camera images can be recorded or transmitted at either 5 or 30 Hz, depending on the desired field of view. The intensifier gain can be controlled to provide a radiometric dynamic range greater than 10^6.
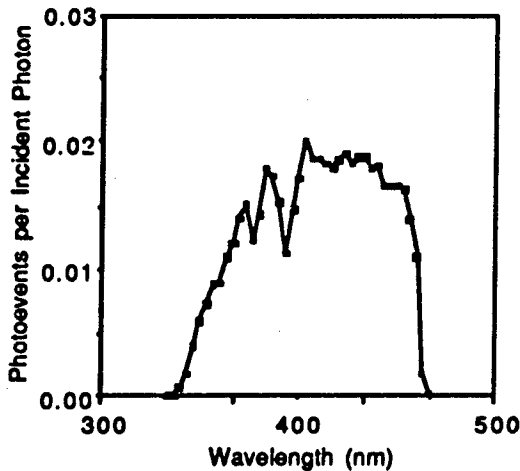
Fig. 1 - Tracker camera: net quantum efficiency curve
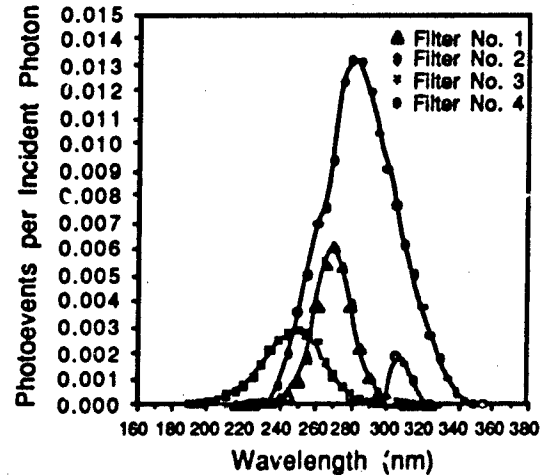
Fig. 2 - Plume camera: net quantum efficiency curves

Table 1 summarizes the instrument characteristics and telemetry rates. Note that the "field of view per pixel" values are updates of those listed in the plume data methodology report [1] and the in the Strypi plume report [2].

Table 1 - Instrument Characteristics

Parameter		Tracker Camera	Plume Camera
Shared telescope type		Cassegrain	Cassegrain
Telescope diameter		10 cm	10 cm
Focal length		60 cm	600 cm
Field of view		2.62 x 1.97 deg	.180 x .135 deg
Field of regard		100 x 97 deg	100 x 97 deg
Field of view per pixel		180.5 x 143.9 μrad	12.8 x 15.0 μrad
Pixel footprint @ 500 km		90 x 72 m	6.4 x 5.0 m
System resolution (FWHM)		220 to 250 μrad	80 to 100 μrad
Spectral region		255-450 nm	195-350 nm
Number of filters		1	4
Photocathode material		Bialkali	CsTe
Time for filter change		n/a	1.7 s
Digitization		8 bits/pixel	8 bits/pixel
Digital data rate		2.5 Mbps	2.5 Mbps
Image rate:	normal	5 per s	5 per s
	zoom*	30 per s	30 per s
Pixels:	normal	251 x 240	251 x 240
	zoom	91 x 112	91 x 112
Pixel exposure time		.16 to 33.3 ms	33 ms
Frames integrated		n/a	1 - 6
Exposure range		$>10^6$	$>10^6$

*Reduced field of view.

1.3 Scientific Objectives for UVPI

The primary goal of the Starbird mission [6,7] for UVPI was to collect spatially resolved, radiometric UV plume data. This was to be accomplished for the third and fourth stages of the rocket by using UVPI's capabilities for tracking and imaging a moving target at long range. The plume-camera filters were cycled to vary the wavebands. Emphasis was placed on the mid-UV bands because these data can be obtained only from a space-based sensor, and this waveband has the best potential for high signal-to-background contrast. Pointing accuracy was optimized because that simplifies registration of images when superposed, a necessary procedure for improving statistics. The UVPI observation was coordinated with ground observations providing infrared and visible band data as an important supplement to the UV data.

A secondary goal was to observe any serendipitous special events such as transients, puffs, chuffing, clouds, or contrails. The brightness, size, frequency, and persistence of such phenomena would provide useful information.

The specific objectives of the mission, related to UVPI data, are given in the following subsections. They revolve around a number of questions concerning plume radiance, spatial extent, temporal variability, and spectral shape of the UV emissions [7-9]. The objectives are grouped under headings reflecting these subjects.

1.3.1 *Specific Objectives Related to Radiometrics*

The following four objectives are basic to those listed in the subsequent subsections.

* Obtain isoradiance contours for multiple plume-camera bandpasses for the Starbird third and fourth stage plumes.
* Obtain radiant intensity measurements in multiple plume-camera bandpasses for the Starbird third- and fourth-stage plumes based on the entire field of view of the plume camera and on a subregion corresponding approximately to a plume core.
* Compare radiometric measurements for Starbird third- and fourth-stage plumes with other measurements or expectations.
* Provide radiometric measurements for nonplume, transient phenomena, if any.

1.3.2 *Specific Objectives Related to Spatial Features*

* Obtain the length of each of the Starbird third- and fourth-stage plume central regions and investigate implications for cooling rate and emissivity of particles.
* Obtain the shape of the shock boundary/mixing layer of the rocket.
* Identify asymmetries in plume shape and investigate angle-of-attack and uneven burning as possible causes.

1.3.3 *Specific Objectives Related to Temporal Features*

* Identify temporal trends in radiometrics and investigate possible dependence on rocket velocity at fixed altitude.
* Investigate radiometric fluctuations to determine whether short-term variations in brightness are observed.
* Identify changes with time in the shape of the plumes' outer regions, if any, and investigate possible dependence on rocket velocity at fixed altitude.
* Identify persistence and cumulative effects, if any, in plumes or non plume phenomena.

1.3.4 *Specific Objectives Related to Spectral Features*

- Compare the shape of the plume central region's emission spectrum from the multiple bandpass measurements with a reference spectral shape and spectral shape determinations based on other sensors.

- Relate tracker-camera measurements to visible and infrared measurements made by other sensors.

- Characterize the emission spectrum for the plumes' outer regions, if any.

1.4 Experiment Concept

1.4.1 *Starbird Trajectory and Description*

Since the Starbird rocket was designed to be observed by the space shuttle flying at an altitude of about 170 km, the planned trajectory was a depressed one, with a burnout altitude for the last stage of about 105 km. The trajectory called for Starbird to be launched from the Kennedy Space Center, flying in an east-southeast direction, and landing in the Atlantic Ocean, 425 km downrange after about 7 minutes of flight time. The Talos and Sergeant stages were to burn out at 6 and 47 s after launch, respectively, followed by a coast period of 50 s. The Orbus stages were to burn one after the other with a 6 s coast between the two.

The Starbird Developmental Launch Vehicle was a four-stage rocket, with the Talos and Sergeant as the first and second stage, respectively; two identical Orbus motors made up the third and fourth stages (Fig. 3). The Orbus motor had an average thrust of about 7,000 lb with a burn time of 39 s. The motor used an axisymmetric nozzle, 40 cm in diameter, with an expansion ratio of 46.4 and a divergence angle of 15.54°. The propellant for the Orbus was a composite consisting of ammonium perchlorate, cyclo-tetramethylene-tetranitramine, powdered aluminum and HTPB (hydroxol terminated polybutadiene) rubber binder of Class 1.3 UTP-19, 687A. The propellant had an aluminum loading of 20% and a flame temperature of 3338 K. Figure 4 is a sketch of the Orbus motor. Table 2 summarizes Starbird XI rocket motor characteristics; Table 3 provides parameter values for the Orbus motor.

Payload	4th Stage	3rd Stage	2nd Stage	1st Stage
	Orbus Motor	Orbus Motor	Sergeant (XM-100)	TALOS

Shroud GCA Module Interstage Aft Skirt Interstage
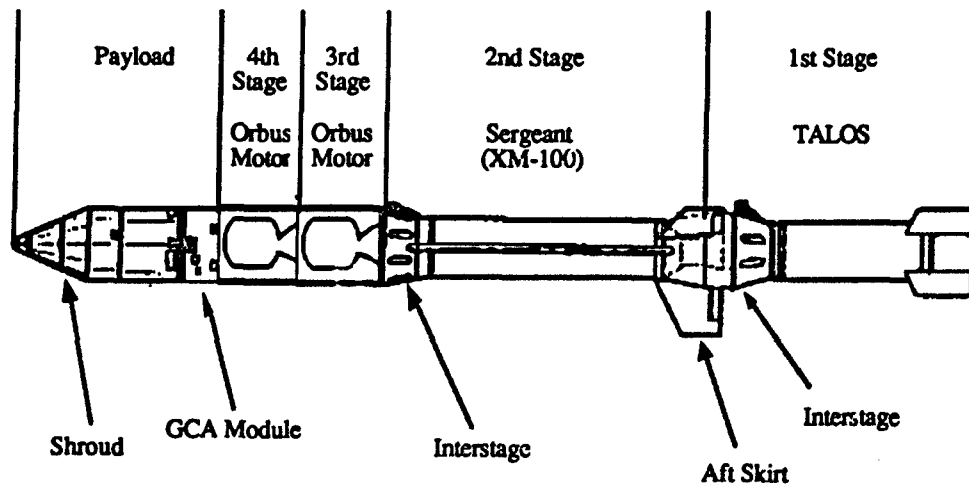
*Figure reprinted from Ref. 7.

Fig. 3 - Starbird XI rocket schematic

Case insulation silica-filled EPDM
Case, T-40 graphite composite
Liner, UTL-0040D
Skirt, T-40 graphite epoxy
Class 1.3
HTPB propellant
UTP-19,867A
Toroidal pyrogen igniter
Movable nozzle assembly
• Flexseal TVC joint
• 4D carbon-carbon throat
• Carbon-phenolic insulators
• Exit cone
  • HD/LD carbon phenolic
  • Graphite-epoxy overwrap
Attach flange aluminum
2124-T851
Thrust vector actuation system
(2 axis)
• High output electric motors
• Gear box
• Drive and loop closure electronics
• Thermal battery

Motor ignition/TVA
thermal battery cable
(270°)
TVA system electronics
• Drive and loop
  closure electronics
• Thermal Battery
Yaw actuator
(180°)
(0°)
Pressure
transducers (2)
TBI initiator (2)
(90°)
Pitch actuator
FTS system
• Glass-epoxy tunnel
• FLSC 125 gr/ft
• Aluminum detonator covers

Fig. 4 - Orbus rocket motor

Table 2 - Summary Of Starbird XI Rocket Motor Characteristics

Motor	Stage	Burn Time (s)	Avg Thrust (lb)	Total Impulse (lb-s)	Altitude (km)	Velocity (km/s)
TALOS TX-33-39 S/N 726	1	6.0	110,000 (vac)	1,900,900	0-1.0	0.0-0.32
Sergeant	2	34.0	50,000 (sl)	59,700	10-26	.25-1.0
Orbus	3	39.0	7,000 (vac)	71,200	60-85	.54-1.06
Orbus	4	38.0	7,000 (vac)	214,300	90-105	1.03-2.2

Note: vac = vacuum, sl = sea level.
Based on information from Ref. 7.

Table 3 - Orbus motor parameters

Nozzle Characteristics

Initial throat diameter	6.67 in.
Final throat diameter	5.51 cm.
Exit plane diameter	37.52 cm.
Exit cone half-angle	16.9°
Expansion ratio	46.39

CYI-75 Propellant Constituents

	(wt %)
Ammonium perchlorate (oxidizer)	58.0
Cyclotetramethylene tetranitramine (oxidizer)	12.0
Aluminum (fuel)	20.0
Stabilizer	3.14

Typical Exhaust Gas Composition

	mole (fraction)
CO_2	.015762
CO	.2176
H_2O	.109803
HCl	.115542
H_2	.293115
N_2	.115421
H	.015082
Al_2O_3 (solid)	.094148

1.4.2 Radiometrics

The Starbird third- and fourth-stage rocket motor propellant is a composite having a composition of 70% oxidizer, 20% powdered aluminum, and a small amount of hydrocarbon binder. The combustion products for both rocket motors are Al_2O_3 particles, H_2O, CO, CO_2, and other gases. The temperature inside the rocket motor chamber is typically 3200 K, which is hot enough to melt the Al_2O_3 (melting point = 2320 K) but not hot enough to vaporize it (boiling point approximately = 3700 K). As the exhaust exits the rocket nozzle it cools, and the Al_2O_3 begins to solidify. The temperature of the exhaust decreases further as it moves away from the rocket [7].

In the ultraviolet, the emission from the plume central regions of these rocket motors is expected to be dominated by thermal emission from hot particles of Al_2O_3. In a simplified model,

the temperature of the Al_2O_3 particles is taken to be constant at the solidification temperature of 2320 K because the latent heat of fusion causes the temperature of the particles to pause momentarily at this point as they cool. In the outer region, other thermophysical processes can produce emission bands arising from exhaust gases or atmospheric constituents, and these will contribute to the spectrum.

Even in the simplified model, in which the Al_2O_3 particles in the plume are assumed to be at a uniform temperature of 2320 K, the plume emission is different from a 2320 K blackbody for two primary reasons. First, the plume consists of a rather transparent cloud of particles such that the total emission from the cloud is substantially less than would be the case from a solid object the same size as the plume. Second, the Al_2O_3 particles are typically a few microns in size and are inefficient emitters of visible and longer wavelengths. The effective emissivity for 2.3-μm particles of Al_2O_3 is considered typical of particles in the plume. This is further discussed in Section 3.

The rocket's emission was estimated for all four filter bandpasses of the UVPI's plume camera by using a modified version of the CHARM 1.3 code. The results are given in Tables 4 and 5. This information was used to determine the desired sequence of the plume camera filters for the Orbus burns.

Filter PC-4 was selected to begin the observation of the Starbird because its wider bandpass would provide the brightest signature. Filter PC-4 responds to wavelengths longer than 300 nm, which pass through the ozone layer, and its primary purpose would be to obtain a few seconds of data for comparison with that from ground-based and airborne sensors. Filters PC-1 and PC-3 observe wavelengths that do not pass through the ozone layer and, thus, cannot be observed from the ground. Use of these filters would provide unique data. Since the UVPI plume camera filters must be cycled in sequence, a few seconds of data using filter PC-2 would be collected to complete the data set even though PC-2 passes wavelengths that can be observed from the ground. Therefore, the filter selection for the Starbird third-stage burn should start with a few seconds of using filter PC-4, then switch to PC-3 for several seconds, then switch to PC-2 for a brief data collection opportunity, and end in PC-1 for several seconds of data prior to and including the burnout.

The filter sequence for the fourth stage burn should emphasize the use of filters PC-1 and PC-3, which pass wavelengths that are invisible from the ground. Therefore, the fourth-stage observation should start with filter PC-1 for several seconds, then collect data for a few seconds using PC-2, and then switch to PC-3 and use that filter for the remainder of the Starbird fourth-stage burn. This will allow collection of data from the burnout of the Starbird fourth stage in a band that is invisible to ground-based and airborne sensors.

Table 4 - Expected Intensities for Starbird Third Stage

Filter	W/sr	Photoevents/Frame
PC-1	15.0	13.8
PC-2	9.6	13.1
PC-3	3.8	2.4
PC-4	44.2	179.

Table 5 - Expected Intensities for Starbird Fourth Stage

Filter	W/sr	Photoevents/Frame
PC-1	15.0	15.9
PC-2	9.4	16.5
PC-3	3.8	3.3

2.0 STARBIRD OBSERVATION AND INSTRUMENT PERFORMANCE

2.1 Observation Scenario

2.1.1 *UVPI Operations*

The Starbird plume observation by UVPI was highly successful because of well-coordinated efforts by the LACE team and cooperative efforts by the Starbird launch team.

The following is the sequence of events during this observation. Figure 5 shows the LACE ground track during the encounter.
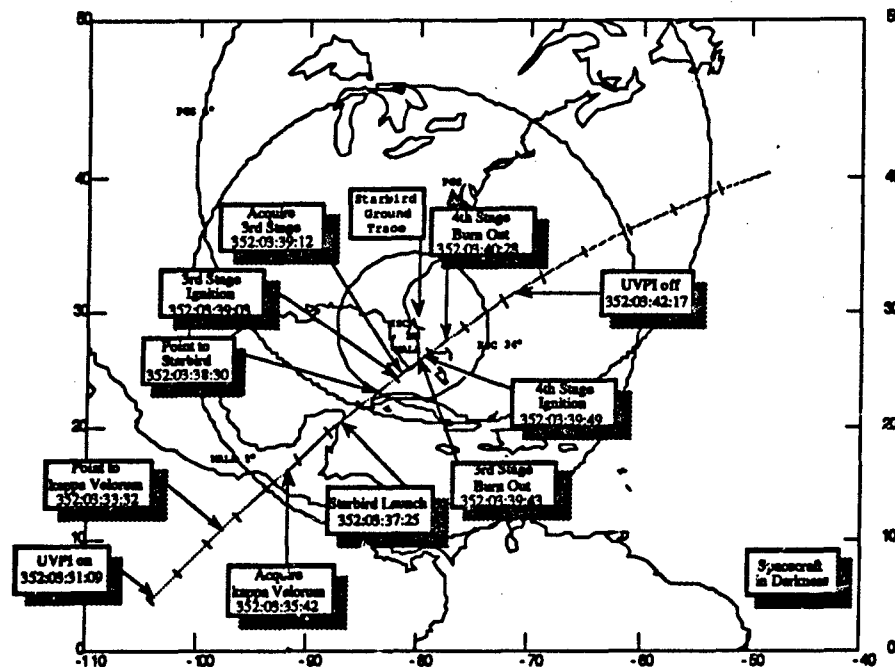
Fig. 5 - LACE ground track for Starbird observation

- Starbird was launched on 18 December 1990, at 03:37:25.089 GMT.

- The UVPI door was fully opened to view Starbird at 03:38:25 and UVPI pointed to the Starbird nominal trajectory using a 0.5° circular scan.

- UVPI observed the third-stage ignition in its tracker camera at 03:39:03. UVPI locked onto the Starbird rocket plume at 03:39:12. The high-rate image transmission mode, plume-to-tracker image ratio of 8:2, and the filter sequence of 4-3-2-1 were successfully exercised before the third-stage burnout at 03:39:42.6.

- UVPI, while in the high-rate image transmission mode, reacquired the Starbird at fourth-stage ignition at 03:39:48.6 and locked onto the target at 03:39:49.7. The filter sequence of 1-2-3 was successfully accomplished before the fourth-stage burnout at 03:40:27.6.

Table 6 shows the preloaded commands and real-time commands for the encounter.

2.1.2 *Sequence of Events*

Figure 6 shows the relationship between time and frame number. Time in Fig. 6 is chosen such that zero time corresponds to the Starbird rocket lift-off time. For this observation, the linear equation for time is: TIME = (FRAME - 10067) / 29.996. Note that there is $1/30$th of a second between frames.
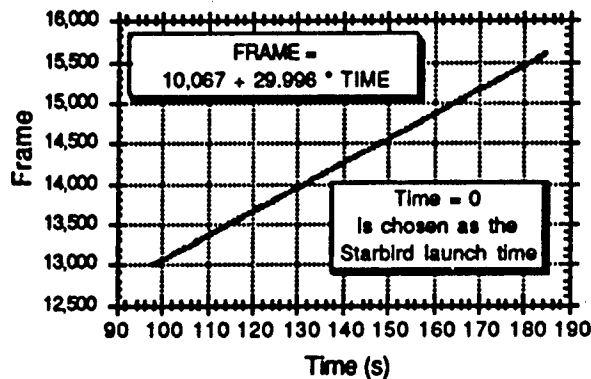
Fig. 6 - Telemetry frame vs time after liftoff

Table 6 - List of Commands

Time (GMT)	TALO (s)	Frame Number	UVPI Delayed Execution Commands	UVPI Real-Time Commands
3:31:09	-376.0		Turn UVPI on	
3:31:44	-341.0		Turn relays K1, K2 on	
3:32:04	-321.0		Set tracker max gain to 10	
3:32:09	-316.0		Initialize tracker	
3:32:19	-306.0		Set filter wheel position to 4	
3:32:58	-267.0		Turn off AGC, set track & plume gains to 0	
3:33:03	-262.0		Set extrapolate timeout to 5 s	
3:33:04	-261.0		Set frame ratio to 1:15 (Plume:Tracker)	
3:33:10	-255.0		Open door to 54.81°	
3:33:30	-235.0		Turn on AGC	
3:33:31	-234.0		Open door one coarse step	
3:33:32	-232.0		INFUNC 118	
3:33:33	-232.0		Set lost track function 198	
3:34:27	-178.0	4733		Close door 1 step
3:34:35	-170.0	4973	*MALA AOS 3°*	
3:34:54	-151.0	5542		Upload fixed STAR pointing function
3:35:03	-142.0	5812	*MALA AOS 5°*	
3:35:23	-122.0	6411		Upload ROCKET pointing function
3:35:33	-112.0	6711		Upload fixed STAR pointing function
3:35:42	-102.0	6981		Acquire star kappa Velorum
3:35:49	-96.0	7212		Change to zoom mode
3:36:02	-82.0	7535		Plume:Tracker frame ratio 8:2
3:36:07	-78.0	7729		Filter wheel position 3

Table 6 - List of Commands (Cont'd.)

Time (GMT)	TALO (s)	Frame Number	UVPI Delayed Execution Commands	UVPI Real-Time Commands
3:36:15	-70.0	7970		Filter wheel position 2
3:36:20	-65.0	8119		Filter wheel position 1
3:36:25	-60.0	8269		Filter wheel position 2
3:36:59	-26.0	9288		Turn zoom off
3:37:25	0.0	10067	<<<<<<<<<< STARBIRD LAUNCH >>>>>>>>>>	
3:37:32	7.0	10277	*Starbird 1st Stage Burnout*	
3:37:39	14.0	10487	*Starbird 2nd Stage Ignition*	
3:37:48	22.0	10756		Upload fixed STAR pointing function
3:37:55	30.0	10966		Point using fixed STAR function
3:37:59	34.0	11086	Set filter wheel position to 4	
3:38:00	35.0	11116	*PGS AOS 5°*	
3:38:07	42.0	11326	Turn off zoom	
3:38:08	42.0	11356	Set frame ratio to 2:8 (P:T)	
3:38:09	44.0	11386	Point to gimbal position 0,0	
3:38:10	45.0	11416	Open door fully for Starbird viewing	
3:38:11	46.0	11446	Initialize tracker	
3:38:14	49.0	11535	*STARBIRD 2nd Stage Burnout*	
3:38:20	55.0	11715	Load mass and intensity run block	
3:38:30	65.0	12015	Point to Starbird using rocket function	
3:38:31	66.0	12045	Set lost track function to rocket function	
3:38:35	70.0	12165	Turn on tape recorder, tape unit A	
3:39:03	98.0	13004	*Starbird 3rd Stage Ignition*	
3:39:12	107.0	13274		Acquire using rocket function
3:39:17	112.0	13423		Change to zoom mode
3:39:22	117.0	13573		Plume:Tracker ratio 8:2
3:39:29	124.0	13783		Filter wheel position 3
3:39:34	129.0	13933		Filter wheel position 2
3:39:37	132.0	14023		Filter wheel position 1
3:39:43	138.0	14202	*Starbird 3rd Stage Burnout*	
3:39:49	144.0	14382	*Starbird 4th Stage Ignition*	
3:40:02	157.0	14772		Filter wheel position 2
3:40:07	162.0	14922		Filter wheel position 3
3:40:28	182.0	15551	*Starbird 4th Stage Burnout*	
3:40:43	198.0	16000	Set frame ratio to 1:15 (P:T)	
3:40:45	200.0	16060	Zoom off	
3:40:46	201.0	16090	Close door to 54.81°	
3:41:11	226.0	16840	Swing gimbal to left	(Az=-5.0°, El=+4.5°)
3:41:16	231.0	16989	Swing gimbal to right	(Az=+4.8°, El=+2.8°)
3:41:21	236.0	17139	Turn off AGC	
3:41:22	237.0	17169	Set track and plume MCP gains to 0	
3:41:25	240.0	17259	Park gimbal mirror	

Table 6 - List of Commands (Cont'd.)

Time (GMT)	TALO (s)	Frame Number	UVPI Delayed Execution Commands	UVPI Real-Time Commands
3:41:26	241.0	17289	Close door fully	
3:41:55	270.0	18158	Turn off tape recorder	
3:42:17	292.0			Command UVPI shutdown
3:44:51	446.0		MALA LOS 5°	
3:46:41	556.0		Command UVPI shutdown	
3:46:41	556.0		PGS LOS 5°	

2.2 Starbird Performance Summary

The overall performance of the Starbird rocket was somewhat less than nominal. The planned apogee of the trajectory was not attained, and the velocity at fourth-stage burnout was lower than expected. The telemetry data for the Starbird trajectory is given in detail in Appendix A. Figure 7 shows the actual altitude and velocity of the Starbird trajectory. Close examination of the telemetry data and the planned trajectory indicated that the trajectory deviation from nominal was probably caused by the second stage's less-than-nominal performance. The altitude at the second-stage burnout was comparable to the planned trajectory, but the burnout velocity was 0.88 km/s compared to 0.99 km/s for the planned trajectory. This in turn caused the burnout velocity and altitude of the fourth stage to be only 1.86 km/s and 89 km, respectively, compared to 2.2 km/s and 105 km for the planned trajectory.

Figure 8 provides telemetry information for Starbird angle of attack and chamber pressure.

Launch Time (GMT): 12-18-90   3:37:25.089
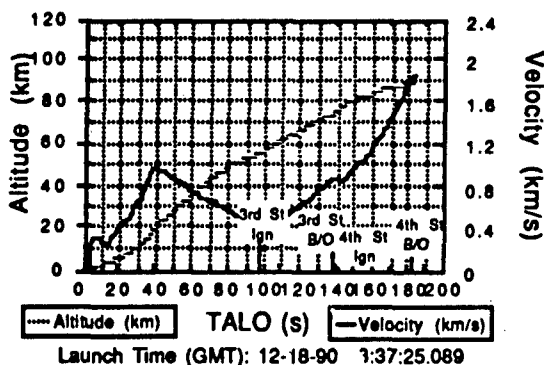
Fig. 7 - Starbird altitude and velocity profiles from telemetry data

Launch Time (GMT): 12-18-90 03:37:25.089
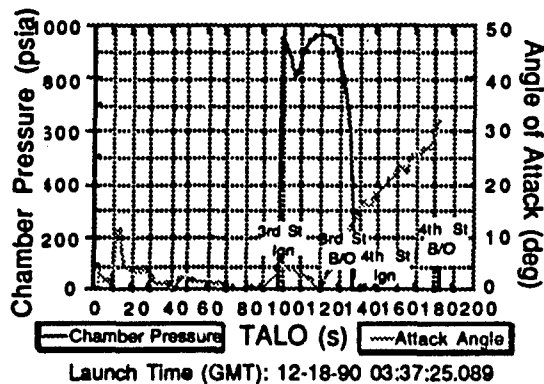
Fig. 8 - Starbird stage-three angle of attack

2.3 Encounter Geometry

From the post-launch telemetry data for the Starbird vehicle's position and attitude, the range and aspect angle vs time after launch were computed and are shown in Fig. 9. The aspect angle is defined as the angle between the line-of-sight vector from UVPI to the target point and the longitudinal axis of the rocket. Zero degree aspect angle means looking "nose on"; 180° means looking up the nozzle. The best range/aspect angle combination occurred toward the end of the fourth-stage burn.

Figure 10 shows the percent vignetting and the orientation angle of the rocket body in the tracker camera's FOV. At the Starbird third-stage ignition, the plume intensity signal was vignetted

by as much as 16%. However, by the time the UVPI plume camera collected data in the proper plume-to-tracker frame ratio and high image transmission rate mode, the signal was vignetted by only 1.2% and became essentially clear of vignetting a few seconds later. The tracking of the fourth stage was clear of any vignetting.

The orientation angle in Fig. 10 is used to assist with the radiometric analysis of the plume. This angle is defined as the angle between the tracker camera's horizontal axis and the projection of the rocket body onto the focal plane of the tracker camera.
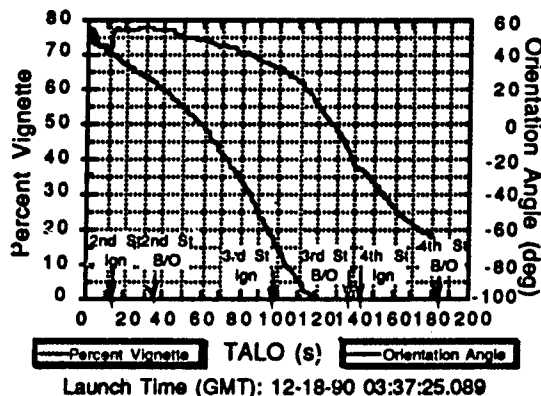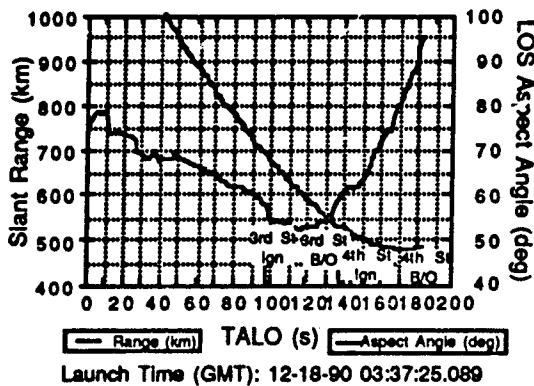
Fig. 9 - Range and aspect angle for UVPI-Starbird encounter

Launch Time (GMT): 12-18-90 03:37:25.089

Fig. 10 - Percent vignette and orientation angle for UVPI-Starbird encounter

Launch Time (GMT): 12-18-90 03:37:25.089

2.4 Pointing Performance Overview

2.4.1 *Mission Mode Sequencing*

The tracker was commanded to the Mass and Intensity Centroid track mode throughout the Starbird observation. Figure 11 shows the sequencing of the various mission modes during the observation.
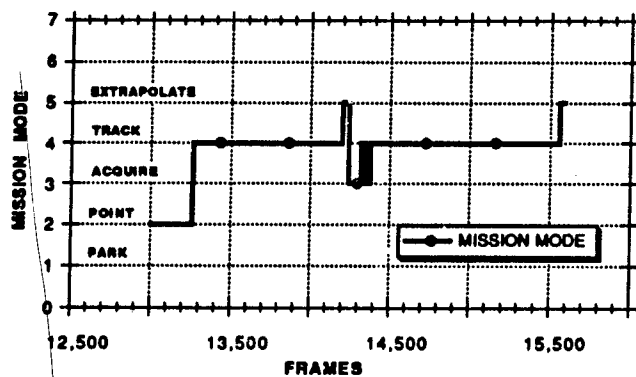
Fig. 11 - Track and mission modes vs frame

The POINT mode was used to scan for the Starbird third-stage rocket until it was within the tracker-camera's field of view, at which time the ACQUIRE mode was commanded from the ground station. The tracker then locked-on, TRACK mode, to the third-stage Orbus rocket, which was tracked

for approximately 31 s. After the tracker locked-on to the fourth-stage Orbus rocket, the tracker followed the rocket for approximately 39 s.

2.4.2 Gimbal Angles

Figures 12 and 13 show the azimuth and elevation gimbal angles, respectively, as a function of frame number. The elevation gimbal angle varied by about 2° during the engagement for either the third stage or the fourth stage. The UVPI gimbaled mirror was initially looking ahead of the satellite at the third-stage ignition; it was looking behind the satellite at the fourth-stage burnout. The azimuth angle varied about 9 deg during the encounter for either the third stage or the fourth stage. The azimuth and elevation gimbal rates were calculated as 0.36 deg/s and 0.07 deg/s, respectively, which were well within the tracker's capability. The dashed lines in these plots represent the Instrument Control Computer (ICC) commanded gimbal angles. At the beginning of the encounter, while operating in the POINT and ACQUIRE modes, the ICC commanded the gimbal angles. When the tracker locked onto the target image, the mode was set to TRACK and the tracker controlled the gimbal angles. Note that the ICC commanded gimbal angles remain fixed to the last commanded value. There is a noticeable transient as the tracker brings the track errors to zero. At the end of the encounter when the tracker loses the target image and goes into the EXTRAPOLATE mode, the ICC extrapolates the immediately previous gimbal angles according to their respective rates. Also, note that the gimbal motion at this time exhibits a transient that is a result of the extrapolation function implementation.
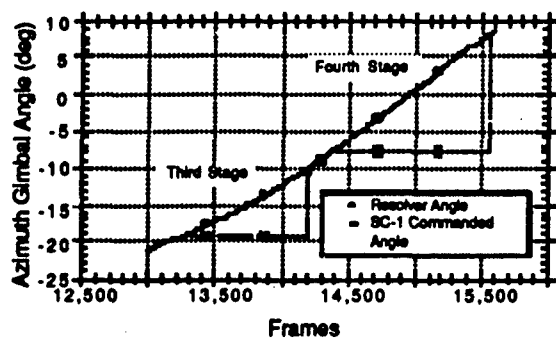
Fig. 12 - Azimuth gimbal angles vs frame number
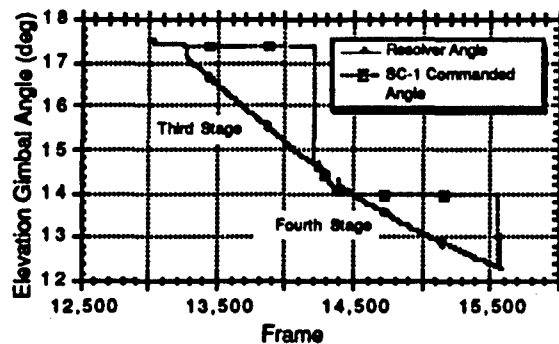
Fig. 13 - Elevation gimbal angles vs frame number

2.5 Tracker Performance Summary

Tracker performance was analyzed for the 13,400 to 15,500 telemetry frame range. This interval is representative of nominal tracking while collecting plume signatures in the plume camera.

2.5.1 Acquisition

The tracker performed within the UVPI tracker specifications. The tracking errors for the acquisition of the third and fourth stages are plotted as a function of time in Figs. 14 and 15, respectively. The servo response was similar to that observed in previous laboratory tests. The tracker acquired the target in less than 0.1333 s and drove the tracking error to zero in less than 1.2 s. The observed jitter was between 6.8 and 12.5 μrad which is better than the tracker system specifications require. It was observed that the tracker was biased approximately +0.5 pixels in the Y-direction. A gimbal-angle transient was observed in both the azimuth and elevation gimbal angles when the tracker transition to the EXTRAPOLATE mode.
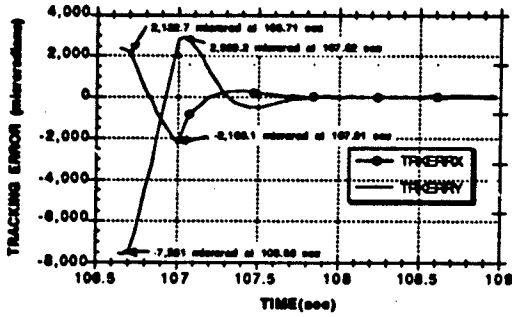
Fig. 14 - Third-stage acquisition tracking error vs time
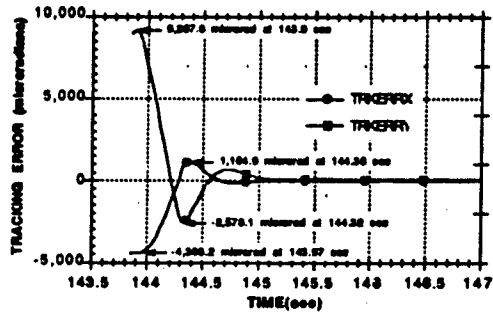
Fig. 15 - Fourth-stage acquisition tracking error vs time

2.5.2 *Tracking Jitter*

The tracking jitter was determined between frames 13400 and 15500. Figure 16 shows the tracking errors plotted as pixels vs the frame numbers; Fig. 17 plots the tracking error in X vs the tracking error in Y. These two different perspectives show that the tracker is biased approximately half a pixel in Y, with an elongated scattering in the X direction that oscillates between ±1 pixel.

Fig. 16 - X and Y tracking errors vs frame

Third Stage
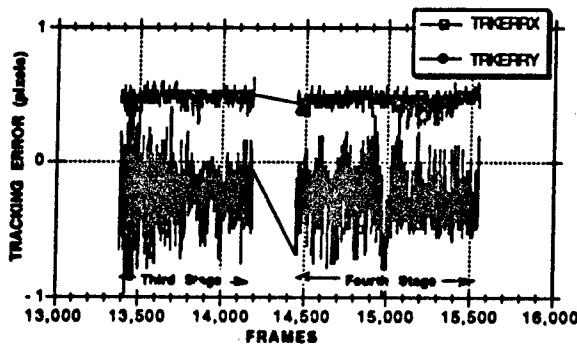
Fourth Stage
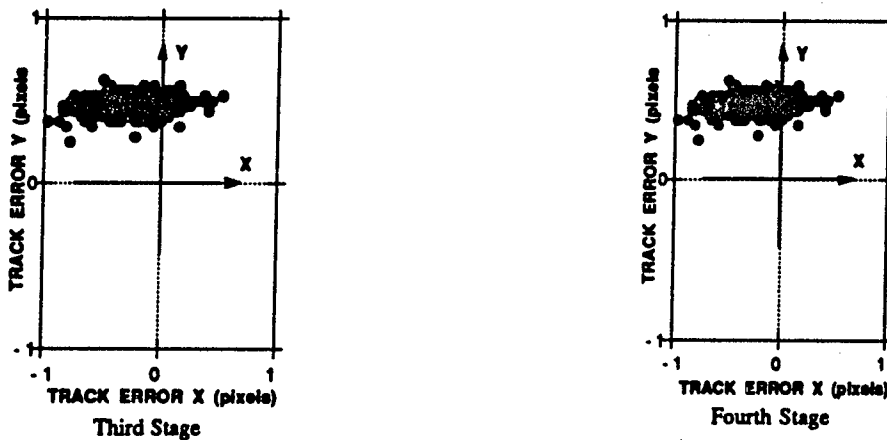
Fig. 17 - Y tracker error vs X tracker error in pixels

A more representative picture is shown in Figs. 18 and 19 where the pixels have been converted to microradians. The statistical results from these plots are also shown in Table 7. The conversion from x-pixels to microradians is 60 μrad per pixel; the conversion from y-pixels to microradians is 143 μrad per pixel. Note that the bias in the Y direction is approximately +67 μrad. The standard deviation is the RMS value about the mean. Hence, the X and Y tracker RMS about their respective means is 12.5 μrad in X and 6.8 μrad in Y. These values are better than the tracking jitter specification of 15 μrad RMS.
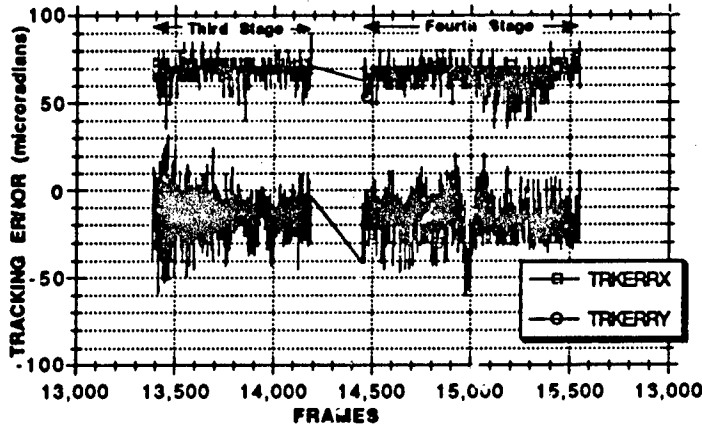
Fig. 18 - X and Y tracking errors vs frame number
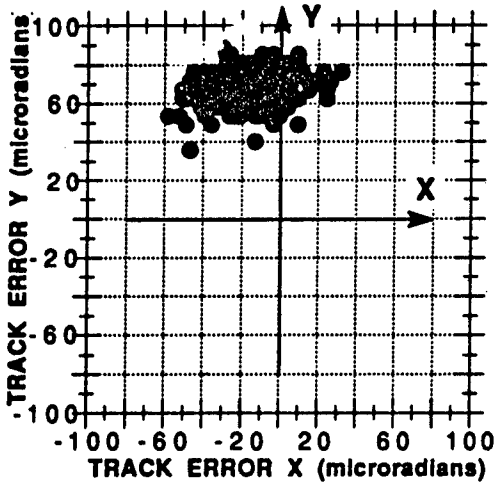
Third Stage
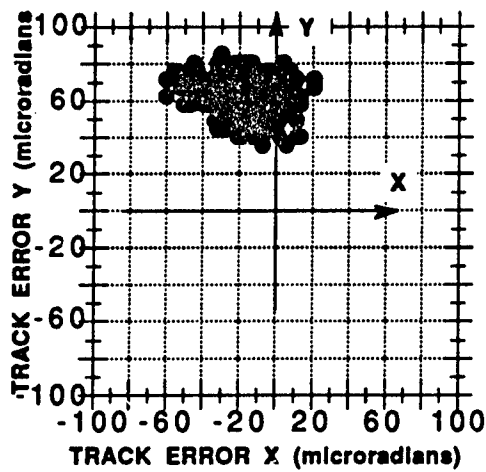
Fourth Stage

Fig. 19 - Y tracker error vs X tracker error in microradians

Table 7 - Tracking Error Statistics During Starbird Third and Fourth Stage Burn

Telemetry Frames	Parameter	Tracking Error X (μrad)	Tracking Error Y (μrad)
13,400 to 15,500	Minimum	-60.0	35.7
	Maximum	31.9	89.4
	Mean	-15.1	67.4
	Std Deviation*	12.5	6.8
	Points	1886	1886

*RMS Jitter

2.5.3 *Comparison with Previous Encounters*

A comparison with tracking errors for other encounters, Nihka and Strypi, is given in Table 8.

Table 8 - Tracking Error Comparison

Rocket Encounter	Mean Tracking Error		RMS Jitter	
	X (μrad)	Y (μrad)	X (μrad)	Y (μrad)
Strypi Second Stage	-3 to 3	-47 to -62	7 to 10	6 to 13
Strypi Third Stage	-1 to -19	-45 to -54	16 to 187	18 to 167
Nihka	2	-67	13	10
Starbird Third and Fourth Stage	-15	67	13	7

This table shows that the tracking jitter has remained consistent and within specifications for the Nihka, Starbird, and Strypi second-stage observations. These exhibited approximately 100% peak video value. The one exception is the tracking of the Strypi third-stage rocket. It did not track within jitter specifications, less than 15 μrad RMS, because the tracker-camera gain level was held to a low limit. This resulted in a low percentage of peak video value in the presence of a weak plume signature and yielded poor tracking stability.

3.0 EXTRACTION OF RADIOMETRIC QUANTITIES

Three levels of data reduction are useful for any radiometric experiment. At the first level, data are merely reduced to instrument readings or counts at the image plane; at the second level, instrument readings are converted by instrument-specific factors (which may be approximate) into approximate measures of physical quantities (e.g. radiance) with no assumed spectral shape for the source being used; and at the third level of reduction, a spectral shape is assumed to reduce data and present it.

A spectral shape must be assumed because instrument efficiency is a function of wavelength within each band, and the spectral distribution of incident photons is needed to provide the appropriate weighting at each wavelength within the pass band of integrated response. Since the spectral shape is not known from the data, a spectral shape must be assumed to determine this weighted distribution. Once a spectral shape has been assumed, the number of photoevents measured is used to infer the amplitude or intensity of the emission with that spectral shape.

3.1 Data Calibration Procedure

The raw image data transmitted from the satellite are in the form of arrays of 8-bit binary numbers Q_k, representing the intensity of light falling on the kth pixel of the CCD. From Q_k, an

estimate of the number of photoevents P_k occurring at the corresponding photocathode pixel during the image frame can be obtained by using

$$P_k = \left(\frac{1}{G_g}\right)\left(\frac{Q_k - D_k}{U_k}\right),$$
(1)

where

G_g is gain conversion factor for gain step g, i.e., the value of Q_k for a single photoevent, assumed to be the same for all pixels k;

D_k is the measured dark value for the kth pixel; and

U_k is the measured gain nonuniformity correction factor for the kth pixel.

The pulse height distribution of the image intensifier will cause noninteger values for P_k. The conversion of CCD response peaks to integral photoevent counts is possible only on the weakest images because of the overlap of photoevent images. Hence, P_k values are treated as continuous variables. The G_g, D_k, and U_k factors are discussed in detail along with the data calibration procedure in Section 2.0 of Ref. 1.

3.1.1 *Statistical Discrimination of Photoevents*

When a single photoevent is generated in the microchannel plate (MCP) of the UVPI plume camera, it is registered as a spatial distribution of charge in the CCD focal plane array (FPA). In general, a photoevent gets registered within a 3x3 pixel region, with the largest FPA response at the center pixel. Note that the blurring of a single photoevent is a relatively small component of the overall system point spread function.

When UVPI is looking at a dim source, relative to the instrument sensitivity, the instrument gain is automatically set high, say gain 13. At these high gains the calibration procedure (the estimation of photoevents from the measured DN) is sensitive to any error in the measurement of dark field level used for calibration. Although a small bias error in the dark field would have a small impact on the photoevent estimate for a single pixel, it could have a large impact on the results when summing the contribution of groups of pixels. Hence, for dim signal levels such as the Starbird rocket plume, a statistical discrimination scheme was developed that estimates the probability of false alarm for every pixel. In the context of calibrating UVPI data, a false alarm occurs when the noise in a pixel that contains no target is large enough to be considered part of a photoevent.

Working with the already calibrated images, the discrimination scheme consists of estimating a statistical decision threshold for each image. The threshold is given in terms of the background mean, standard deviation, and the acceptable probability of false alarm. Estimates for each image of the background mean and variance are made by using 4 image blocks located at each corner of the image and with dimensions of 8x8 pixels. The estimated threshold will exactly correspond to a probability of false alarm of PF if the following assumptions hold [10]:

- the local mean and local variance background statistics are the same over the whole FPA, and
- the density function of the background follows a Gaussian distribution.

Mathematically the decision threshold is given by

$$t = \mu + \sigma \cdot t'$$

where

μ is the estimated background mean,

σ is the estimated background standard deviation, and

t' must satisfy the integral equation

$$PF = \text{erfc}\,(t').$$

All the plume-camera images used in this report to estimate radiance or radiant intensities were subjected to the above discrimination scheme by using a probability of false alarm of 0.0001. False alarms were in fact observed in approximately 1 out of every 10,000 pixels, indicating that the two assumptions stated above are generally representative of these data. Recalling that a photoevent may spread over a 3x3 pixel region, for all those pixels where a photoevent took place, immediate neighbors are also included as possible signal contributors. A new estimate for the number of photoevents from the kth pixel was computed based on the following rule,

$$P_k = \max(0, P_k - \mu) \quad \text{if condition (A) holds, or} \quad P_k = 0, \text{ otherwise}$$

Condition (A) states that if any pixel in the local neighborhood of the kth pixel exceeds t' then the value at the kth pixel is adjusted to be the maximum of zero or $P_k - \mu$. Thus, pixels containing no photoevent contribution are set to exactly zero, eliminating the possibility of an erroneous contribution due to uncertainties in the dark field estimate for that pixel. This adjustment can be significant when large numbers of pixels contain no photoevents, i.e., few photoevents per image.

Figures 20 and 21 show a composite image created with no statistical discrimination and a composite image using statistical discrimination.

Fig. 20 - Composite image using no statistical discrimination

NRL/BENDIX STARBIRD Observation
Third Stage

PC=3 (195-295nm)
41 Superposed Images
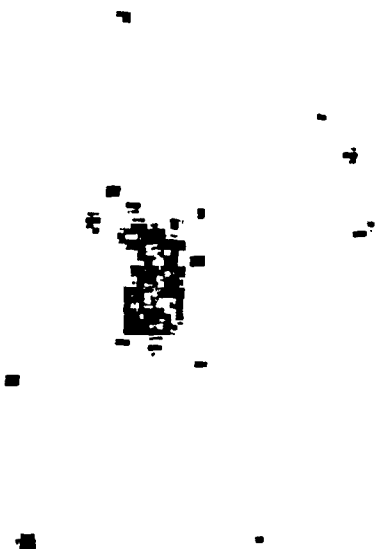
NRL/ACT 3/30/9%

Fig. 21 - Composite image using statistical discrimination

3.2 Relation of Photoevents to Source Radiance

Presumably, the photoevents at the image plane are the result of a radiation source in the field of view. If the radiation source is isotropic and uniform over an emitting region of area A_s then an expression for the photon flux ϕ_{in}, incident on the face of the telescope, in photons/second is:

$$\Phi_{in} = \left(\frac{A_s \Omega_s}{hc}\right) \int \lambda L(\lambda) d\lambda, \tag{2}$$

where

$L(\lambda)$	is source spectral radiance in W/m²-nm-sr,
A_s	is area of emitting region,
Ω_s	is solid angle of emission subtended by the telescope,
h	is Planck's constant,
c	is speed of light.

The factor λ/hc converts the spectral radiance $L(\lambda)$ to a photon radiance (photons/s-m²-nm-sr).

By setting the size of the emitting region equal to the footprint area of a pixel, the following reciprocity relation results:

$$A_p \Omega_s = \frac{A_s A_c}{R^2} = A_c \Omega_p,$$

where

A_c is system aperture area,
Ω_p is pixel field of view,
R is range from the detector to the emitting region.

The general expression for the number of photoevents P_k in pixel k at the image plane, due to an emitting source of spectral radiance $L(\lambda)$ filling the pixel field of view, is then given by [11]:

$$P_k = \left(\frac{A_c \Omega_p \tau}{hc} \right) \int \lambda Q(\lambda) L(\lambda) d\lambda, \tag{3}$$

where

τ is exposure time,
$Q(\lambda)$ is wavelength-dependent photoelectronic conversion efficiency, or net quantum efficiency, of the optics and detector.

In general, the exposure time τ is $1/30$th s for the plume camera and variable to a maximum of $1/30$th s for the tracker camera. The pixel field of view Ω_p is 12.8 by 10.0 μrad = 1.28×10^{-10} sr for the plume camera, and 180.5 by 143.9 μrad = 2.6×10^{-8} sr for the tracker camera. At the typical range of 500 km, these pixel fields of view correspond to 6.4 by 5.0 m and 90 by 72 m, respectively.

For further insight into the relationship of photoevents to source radiance, several forms of approximation can be helpful. Eq. (3) can be rearranged as

$$\int \lambda Q(\lambda) L(\lambda) d\lambda = \left(\frac{P_k}{\tau} \right) \left(\frac{hc}{A_c \Omega_p} \right) \tag{4}$$

Now note that the integral on the left is similar to the source radiance integral, $\int L(\lambda) d\lambda$, except for the λ and $Q(\lambda)$ factors. One quick and simple approximation involves substituting constant values for λ and $Q(\lambda)$, allowing them to come out from under the integral and move to the right side. For example, $\lambda_o = (\lambda_1 + \lambda_2)/2$ and $Q_o = Q_{max}/2$ provide estimated "average" values that allow reduction of the integral to an approximate radiance. The sensitivity of this approximate radiance to λ and $Q(\lambda)$ for various assumed spectra is discussed in Section 4.6 of Ref. 1. A more frequently used approximation, the peak normalized radiance, is discussed in the next section.

3.3 The Peak Normalized Radiance Approximation

The second level of data reduction involves manipulation of instrument-specific factors to obtain approximate measures of radiance and other similar quantities. One common method is called peak normalization in which both sides of Eq. (4) are divided by the quantities λ_m and $Q(\lambda_m)$. The definition of λ_m is the wavelength of peak net quantum efficiency and the definition of $Q(\lambda_m)$ is the peak net quantum efficiency. The result is called the peak normalized radiance L_{pn}, which is defined as

$$L_{pn} = \frac{\int \lambda Q(\lambda) L(\lambda) d\lambda}{\lambda_m Q(\lambda_m)}. \tag{5}$$

In practice, the evaluation of L_{pn} is based on the measured P_k using:

$$L_{pn} = \left(\frac{P_k}{\tau}\right)\left(\frac{hc}{\lambda_m}\right)\left(\frac{1}{A_c \Omega_p Q(\lambda_m)}\right). \tag{6}$$

Table 9 gives the values of λ_m, $Q(\lambda_m)$, and $\lambda_m Q(\lambda_m)$ for each of the filters and the quantity $hc/A_c\Omega_p = 1.98 \times 10^{-8}$ J-nm/cm^2-sr.

Even though Eq. (5) is an exact expression, it is not a true radiance because the integral contains terms other than $L(\lambda)$. L_{pn} approaches the true radiance as $[\lambda Q(\lambda)/\lambda_m Q(\lambda_m)]$ approaches 1. For UVPI, λ/λ_m is usually about equal to 1, but $Q(\lambda)/Q(\lambda_m) \ll 1$ for efficiency curves like PC-1 and PC-3 with long, low wings. On the other hand, efficiency curves for PC-2 and the tracker camera are more box-like, and $Q(\lambda)/Q(\lambda_m)$ is close to one. This is discussed further in Ref. 1.

Table 9 - Plume Camera Filter, λ_m, and Peak Quantum Efficiency

Filter	λ_m (nm)	$Q(\lambda_m)$	$\lambda_m Q(\lambda_m)$ (nm)
Plume PC-1	270	.00606	1.64
Plume PC-2	305	.00182	0.555
Plume PC-3	250	.00284	0.710
Plume PC-4	280	.0131	3.67
Tracker	355	.0200	7.10

Table 10 presents peak normalized radiance values and reference spectrum values obtained from an observation of the Starbird third-stage rocket by using measured P_k from the brightest pixel only. The ratio of the two radiances is included in the last column. The peak normalized approximation underestimates the reference spectrum result by a factor of 5 or more for filters PC-1 and PC-3, which have efficiency wings. On the other hand, L_{pn} is only low by about a factor of two for PC-2.

Table 10 - P_k/τ and L_{pn} for Brightest Pixel

Filter	P_k/τ (photoevents/s)	L_{pn} (μW/sr-cm^2)	L_e (μW/sr-cm^2)	L_{pn}/L_e
Plume PC-1	5.19	.063	.514	0.12
Plume PC-2	5.95	.212	.370	0.57
Plume PC-3	4.11	.114	.535	0.21
Plume PC-4	55.1	.297	.997	0.30

Thus, the peak normalized radiance is an approximate measure of the total radiance in the passband of the filter. A corrected radiance can be obtained if the true spectrum is used to evaluate the integral [12]. To better estimate the true in-band radiance, the approximate shape of the plume spectrum must be known.

3.4 Reference Spectrum for Aluminum-Loaded Propellants

The third level of data reduction requires the assumption of a spectrum for the emitting region. The amplitude of the assumed spectrum plays no role, but the shape acts as a weighting function within the passband to determine the distribution of photons as a function of wavelength. This is important because the instrument efficiency is different at each wavelength within a passband. Thus, the implied photon flux at the telescope face for a fixed measurement of photoevents, P_k will depend on how the photons are distributed across that wavelength interval. What is needed is the spectral shape. Such a spectral shape is not provided by the instrument. Fortunately, previous measurements and theoretical predictions can aid in making the assumption, as explained below. The sensitivity of the resulting radiometric values to several different spectral shapes is discussed in Section 4.5 of Ref. 1.

The solid rocket motors under consideration contain powdered aluminum in their propellant. This aluminum oxidizes and emerges as an incandescent mist in the rocket exhaust. It is this mist of oxidized aluminum particles or droplets that emits much of the UV radiation seen by UVPI in the plume central region. This mist is optically thin. The plumes are, thus, partially transparent. Because the heat of fusion for aluminum oxide is very high and the rate of cooling for micron-sized particles is relatively low, the particles remain at roughly the melting temperature throughout the length of the plume. Thus, most of the light in the plume will be from this nearly transparent cloud of micron-sized Al_2O_3 particles at the melting point, 2320 K.

The assumed spectral shape that will be used is that of a 2300 K blackbody times an emissivity function $\varepsilon_{Al}(\lambda)$, shown in Fig. 22 [13]. This emissivity curve is basically characteristic of hot alumina particles of the size found in rocket exhaust plumes [9].

The resulting normalized spectral shape is fairly generic to all solid-fueled boosters with aluminum-loaded fuel and is termed the reference spectrum $R(\lambda)$. Mathematically,

$$R(\lambda) = \varepsilon_{Al}(\lambda) L_{BB}(\lambda),\qquad (7)$$

where $L_{BB}(\lambda)$ is the 2300 K blackbody spectrum. The reference spectrum, compared to a blackbody spectrum, is shown in Fig. 23. The spectral shape is a good approximation to actual rocket plume spectra as verified by on-board spectrometers looking back into rocket plumes [14].
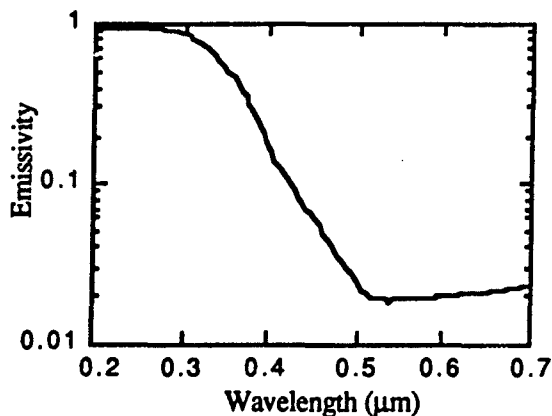
Fig. 22 - Emissivity curve for aluminum particles in rocket plumes
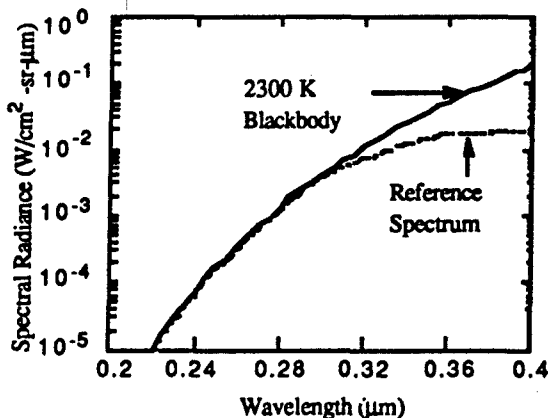
Fig. 23 - Assumed reference spectrum

3.5 Use of the Reference Spectrum to Calculate a Scaling Constant

Assuming that the reference spectrum $R(\lambda)$ gives the proper spectral shape for $L(\lambda)$ is equivalent to saying that $L(\lambda)$ and $R(\lambda)$ are related by a scaling constant α that is independent of λ:

$$\alpha = \frac{L(\lambda)}{R(\lambda)}. \tag{8}$$

The scaling factor α for a pixel can be obtained by first calculating the number of photoevents expected for the unscaled reference spectrum P_k' using the expression,

$$P_k' = \left(\frac{A_c \Omega_p \tau}{hc}\right) \int \lambda \mathcal{Q}(\lambda) R(\lambda) d\lambda, \tag{9}$$

where the calculated value is the same for all k (i.e., k is superfluous). Then, using the ratio of Eq. (3) to Eq. (9), namely,

$$\frac{P_k}{P_k'} = \frac{\int \lambda \mathcal{Q}(\lambda) L(\lambda) d\lambda}{\int \lambda Q(\lambda) R(\lambda) d\lambda} = \frac{\alpha \int \lambda Q(\lambda) R(\lambda) d\lambda}{\int \lambda Q(\lambda) R(\lambda) d\lambda} = \alpha_k. \tag{10}$$

Therefore, α_k can be determined for each passband and for each pixel by comparing the measured value of P_k to the calculated value P_k':

$$\alpha_k = \alpha_k = \frac{P_k}{P_k'}, \tag{11}$$

which gives an in-band, effective value of α_k for that pixel. Actually, these plumes are optically thin and α_k, in some sense, provides a measure of the thinness or density of emitters along the line of sight of that pixel.

After α is known, the source spectral radiance function $L(\lambda)$ can be calculated by using Eq. (8) and, in turn, used to calculate in-band total radiance for the plume data in various filter bandpasses. All the radiometric values presented in this report can be obtained from the source function $L(\lambda)$, defined by Eqs. (8) and (11). The values for P_k/τ and P_k'/τ, obtained as an average for the brightest pixel over several frames for the Starbird third-stage plume in the various filter bands, are given in Table 11.

Table 11 – Photoevents per Second from Starbird Third-Stage
Plume and Reference Spectrum Model for Brightest Pixel
and Ratios of These Values

Filter	P_k/τ (PE/s)	P_k'/τ (PE/s)	α_k
Plume PC-1	5.19	1898	2.73×10^{-3}
Plume PC-2	5.95	1960	3.04×10^{-3}
Plume PC-3	4.11	371	1.11×10^{-2}
Plume PC-4	55.1	28400	1.94×10^{-3}

3.6 Centroid Wavelength Determination

The procedure above yields a function $L(\lambda)$ that describes the amplitude of the spectral shape that corresponds to the observed number of photoevents. Describing this function with a single numerical value is difficult because of the extremely rapid variation of the spectral radiances evident in Figs. 26, through 28 found in Section 4. It is sometimes desirable to provide single numerical values of plume spectral radiance and spectral radiant intensity despite this rapid variation. This is achieved simply by taking $L(\lambda)$ of Eq. (8) at a specific characteristic wavelength λ_c, for each filter passband. This could have been selected to be the center of each filter passband, but this choice would neglect the shift in the effective response because of the spectrally varying source. A response centroid wavelength, weighted by the reference spectral function, was defined:

$$\lambda_c = \frac{\int \lambda^2 R(\lambda)Q(\lambda)d\lambda}{\int \lambda R(\lambda)Q(\lambda)d\lambda}. \tag{12}$$

This describes the wavelength of average contribution to the UVPI response for each filter. These centroid wavelengths were computed for various spectral shapes and are shown in Table 12, for which the integrals of Eq. (12) have been evaluated as discrete summations over the range of $Q(\lambda)$ that is not negligible. *The numbers in parentheses under the exact reference spectrum values are the rounded values that are actually used throughout the report.*

Table 12 – Centroid Wavelength λ_C for Various Spectra

	PC-3 (nm)	PC-1 (nm)	PC-2 (nm)	PC-4 (nm)	Tracker (nm)
1800K Blackbody	270.4	282.4	310.0	314.1	416.2
2300K Blackbody	265.8	279.2	309.7	308.5	409.7
Reference Spectrum (Rounded)	265.8 (265)	279.1 (280)	309.6 (310)	306.4 (305)	389.4 (390)
Flat Spectrum	248.1	270.7	309.0	287.3	369.5
Peak Normalized	250.0	270.0	310.0	280.0	355.0

Defining λ_c is simply a means of selecting a nominal characteristic wavelength for describing the result of the fitting of the spectral shape to the instrument measurement as single numerical values. Other procedures could have been used for selecting a reference wavelength for describing the spectral radiance function. One could, for example, have taken the central wavelength for each filter and cited the numerical value of the fit function at those wavelengths. This would yield different

values for the nominal spectral radiances, without changing the function $L(\lambda)$ at all. In short, these single numerical values for the rapidly varying spectral radiometric parameters must be treated with caution.

3.7 Calculations of Radiance and Radiant Intensity

After the spectral radiance is known, the spectral integrals can be evaluated to obtain values for the radiance:

$$L_e = \int_{\lambda_L}^{\lambda_U} L(\lambda)d\lambda = \alpha \int_{\lambda_L}^{\lambda_U} R(\lambda)d\lambda. \tag{13}$$

The units of L_e are (power)/(area)(solid angle), or W/m^2-sr. The evaluation of these integrals is limited to the nominal bandwidth of the pertinent filter. Note that the integrand of Eq. (13) does not include the response function $Q(\lambda)$ and, therefore, does not become small outside the filter passbands. The values obtained for L_e will depend very strongly on the limits of integration.

Conversion to radiant intensity can be achieved from the preceding expressions by multiplying by $R^2\Omega_p$, where R is the range to the source and Ω_p is the pixel field of view. The result is then summed over the pixels containing signal. This is equivalent to summing the apparent radiance or spectral radiance over the projected pixel area and attributing it to a point source within the field of view of the pixel. The spectral radiant intensity $I(\lambda)$ and the radiant intensity I_e can be obtained directly from the corresponding expressions for the spectral radiance and radiance, Eqs. (8) and (13), respectively:

$$I(\lambda) = R^2\Omega_p L(\lambda) = R^2\Omega_p \alpha R(\lambda), \tag{14}$$

and

$$I_e = \int_{\lambda_L}^{\lambda_U} I(\lambda)d\lambda = R^2\Omega_p L_e. \tag{15}$$

The units of $I(\lambda)$ are (power)/(spectral bandwidth)(solid angle), or W/nm-sr, and the units of I_e are (power)/(solid angle), or W/sr. As with the radiance, the radiant intensity is an integral across a limited portion of the spectrum defined by the nominal filter edges. The value so obtained is far smaller than that for the full spectrum radiant intensity. It will also be very sensitive to the limits of integration chosen for Eq. (15).

3.8 Summary of Radiometric Conversion Constants

Table 13 summarizes the definitions of conversion constants most often encountered in calculating one radiometric quantity from another. Table 14 gives the specific values for the conversion constants based on the assumed reference spectrum. Any revised spectral shape assumption will lead to a different set of conversion constants. Table 15 lists the radiometric values corresponding to one photoevent per second. The radiant intensity values refer to a range of 500 km. The values of the spectral radiance $L(\lambda_c)$ and the radiance L_e are based on a single photoevent per second per pixel. Any arbitrary number of photoevents measured in a particular pixel is multiplied by the value in the table to determine the radiance of the source in that pixel's field of view. The values of the spectral radiant intensity $I(\lambda_c)$ and radiant intensity I_e are per pixel even though these terms are used more often to refer to the total number of photoevents measured in the entire plume image.

Table 13 – Summary of Formulas Defining Conversion Constants

From	To	Op	Formula
P_k/τ (photoevents/s)	ϕ_{in} (photons/s)	*C_1	$C_1 = \dfrac{\int \lambda R(\lambda)d\lambda}{\int \lambda R(\lambda)Q(\lambda)d\lambda}$
ϕ_{in} (photons/s)	P_{in} (watts)	*C_2	$C_2 = \dfrac{hc\int R(\lambda)d\lambda}{\int \lambda R(\lambda)d\lambda}$
P_{in} (watts)	I_e (W/sr)	+C_3	$C_3 = A_c/R^2$
L_e (W/sr-cm^2) I_e (W/sr)	$L(\lambda_c)$ (W/cm^2-sr-nm) $I(\lambda_c)$ (W/sr-nm)	+C_4	$C_4 = \dfrac{\int \lambda L(\lambda)d\lambda}{L(\lambda_c)}$
I_e (W/sr) $I(\lambda_c)$ (W/sr-nm)	L_e (W/cm^2-sr) $L(\lambda_c)$ (W/cm^2-sr-nm)	+C_5	$C_5 = R^2\Omega_p$

Table 14 - Conversion Constants for the Reference Spectrum

Constant	Units	PC-3	PC-1	PC-2	PC-4	Tracker
		(λ_c=265 nm)	(λ_c=280 nm)	(λ_c=310 nm)	(λ_c=305 nm)	(λ_c=390 nm)
C_1	photons/PE	1840	1510	976	294	66.2
C_2	joules/photon	7.11×10^{-19}	6.61×10^{-19}	6.41×10^{-19}	6.19×10^{-19}	5.11×10^{-19}
C_3	steradians	3.12×10^{-14}	3.12×10^{-14}	3.12×10^{-14}	3.12×10^{-14}	3.12×10^{-14}
C_4	nm	104.5	150.2	20.4	105.5	125.2
C_5	cm^2	31.9×10^4	31.9×10^4	31.9×10^4	31.9×10^4	6510×10^4

Table 15 - Radiometric Values for One Photoevent Per Second

Units	PC-3	PC-1	PC-2	PC-4	Tracker
	(λ_c=265 nm)	(λ_c=280 nm)	(λ_c=310 nm)	(λ_c=305 nm)	(λ_c=390 nm)
P_k/τ (photoevents/s)	1	1	1	1	1
ϕ_{in} (photons/s)	1840	1510	976	294	66.2
P_{in} (watts)	1.31×10^{-15}	9.95×10^{-16}	6.26×10^{-16}	1.82×10^{-16}	3.38×10^{-17}
I_e (W/sr)	4.16×10^{-2}	3.17×10^{-2}	1.99×10^{-2}	5.80×10^{-3}	1.08×10^{-3}
$I(\lambda_c)$ (W/sr-nm)	3.96×10^{-4}	2.11×10^{-4}	9.76×10^{-4}	5.50×10^{-5}	8.60×10^{-6}
L_e (W/sr-cm^2)	1.30×10^{-7}	9.94×10^{-8}	6.24×10^{-8}	1.82×10^{-8}	1.65×10^{-11}
$L(\lambda_c)$ (W/sr-cm^2-nm)	1.24×10^{-9}	6.61×10^{-10}	3.06×10^{-9}	1.72×10^{-10}	1.32×10^{-13}

Note that the conversion constants associated with $I(\lambda_c)$ and $L(\lambda_c)$ use the rounded reference spectrum centroid wavelength values shown in parentheses in Table 12.

4.0 PLUME DATA

In this section the observed plume data are presented. The data intervals used in this report are defined in 4.1, and an overview of the intensity history observed by each camera is given in 4.2. Examples of single plume-camera images are given in 4.3. Composite images with corresponding contour plots for the defined data intervals for the plume and tracker cameras are presented in 4.4 and 4.5, respectively. Subsection 4.6 discusses the error in the radiometric observations. The concluding subsection, 4.7, discusses the noise equivalent radiance for the UVPI.

4.1 Data Intervals

4.1.1 *Description of Intervals*

Table 16 summarizes the Starbird third- and fourth-stage data intervals used in this report. Also included are the number of plume-camera images and tracker-camera images analyzed in each interval. Table 17 reports important calibration parameters associated with the intervals. The UVPI-Starbird range is used to determine source radiant intensity, as discussed in 4.2. The image angle variation associated with a sequence of frames is a measure of the variation in plume-image axis orientation with respect to TV lines in the image display. This parameter is relevant to the spatial analysis presented in Section 5.0.

The Starbird third-stage plume was first observed in the plume camera around frame 13013. Because of gain changes and ensuing transients in the plume camera, data analysis was limited to intervals 1 through 4 of Table 16. Approximately 6.7 s of filter 4 data, 1.8 s of filter 3 data, 2.0 s of filter 2 data, and 2.0 s of filter 1 data were collected during this time. Analysis of tracker camera data was restricted to these same intervals.

The Starbird fourth-stage plume was first observed in the plume camera around frame 14368. Because of gain changes and ensuing transients in the plume camera, analysis of both tracker- and plume-camera data was limited to intervals 5 through 7 of Table 16. Approximately 6.7 s of filter 3 data, 1.4 s of filter 2 data, and 4.4 s of filter 1 data were collected during this time.

Table 16 - Definitions of Data Intervals

Data Interval	Starbird Stage	GMT	TALO (s)	Plume Camera Filter	Telemetry Frame Range	No. of Plume Images	No. of Tracker Images
1	3	3:39:20.64 - 3:39:27.31	115.6 - 122.3	PC-4	13543-13743	157	40
2	3	3:39:31.54 - 3:39:33.32	126.5 - 128.3	PC-3	13870-13923	41	11
3	3	3:39:34.91 - 3:39:36.88	129.9 - 131.9	PC-2	13971-14030	48	12
4	3	3:39:40.79 - 3:39:42.56	135.8 - 137.8	PC-1	14147-14200	44	10
5	4	3:39:55.33 - 3:39:59.76	150.3 - 154.8	PC-1	14583-14716	108	26
6	4	3:40:04.68 - 3:40:06.10	159.7 - 161.1	PC-2	14863-14906	36	8
7	4	3:40:08.01 - 3:40:14.75	163.0 - 169.8	PC-3	14963-15165	153	38

4.1.2 *Calibration Parameters Associated with Intervals*

There were basic camera parameters that were pertinent to the radiometric calibration of the data for all frames during which the Starbird third and fourth stages were observed. These parameters, which are listed in Appendix B, included time, telemetry frame number, gain level for both cameras, and exposure time for both cameras. The plume camera has a constant $1/30$th of a second exposure time for each frame. The tracker camera has an electronic gate that can vary the exposure time to a maximum of $1/30$th of a second. Figure 24 shows the camera gain levels for both tracker and plume cameras. Figure 25 shows exposure time for both cameras as a function of telemetry frame number. In these figures, the data intervals are depicted as horizontal, bold, solid lines.

Table 17 – Parameters Associated With Data Intervals

Data Interval	Starbird Stage	Plume Camera Filter	Bandpass (nm)	Plume to Tracker Ratio	UVPI-Starbird Range (km)	Image Angle Variation (deg)
1	3	PC-4	235-350	8:2	596	10.3
2	3	PC-3	195-295	8:2	565	2.8
3	3	PC-2	300-320	8:2	553	3.0
4	3	PC-1	200-320	8:2	535	3.6
5	4	PC-1	200-320	8:2	499	5.9
6	4	PC-2	300-320	8:2	488	1.7
7	4	PC-3	195-295	8:2	483	6.4
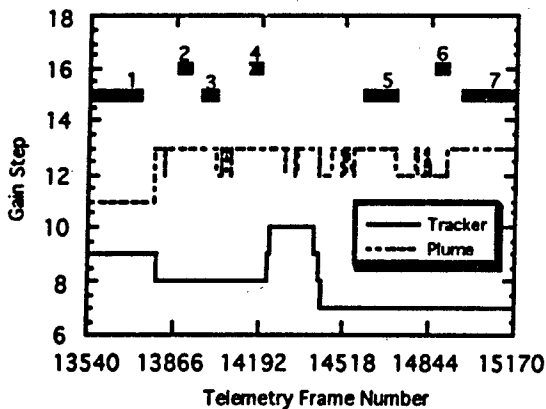
Fig. 24 - Tracker and plume camera gain
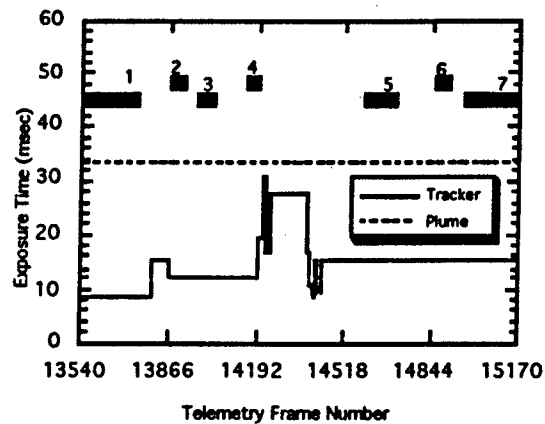
Fig. 25 - Tracker and plume camera exposure times

4.2 Intensity History Overview

As a quick overview, Figs. 26 and 27 show plume-camera long-term trends in the central region and total spectral radiant intensity, respectively. The values plotted were derived by assuming the reference spectral shape. Figure 28 shows similar results for the tracker-camera total spectral radiant intensity in a 19 by 19 pixel region containing the plume camera field of view. Notice that the tracker camera mean changes from interval to interval. Consequently, part of the difference among measurements taken with the four filters of the plume camera is attributable to long-term temporal variations rather than to spectral differences.

For these figures, all curves specify spectral radiant intensity at the reference centroid wavelength for each interval.
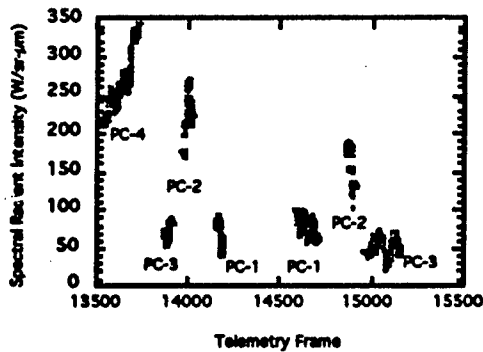
Fig. 26 - Spectral radiant intensity, plume camera, Starbird
central region
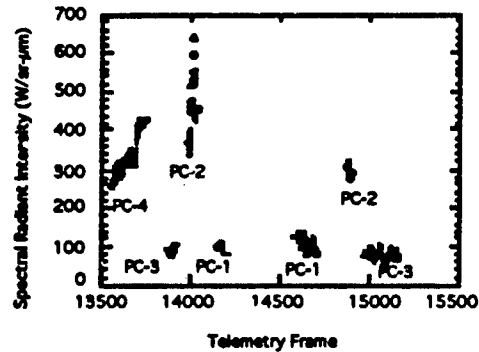
Fig. 27 - Spectral radiant intensity, plume camera, Starbird
total
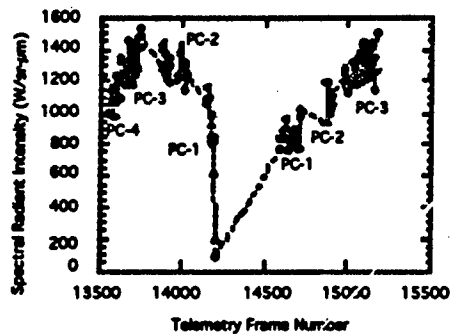
Fig. 28 - Spectral radiant intensity, tracker camera

4.3 Single Images

This subsection presents raw plume-image data. Given the characteristics of the UVPI cameras, e.g., exposure time, optics aperture, and the rocket-plume radiant intensity, the number of photoevents that are registered within the focal plane array of a camera can be individually counted as isolated events. In this respect, UVPI can be used as a photon-counting instrument.

Figure 29 shows single images, in zoom image transmission rate, of the Starbird third-stage burn for the different filters. The image in the upper left corner is frame 13657, PC-4; the upper right corner is frame 13886, PC-3; the lower left corner is frame 14018, PC-2; and the lower right corner is frame 14164, PC-1. Pixel radiance is encoded as image brightness, where dark and bright are, respectively, relatively smaller and larger radiance. The images demonstrate that the shapes of the plume central region and outer region are not necessarily clearly delineated in a single frame.

Every bright spot on the image corresponds to one or more photoevents that pile up at that particular pixel during the exposure time of the camera. Figure 30 illustrates the number of photoevents per second measured at each pixel location in the center 64 by 64 pixels of the lower-left-corner image shown in Fig. 29. The z axis corresponds to the number of photoevents per second while the x and y axes correspond to row and column indices. The actual procedure used to compute the number of photoevents from the measured digital number in the UVPI telemetry stream was discussed in Section 3 and in Ref. 1. Figure 30 is also representative of single images during the fourth-stage burn.
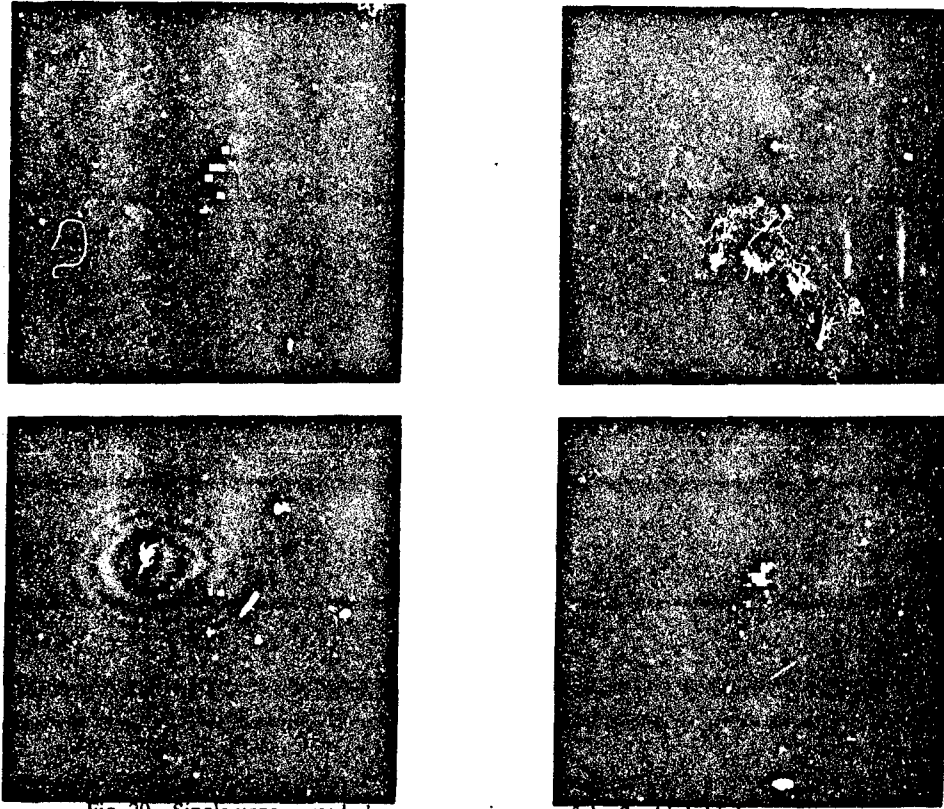
Fig. 29 - Single unprocessed plume camera images of the Starbird third-stage plume
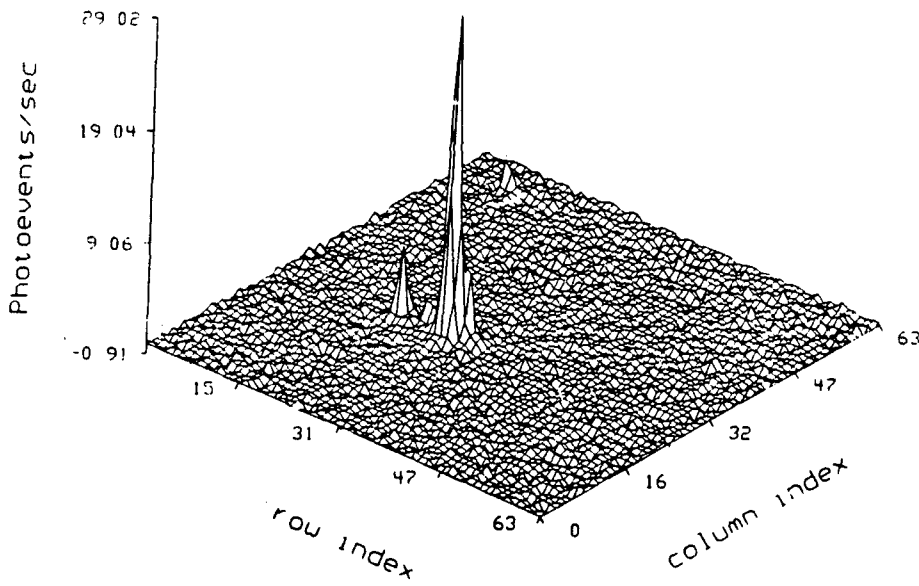
Fig. 30 - Single image of the Starbird third-stage plume

4.4 Composite Plume Camera Images and Contour Plots

In this subsection composite plume camera images and their corresponding contour plots are presented that show the spatial distribution of the time-averaged plume radiance. The composite images are made from calibrated versions of images formed while observing the Starbird third and fourth stages during the seven data intervals listed in Table 16 of Section 4. As explained in Section 3, the reference emission spectrum is assumed to convert UVPI measurements into units of radiance, (W/sr-cm^2), for both the Starbird third- and fourth-stage data. Within each interval the plume-to-tracker image ratio is 8 to 2, and the exposure time for each individual plume camera image is ^{1}/30th of a second. Many individual images are superposed to form each composite image.

The limiting resolution of the UVPI cameras is described by the point spread function. Observation of a ground-based beacon, a source less than 5 m across, shows that the full-width-half-maximum of the point source response in the plume camera is about 9 pixels, or about 90 μrad, which is equivalent to 40 m at a 450-km range. Figure 31 shows a plume-camera image of the beacon on the same scale as the plume images that follow. This is representative of the plume-camera's point spread function. Figure 32 shows the contour plot for the ground beacon, a point source, on the same scale as Figs. 34, 36, 38, 40, 42, 44, and 46, discussed below. This figure indicates th·· resolution of the plume-camera contour plots as the result of the point spread function.

The Starbird third stage was observed with the four plume-camera filters and the Starbird fourth stage with only three of the four filters. Figures 33, 35, 37, 39, 41, 43 and 45 show the resulting calibrated composite images for the seven data intervals. In these images, the radiant intensity has been mapped to a false-color scale with black representing the highest intensity, light blue the middle intensity, and white the lowest intensity. A horizontal color bar depicting the mapping of radiant intensity into colors is shown on the lower left corner of each image. A histogram of the image intensity values is shown above the color bar in the form of white dots.

Figures 34, 36, 38, 40, 42, 44 and 46 are contour plots for the seven data intervals, starting with filter 4 in the third stage and ending with filter 3 in the fourth stage. Table 18 contains the value of the maximum apparent pixel radiance measured for the brightest pixel for the plume camera as a function of data interval. With each picture or plot a companion summary table provides relevant information for the quantitative interpretation of the image or plot. The parameters presented in these tables are described in Table 19.

Table 18 – Plume Camera Apparent Peak Radiometric Values

Interval	Stage	Filter	Apparent Peak Radiance (μW/sr-cm^2)	Apparent Peak Spectral Radiance (μW/sr-cm^2-μm)	Centroid Wavelength (nm)
1	3	PC-4	9.97×10^{-1}	9.44	305
2	3	PC-3	5.35×10^{-1}	5.12	265
3	3	PC-2	3.70×10^{-1}	1.81×10^1	310
4	3	PC-1	5.14×10^{-1}	3.43	280
5	4	PC-1	7.50×10^{-1}	5.00	280
6	4	PC-2	3.69×10^{-1}	1.81×10^1	310
7	4	PC-3	3.24×10^{-1}	3.10	265

The black, blue, and red contours represent, respectively, plume radiance contours at 95%, 50%, and 9.5% of the maximum radiance in the image. The radiance units are watts per steradian per square centimeter, and the horizontal and vertical axes are scaled in meters.

Table 19 – Description of Basic Parameters

Aspect Angle	Angle, in degrees, between the line of sight and the rocket body longitudinal vector
Average Range	Average distance, in kilometers, between UVPI and the plume target
Camera	Camera used, either tracker or plume
Displayed Image Size	Size in pixels (picture elements) of the image being displayed
Number of Superposed Images	Number of images averaged together to generate the composite image. Because of the tracker-to-plume image ratio, this number is not equal to the number of frames in the range.
Pixel Foot Print	Projected pixel dimensions, in meters, at target range. This number does not account for any spreading introduced by the optics or jitter because it incorporates only the instantaneous field of view.
Range of Frames Used	Range of frames containing the set of tracker- or plume-camera images superposed.
Spectral Band	Spectral band, in nanometers, covered by all images within the set. This band includes more than 99% of the net quantum efficiency response curve.
Target Observed	Either Stage 3 or Stage 4
Total Photoevents/s	Sum of all photoevent-per-second pixel values over the specified region of the focal plane
Total Radiant Intensity (W/sr)	Radiant intensity associated with the total photoevents per second
Total Spectral Radiant Intensity (W/sr-µm)	Spectral radiant intensity at the specified centroid wavelength associated with the total photoevents per second.
Apparent Peak Radiance (μW/sr-cm^2)	The apparent radiance measured at the brightest pixel in an image. Because of the size and structure of UVPI's point spread function, the value given is likely not to be a good measure of the true peak radiance at the source. The value is useful for rough comparisons and order of magnitude estimates.
Apparent Peak Spectral Radiance (μW/sr-cm^2-µm)	The apparent spectral radiance at the specified centroid wavelength measured at the brightest pixel in an image. Because of the size and structure of UVPI's point spread function, the value given is likely not to be a good measure of the true peak spectral radiance at the source. The value is useful for rough comparisons and order of magnitude estimates.
Error (%)	The total error associated with the above radiometric values. This error includes gain conversion factor error and the error attributable to photon shot noise and detector noise. The error estimate is based on the total number of images superposed. See Section 4.6 for in-depth discussion.

Because of the UVPI's dynamic range of 256 levels in the analog to digital converter, it is difficult to get well-defined plume contours at levels below 9.5% of the maximum radiance unless a large number of images are superposed.

Table 18 also shows apparent peak spectral radiance reported at the specified centroid wavelength. Because of the size and structure of UVPI's point spread function, values given are primarily useful for rough comparisons and order of magnitude estimates. Estimates of true source peak radiance require further analysis. A comparison of UVPI apparent peak radiance measurements with CHARM 1.3 code predictions is presented in Section 5.3.

Note that the number of images superposed in each data interval can be significantly different. For example, only 36 images were used for interval 6, and 157 were used for interval 1. For each interval, as many images as possible were superposed.

Because of the relatively long observation time, the apparent rocket velocity vector changes from interval to interval. The velocity is directed out of the page toward the viewer at an angle that is the complement of the aspect angle shown in Fig. 9. Over the period of observation, the direction of the rocket velocity vector projected on the image plane changes significantly. Table 20 summarizes the direction of the velocity vector projected on the image plane.

Table 20 - Apparent Velocity Vector Direction for Each Interval

Interval	Stage	Filter	Direction of Motion Relative to Tracker-Camera X Axis (deg)
1	3	PC-4	12.4
2	3	PC-3	-0.88
3	3	PC-2	-6.24
4	3	PC-1	-17.5
5	4	PC-1	-38.3
6	4	PC-2	-48.0
7	4	PC-3	-54.0
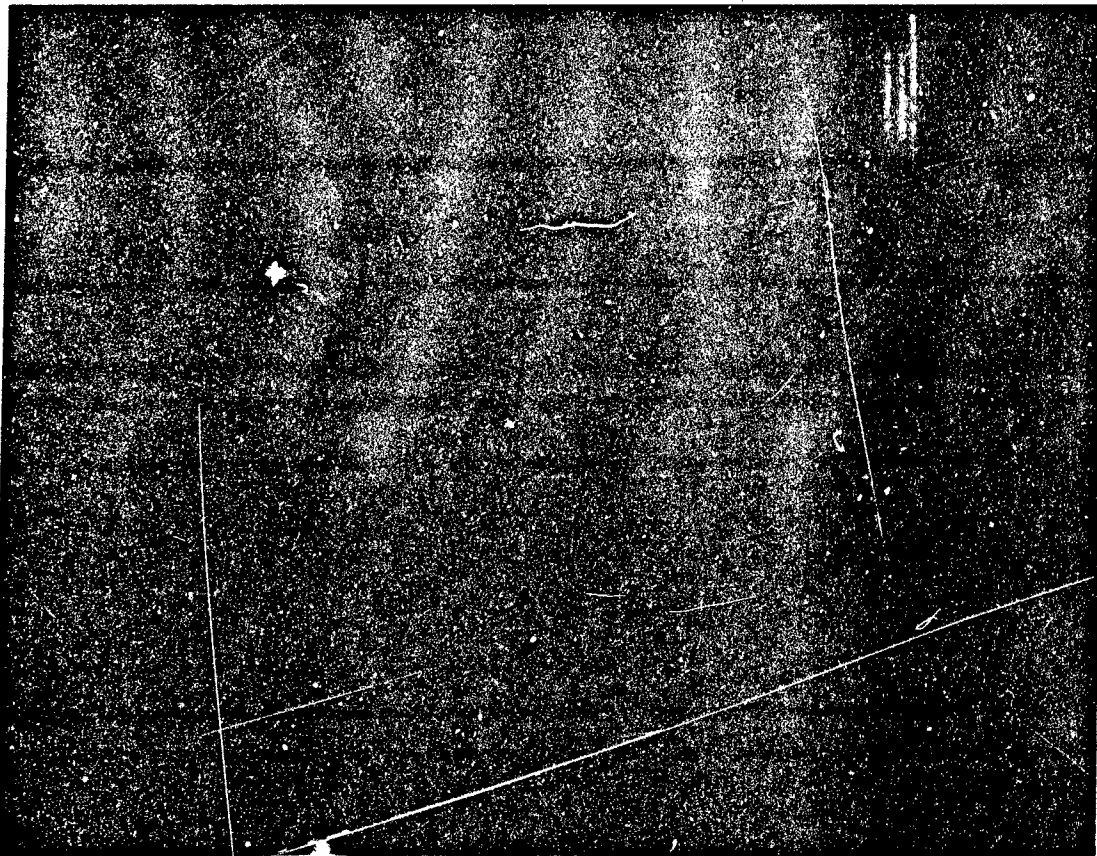
Observing Sensor:	UVPI
Target Observed:	UVPI Ground-Based Beacon
Orbit Number:	1173
Range of Frames Used:	12778-12778
Camera:	Plume
Displayed Image Size (pixels):	112 (vertical) x 91 (horizontal)
Average Range (km):	450

Fig. 31 - Plume-camera image of ground-based beacon illustrating the point spread function

PSF Estimate : Range=480km

Column Axis (meters)

Row Axis (meters)
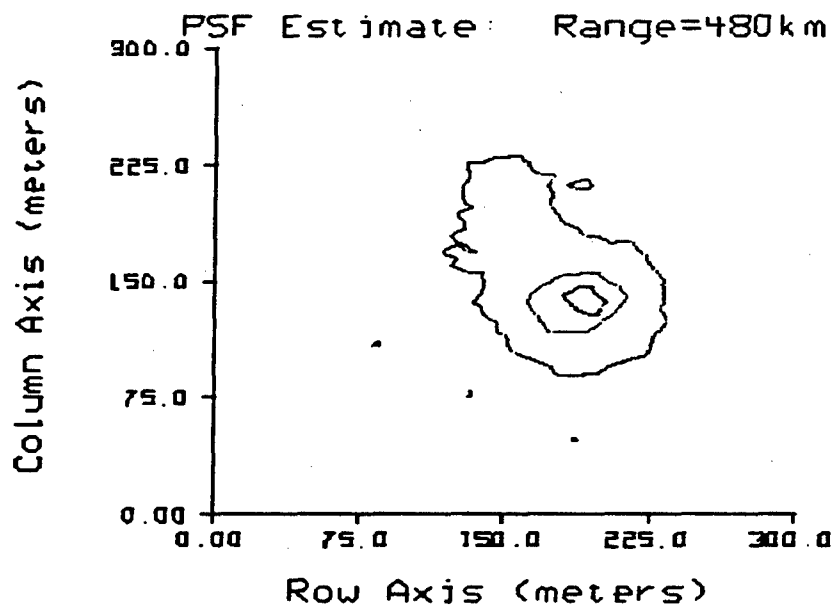
$| = 0.095*max \quad | = 0.50*max \quad | = 0.95*max$

Observing Sensor:	UVPI
Target Observed:	UVPI Ground-Based Beacon
Orbit:	1173
Range of Frames Used:	12778-12778
Camera:	Plume
Average Range (km):	450

Fig. 32 - Plume-camera contour plot for ground-based beacon

NRL/BENDIX STARBIRD Observation   PC=4 (235-350nm)
Third Stage   157 Superposed Images

NRL/ACT 3/30/92.

Observing Sensor:	UVPI (Dec. 18, 1990)
Target Observed:	Starbird, Stage 3
Range of Frames Used:	13543-13743
Number of Superposed Images:	157
Camera:	Plume
Spectral Band (nanometers):	235-350 (PC-4)
Displayed Image Size (pixels):	112 (vertical) x 91 (horizontal)
Average Range (km):	596
Pixel Footprint (m) @ Range:	5.96 (vertical) x 7.63 (horizontal)
Aspect Angle (deg):	45.6
*Total Photoevents/s:	4.29×10^3
*Total Radiant Intensity (W/sr):	3.53×10^1
*Total Spectral Radiant Intensity @ 305 nm (W/sr-mm):	3.34×10^2
*Error (%):	13.6

*For full image.

Fig. 33 - Composite plume-camera image for interval 1

Third Stage (PC=4 235-350nm)

max=0.99uW/sr-cm2
| =0.095*max | =0.50*max | =0.95*max

NRL/ACT 3/30/92

Observing Sensor:	UVPI (Dec. 18, 1990)
Target Observed:	Starbird, Stage 3
Range of Frames Used:	13543-13743
Number of Superposed Images:	157
Camera:	Plume
Spectral Band (nanometers):	235-350 (PC-4)
Displayed Image Size (pixels):	67.1 (vertical) x 52.4 (horizontal)
Average Range (km):	596
Pixel Footprint (m) @ Range:	5.96 (vertical) x 7.63 (horizontal)
Aspect Angle (deg):	45.6
*Photoevents/s:	5.51×10^1
*Apparent Peak Radiance (μW/sr-cm^2):	9.97×10^{-1}
*Apparent Peak Spectral Radiance @ 305 nm (μW/sr-cm^2-μm):	9.44

*For brightest pixel.

Fig. 34 - Plume camera contour plot for interval 1

NRL/BENDIX STARBIRD Observation   PC=3 (195-295nm)
Third Stage   41 Superposed Images

NRL/ACT 3/30/92

Observing Sensor:	UVPI (Dec. 18, 1990)
Target Observed:	Starbird, Stage 3
Range of Frames Used:	13870-13923
Number of Superposed Images:	41
Camera:	Plume
Spectral Band (nanometers):	195-295 (PC-3)
Displayed Image Size (pixels):	112 (vertical) x 91 (horizontal)
Average Range (km):	565
Pixel Footprint (m) @ Range:	5.65 (vertical) x 7.23 (horizontal)
Aspect Angle (deg):	46.9
*Total Photoevents/s:	1.78×10^2
*Total Radiant Intensity (W/sr):	9.46
*Total Spectral Radiant Intensity @ 265 nm (W/sr-mm):	9.06×10^1
*Error (%):	13.2

*For full image.

Fig. 35 - Composite plume-camera image for interval 2

Third Stage (PC=3 195-295 nm)

max=0.53uW/sr-cm2
| =0.095%max | =0.50%max | =0.95%max

NRL/RCI 3/30/92

Observing Sensor:	UVPI (Dec. 18, 1990)
Target Observed:	Starbird, Stage 3
Range of Frames Used:	13870-13923
Number of Superposed Images:	41
Camera:	Plume
Spectral Band (nanometers):	195-295 (PC-3)
Displayed Image Size (pixels):	70.8 (vertical) x 55.3 (horizontal)
Average Range (km):	565
Pixel Footprint (m) @ Range:	5.65 (vertical) x 7.23 (horizontal)
Aspect Angle (deg):	46.9
*Photoevents/s:	4.11
*Apparent Peak Radiance (μW/sr-cm^2):	5.35×10^{-1}
*Apparent Peak Spectral Radiance @ 265 nm (μW/sr-cm^2-μm):	5.12

*For brightest pixel.

Fig. 36 - Plume-camera contour plot for interval 2

NRL/BENDIX STARBIRD Observation   PC=2 (300-320nm)
Third Stage   48 Superposed Images

NRL/ACT 3/30/92

Observing Sensor:	UVPI (Dec. 18, 1990)
Target Observed:	Starbird, Stage 3
Range of Frames Used:	13971-14030
Number of Superposed Images:	48
Camera:	Plume
Spectral Band (nanometers):	300-320 (PC-2)
Displayed Image Size (pixels):	112 (vertical) x 91 (horizontal)
Average Range (km):	553
Pixel Footprint (m) @ Range:	5.53 (vertical) x 7.08 (horizontal)
Aspect Angle (deg):	47.7
*Total Photoevents/s:	3.89×10^2
*Total Radiant Intensity (W/sr):	9.48
*Total Spectral Radiant Intensity @ 310 nm (W/sr-μm):	4.65×10^2
*Error (%):	16.2

*For full image.

Fig. 37 - Composite plume-camera image for interval 3

Third Stage (PC=2 300-320 nm)

max=0.37uW/sr-cm2
⌷ =0.095*max ⌷ =0.59*max ⌷ =0.95*max

NRL/ACT 3/30/92

Observing Sensor:	UVPI (Dec. 18, 1990)
Target Observed:	Starbird, Stage 3
Range of Frames Used:	13971-14030
Number of Superposed Images:	48
Camera:	Plume
Spectral Band (nanometers):	300-320 (PC-2)
Displayed Image Size (pixels):	72.3 (vertical) x 56.5 (horizontal)
Average Range (km):	553
Pixel Footprint (m) @ Range:	5.53 (vertical) x 7.08 (horizontal)
Aspect Angle (deg):	47.7
*Photoevents/s:	5.95
*Apparent Peak Radiance ($\mu W/sr$-cm^2):	3.70×10^{-1}
*Apparent Peak Spectral Radiance @ 310 nm ($\mu W/sr$-cm^2-μm):	1.81×10^1

*For brightest pixel.

Fig. 38 - Plume-camera contour plot for interval 3

NRL/BENDIX STARBIRD Observation   PC=1 (220-320nm)
Third Stage   44 Superposed Images

NRL/ACT 3/30/92

Observing Sensor:	UVPI (Dec. 18, 1990)
Target Observed:	Starbird, Stage 3
Range of Frames Used:	14147-14200
Number of Superposed Images:	44
Camera:	Plume
Spectral Band (nanometers):	220-320 (PC-1)
Displayed Image Size (pixels):	112 (vertical) x 91 (horizontal)
Average Range (km):	535
Pixel Footprint (m) @ Range:	5.35 (vertical) x 6.85 (horizontal)
Aspect Angle (deg):	51.0
*Total Photoevents/s:	3.36×10^2
*Total Radiant Intensity (W/sr):	1.22×10^1
*Total Spectral Radiant Intensity @ 280 nm (W/sr-μm):	8.131×10^1
*Error (%):	14.4

*For full image.

Fig. 39 - Composite plume-camera image for interval 4

Third Stage (PC=1 220-320nm)

max=0.51uW/sr-cm2

│ =0.095%max │ =0.50%max   │ =0.95%max

NRL/ACT 3/30/92

Observing Sensor:	UVPI (Dec. 18, 1990)
Target Observed:	Starbird, Stage 3
Range of Frames Used:	14147-14200
Number of Superposed Images:	44
Camera:	Plume
Spectral Band (nanometers):	220-320 (PC-1)
Displayed Image Size (pixels):	74.8(vertical) x 58.4(horizontal)
Average Range (km):	535
Pixel Footprint (m) @ Range:	5.35 (vertical) x 6.85 (horizontal)
Aspect Angle (deg):	51.0
*Photoevents/s:	5.19
*Apparent Peak Radiance (μW/sr-cm^2):	5.14×10^{-1}
*Apparent Peak Spectral Radiance @ 280 nm (μW/sr-cm^2-μm):	3.43

*For brightest pixel.

Fig. 40 - Plume-camera contour plot for interval 4

NRL/BENDIX STARBIRD Observation   PC=1 (220-320nm)
Fourth Stage   108 Superposed Images

NRL/ACT 3/30/92

Observing Sensor:	UVPI (Dec. 18, 1990)
Target Observed:	Starbird, Stage 4
Range of Frames Used:	14583-14716
Number of Superposed Images:	108
Camera:	Plume
Spectral Band (nanometers):	220-320 (PC-1)
Displayed Image Size (pixels):	112 (vertical) x 91 (horizontal)
Average Range (km):	499
Pixel Footprint (m) @ Range:	4.99 (vertical) x 6.38 (horizontal)
Aspect Angle (deg):	54.4
*Total Photoevents/s:	4.94×10^2
*Total Radiant Intensity (W/sr):	1.56×10^1
*Total Spectral Radiant Intensity @ 250 nm (W/sr-μm):	1.04×10^2
*Error (%):	11.7

*For full image.

Fig. 41 - Composite plume-camera image for interval 5

Fourth Stage (PC=1 220-320nm)

max=0.75uW/sr-cm2
| =0.095*max | =0.50*max | =0.95*max

NRL/ACI 3/30/92

Observing Sensor:	UVPI (Dec. 18, 1990)
Target Observed:	Starbird, Stage 4
Range of Frames Used:	14583-14716
Number of Superposed Images:	108
Camera:	Plume
Spectral Band (nanometers):	220-320 (PC-1)
Displayed Image Size (pixels):	80.2 (vertical) x 62.7 (horizontal)
Average Range (km):	499
Pixel Footprint (m) @ Range:	4.99 (vertical) x 6.38 (horizontal)
Aspect Angle (deg):	54.4
*Photoevents/s:	7.57
*Apparent Peak Radiance (μW/sr-cm^2):	7.50×10^{-1}
*Apparent Peak Spectral Radiance @ 280 nm (μW/sr-cm^2-μm):	5.00

*For brightest pixel.

Fig. 42 - Plume-camera contour plot for interval 5

NRL/BENDIX STARBIRD Observation
Fourth Stage

PC=2 (300-320nm)
36 Superposed Images

NRL/ACT 3/30/92

Observing Sensor:	UVPI (Dec. 18, 1990)
Target Observed:	Starbird, Stage 4
Range of Frames Used:	14863-14906
Number of Superposed Images:	36
Camera:	Plume
Spectral Band (nanometers):	300-320 (PC-2)
Displayed Image Size (pixels):	112 (vertical) x 91 (horizontal)
Average Range (km):	488
Pixel Footprint (m) @ Range:	4.88 (vertical) x 6.24 (horizontal)
Aspect Angle (deg):	83.7
*Total Photoevents/s:	3.19×10^2
*Total Radiant Intensity (W/sr):	6.04
*Total Spectral Radiant Intensity @ 310 nm (W/sr-μm):	2.96×10^2
*Error (%):	16.8

*For full image.

Fig. 43 - Composite plume-camera image for interval 6

Fourth Stage (PC=2 300-320nm)

max=0.37uW/sr-cm2
| =0.095*max | =0.50*max | =0.95*max

NRL/ACT 3/30/92

Observing Sensor:	UVPI (Dec. 18, 1990)
Target Observed:	Starbird, Stage 4
Range of Frames Used:	14863-14906
Number of Superposed Images:	36
Camera:	Plume
Spectral Band (nanometers):	300-320 (PC-2)
Displayed Image Size (pixels):	82.0 (vertical) x 64.1 (horizontal)
Average Range (km):	488
Pixel Footprint (m) @ Range:	4.88 (vertical) x 6.24 (horizontal)
Aspect Angle (deg):	83.7
*Photoevents/s:	5.93
*Apparent Peak Radiance (μW/sr-cm^2):	3.69x10^{-1}
*Apparent Peak Spectral Radiance @ 310 nm (μW/sr-cm^2-μm):	1.81x10^1

*For brightest pixel.

Fig. 44 - Plume-camera contour plot for interval 6

NRL/BENDIX STARBIRD Observation
Fourth Stage

PC=3 (195-295nm)
153 Superposed Image

NRL/ACT 3/30/92

Observing Sensor:	UVPI (Dec. 18, 1990)
Target Observed:	Starbird, Stage 4
Range of Frames Used:	14963-15165
Number of Superposed Images:	153
Camera:	Plume
Spectral Band (nanometers):	195-295 (PC-3)
Displayed Image Size (pixels):	112 (vertical) x 91 (horizontal)
Average Range (km):	483
Pixel Footprint (m) @ Range:	4.83 (vertical) x 6.18 (horizontal)
Aspect Angle (deg):	91.7
*Total Photoevents/s:	2.21×10^2
*Total Radiant Intensity (W/sr):	8.55
*Total Spectral Radiant Intensity @ 265 nm (W/sr-μm):	8.19×10^1
*Error (%):	11.9

*For full image.

Fig. 45 - Composite plume-camera image for interval 7

Fourth Stage (PC=3 195-295nm)

max=0.32uW/sr-cm2

= 0.095*max   = 0.50*max   = 0.95*max

NRL/ACT 3/30/92

Observing Sensor:	UVPI (Dec. 18, 1990)
Target Observed:	Starbird, Stage 4
Range of Frames Used:	14963-15165
Number of Superposed Images:	153
Camera:	Plume
Spectral Band (nanometers):	195-295 (PC-3)
Displayed Image Size (pixels):	82.8 (vertical) x 64.7 (horizontal)
Average Range (km):	483
Pixel Footprint (m) @ Range:	4.83 (vertical) x 6.18 (horizontal)
Aspect Angle (deg):	91.7
*Photoevents/s:	2.49
*Apparent Peak Radiance (μW/sr-cm^2):	3.24×10^{-1}
*Apparent Peak Spectral Radiance @ 265 nm (μW/sr-cm^2-μm):	3.10

*For brightest pixel.

Fig. 46 - Plume-camera contour plot for interval 7

4.5 Calibrated Tracker Camera Images

While the plume camera gathered rocket plume images, the tracker camera gathered images at a lower rate because of the plume-to-tracker image ratio. The tracker camera's exposure time varied over the data intervals as shown in Table 21.

Table 21 – Tracker Camera Exposure Time

Data Interval	Tracker Camera Exposure Time (ms)
1	8.60
2	12.2
3	12.2
4	12.2
5	15.4
6	15.4
7	15.4

The limiting resolution of the UVPI cameras is described by the point spread function. Observation of the ground-based beacon, a source less than 5 m across, showed that the full-width-half-maximum of the point source response in the tracker camera is about 1.5 pixels, or about 230 μrad. This is equivalent to 104 m at a 450-km range. A tracker-camera contour plot of the ground-based beacon is shown in Fig. 47. This is representative of the tracker-camera's point spread function and can be compared with the interval 3 tracker-camera contour plot shown in Fig. 48. Figure 49 shows a tracker-camera image of the ground-based beacon on the same scale as the Starbird tracker-camera images that follow. The corresponding composite tracker-camera images for each of the seven data intervals are shown in Figs. 50 through 56.

With each picture or plot a companion summary table provides relevant information for the quantitative interpretation of the image or plot. The parameters presented in these tables are described in Table 19. Radiometric values reported in the table accompanying each figure are for the central 19 by 19 pixels of the tracker camera. This field of view approximately matches the total field of view of the plume camera. It contains plume central region and a portion of the outer region. Therefore, it cannot reliably be converted to radiant intensity or spectral radiant intensity. However, to provide estimates of the radiant intensity and spectral radiant intensity, values based on reference spectral energy distribution assumptions are reported for the tracker camera observations. These results have been reduced by 16.3% to account for red leakage in the tracker-camera filter.

Note that the number of images superposed in each data interval can be significantly different. For example, only 8 images were used for interval 6, and 40 were used for interval 1. For each interval, as many images as possible were superposed.

Observing Sensor:	UVPI
Target Observed:	UVPI Ground-Based Beacon
Orbit Number:	1173
Range of Frames Used:	12772-12772
Camera:	Tracker
Displayed Image Size (pixels):	112 (vertical) x 91 (horizontal)
Average Range (km):	450

Fig. 47 - Tracker-camera contour plot for ground-based beacon

Tracker Set=3 255-450nm

max=0.33uW/sr-cm2
| =0.095%max | =0.50%max | =0.95%max

NRL/ACT 6/5/92

Observing Sensor:	UVPI (Dec. 18, 1990)
Target Observed:	Starbird, Stage 3
Range of Frames Used:	13971-14030
Number of Superposed Images:	12
Camera:	Tracker
Spectral Band (nanometers):	255-450
Displayed Image Size (km):	2 (vertical) x 2 (horizontal)
Average Range (km):	553
Pixel Footprint (m) @ Range:	79.6 (vertical) x 99.9 (horizontal)
Aspect Angle (deg):	47.7
*Photoevents/s:	2.00×10^5
*Apparent Peak Radiance ($\mu W/sr$-cm^2):	3.33×10^{-1}
*Apparent Peak Spectral Radiance @ 390 nm ($\mu W/sr$-cm^2-μm):	2.65

*For brightest pixel

Fig. 48 - Tracker-camera contour plot for interval 3

Tracker Camera PSF Estimate

NRL/ACT 8/6/92

Observing Sensor:	UVPI
Target Observed:	UVPI Ground-Based Beacon
Orbit Number:	1173
Range of Frames Used:	12772-12772
Camera:	Tracker
Displayed Image Size (pixels):	112 (vertical) x 91 (horizontal)
Average Range (km):	450

Fig. 49 - Tracker-camera image of ground-based beacon illustrating the point spread function

NRL/BENDIX STARBIRD Observation
Tracker Camera   Set 1

NRL/ACT 6/5/92

Observing Sensor:	UVPI (Dec. 18, 1990)
Target Observed:	Starbird, Stage 3
Range of Frames Used:	13543-13743
Number of Superposed Images:	40
Camera:	Tracker
Spectral Band (nanometers):	255-450
Displayed Image Size (pixels):	112 (vertical) x 91 (horizontal)
Average Range (km):	596
Pixel Footprint (m) @ Range:	85.8 (vertical) x 107.6 (horizontal)
Aspect Angle (deg):	45.6
*Total Photoevents/s:	1.07×10^5
*Total Radiant Intensity (W/sr):	1.63×10^2
*Total Spectral Radiant Intensity @ 390 nm (W/sr-μm):	1.30×10^3
*Error (%):	15.6

*For central 19 x 19 pixels.

Fig. 50 - Composite tracker-camera image for interval 1

NRL/BENDIX STARBIRD Observation
Tracker Camera   Set 2

NRL/ACT 6/5/92

Observing Sensor:	UVPI (Dec. 18, 1990)
Target Observed:	Starbird, Stage 3
Range of Frames Used:	13870-13923
Number of Superposed Images:	11
Camera:	Tracker
Spectral Band (nanometers):	255-450
Displayed Image Size (pixels):	112 (vertical) x 91 (horizontal)
Average Range (km):	565
Pixel Footprint (m) @ Range:	81.3 (vertical) x 102.0 (horizontal)
Aspect Angle (deg):	46.9
*Total Photoevents/s:	1.23×10^5
*Total Radiant Intensity (W/sr):	1.69×10^2
*Total Spectral Radiant Intensity @ 390 nm (W/sr-μm):	1.35×10^3
*Error (%):	At least 15.6

*For central 19 x 19 pixels.

Fig. 51 - Composite tracker-camera image for interval 2

NRL/BENDIX STARBIRD Observation
Tracker Camera   Set 3

NRL/ACT 6/5/92

Observing Sensor:	UVPI (Dec. 18, 1990)
Target Observed:	Starbird, Stage 3
Range of Frames Used:	13971-14030
Number of Superposed Images:	12
Camera:	Tracker
Spectral Band (nanometers):	255-450
Displayed Image Size (pixels):	112 (vertical) x 91 (horizontal)
Average Range (km):	553
Pixel Footprint (m) @ Range:	79.6 (vertical) x 99.9 (horizontal)
Aspect Angle (deg):	47.7
*Total Photoevents/s:	1.26×10^5
*Total Radiant Intensity (W/sr):	1.66×10^2
*Total Spectral Radiant Intensity @ 390 nm (W/sr-μm):	1.32×10^3
*Error (%):	At Least 15.6

*For central 19 x 19 pixels.

Fig. 52 - Composite tracker-camera image for interval 3

NRL/BENDIX STARBIRD Observation
Tracker Camera   Set 4

NRL/ACT 6/5/92

Observing Sensor:	UVPI (Dec. 18, 1990)
Target Observed:	Starbird, Stage 3
Range of Frames Used:	14147-14200
Number of Superposed Images:	10
Camera:	Tracker
Spectral Band (nanometers):	255-450
Displayed Image Size (pixels):	112 (vertical) x 91 (horizontal)
Average Range (km):	535
Pixel Footprint (m) @ Range:	77.0 (vertical) x 96.5 (horizontal)
Aspect Angle (deg):	51.0
*Total Photoevents/s:	8.22×10^4
*Total Radiant Intensity (W/sr):	1.01×10^2
*Total Spectral Radiant Intensity @ 390 nm (W/sr-μm):	8.09×10^2
*Error (%):	At least 15.6

*For central 19 x 19 pixels.

Fig. 53 - Composite tracker-camera image for interval 4

NRL/BENDIX STARBIRD Observation
Tracker Camera   Set 5

NRL/RCT 6/5/92

Observing Sensor:	UVPI (Dec. 18, 1990)
Target Observed:	Starbird, Stage 4
Range of Frames Used:	14583-14716
Number of Superposed Images:	26
Camera:	Tracker
Spectral Band (nanometers):	255-450
Displayed Image Size (pixels):	112 (vertical) x 91 (horizontal)
Average Range (km):	499
Pixel Footprint (m) @ Range:	71.8 (vertical) x 90.0 (horizontal)
Aspect Angle (deg):	54.4
*Total Photoevents/s:	9.89×10^4
*Total Radiant Intensity (W/sr):	1.06×10^2
*Total Spectral Radiant Intensity @ 390 nm (W/sr-μm):	8.46×10^2
*Error (%):	18.3

*For central 19 x 19 pixels.

Fig. 54 - Composite tracker-camera image for interval 5

NRL/BENDIX STARBIRD Observation
Tracker Camera   Set 6

NRL/ACT 6/5/92

Observing Sensor:	UVPI (Dec. 18, 1990)
Target Observed:	Starbird, Stage 4
Range of Frames Used:	14863-14906
Number of Superposed Images:	8
Camera:	Tracker
Spectral Band (nanometers):	255-450
Displayed Image Size (pixels):	112 (vertical) x 91 (horizontal)
Average Range (km):	488
Pixel Footprint (m) @ Range:	70.2 (vertical) x 88.0 (horizontal)
Aspect Angle (deg):	83.7
*Total Photoevents/s:	1.30×10^5
*Total Radiant Intensity (W/sr):	1.34×10^2
*Total Spectral Radiant Intensity @ 390 nm (W/sr-μm):	1.07×10^3
*Error (%):	At least 15.6

*For central 19 x 19 pixels.

Fig. 55 - Composite tracker-camera image for interval 6

NRL/BENDIX STARBIRD Observation
Tracker Camera   Set 7

NRL/ACT 6/5/92

Observing Sensor:	UVPI (Dec. 18, 1990)
Target Observed:	Starbird, Stage 4
Range of Frames Used:	14963-15165
Number of Superposed Images:	38
Camera:	Tracker
Spectral Band (nanometers):	255-450
Displayed Image Size (pixels):	112 (vertical) x 91 (horizontal)
Average Range (km):	483
Pixel Footprint (m) @ Range:	69.4 (vertical) x 87.1 (horizontal)
Aspect Angle (deg):	91.7
*Total Photoevents/s:	1.59×10^5
*Total Radiant Intensity (W/sr):	1.60×10^2
*Total Spectral Radiant Intensity @ 390 nm (W/sr-µm):	1.28×10^3
*Error (%):	15.6

*For central 19 x 19 pixels.

Fig. 56 - Composite tracker-camera image for interval 7

4.6 Error Analysis for Radiometric Observations

The complete estimate of the error in determining radiometric values from the digital numbers reported by the UVPI cameras observing a rocket plume is composed of two components: measurement noise, summarized in 4.6.1, which includes photon shot noise and other intrinsic sensor noise sources; and calibration error, summarized in 4.6.2, which is the error contained in the gain conversion factor. Section 4.6.3 summarizes the calculation of the total error based on the error components presented in 4.6.1 and 4.6.2. Detailed discussions of error estimates are found in Ref. 1.

4.6.1 *Error Due to Measurement Noise*

As a result of photon shot noise, the error in the calculated number of photoevents changes as a function of the plume radiant intensity, which could change as a function of time. This error analysis assumes that the radiant intensity statistics are not affected by a small shift in time. A window size of 15 consecutive images was selected for the statistical analysis of the plume-camera data, and a window of 9 consecutive images was selected for the tracker-camera analysis. A larger time window could be used but with the risk of making the locally constant assumption invalid.

Given the number of photoevents as a function of image, the following quantities are defined:

M is number of images in data interval,
N is number of images used within the window,
μ_i is local mean over N images around ith image,
σ_i is local standard deviation around ith image,
t_i is $3.1 \, \sigma_i + \mu_i$, detection threshold,
ε_i is σ_i / μ_i, local error around the ith image,
G_g is gain conversion factor for gain step g, in units of sensor output per photoevent,
$\varepsilon_{1/G}$ is error in $1/G_g$,
ε_N is average local error in the measured number,

$$\varepsilon_N = \frac{1}{M} \Sigma_i \left(\frac{\sigma_i}{\mu_i} \right),$$

(16)

ε_μ is upper bound error in the measured number for the case of M averaged images,

$$\varepsilon_\mu = \frac{\max(\varepsilon_i)}{\sqrt{M}}, \quad \text{over all } i.$$

(17)

To prevent extreme values from affecting the local statistics, the maximum and minimum values within the N window samples were rejected. That is, only N-2 images were used for the local mean and local standard deviation computation. Under the assumption that the mean radiant intensity is high enough for the radiant intensity fluctuations to be modeled by a gaussian distribution, the probability of exceeding the threshold t_i, is no more than 0.001.

Table 22 lists M, the number of images averaged in each data interval, and ε_N, the error due to measurement in the values averaged over the window that consists of N images. There are three columns of ε_N values corresponding to plume-camera central region measurements, plume camera central region plus outer region, and tracker-camera 19 by 19 pixel field of view. The 19 by 19 tracker camera pixels approximately cover the full field of view of the plume camera. The central region and outer region as used in this report are defined in Section 5.1. Note that four of the tracker camera intervals had too few frames to calculate ε_N.

Table 22 – Percent Error per Image Due to Measurement Noise, ε_N

Interval	Images (M)	Plume-Camera Central Region	Plume-Camera Central Region + Outer Region	Tracker Camera 19 x 19
1	157	12.9	14.0	5.8
2	41	48.0	40.9	–
3	48	45.9	45.7	–
4	44	44.8	41.7	–
5	108	42.6	38.6	4.3
6	36	47.1	26.9	–
7	153	60.8	53.5	5.0

4.6.2 *Error in Gain Conversion Factor*

The gain conversion factor G_g, derived from on-orbit calibration as discussed in the methodology report [1], is based on calibration star measurements. On the basis of measurements of several calibration stars over the full set of UVPI camera gains, an estimate of error associated with G_g can be obtained for each camera configuration. This can be done by calculating the deviations of individual calibration star measurements about a mean value for average and maximum deviation from the calibration curve.

Table 23 tabulates the error associated with the gain conversion factor for the plume and tracker cameras. The average deviation is a good error estimate; the maximum deviation gives a worst-case estimate.

Table 23 - Error in $1/G_g$ for Tracker and Plume Cameras

Camera/Filter	Average Deviation from Mean Calibration Curve	Maximum Deviation from Mean Calibration Curve
Tracker	15.6%	17.3%
Plume, PC-1	10.5%	33.3%
Plume, PC-2	15.9%	25.2%
Plume, PC-3	9.9%	24.7%
Plume, PC-4	13.5%	26.0%

4.6.3 *Calculation of Total Error*

The estimated total calibration error depends on the number of images averaged together, M. In this report we define the total error as the ratio of the standard deviations of the number of photoevents to the mean value of the number of photoevents. Assuming that the digital number reported by UVPI for a calibration star and the gain conversion factor G_g are uncorrelated, or weakly correlated, then the total error per image ε_F can be obtained from the relation [15]:

$$\varepsilon_F = \sqrt{\varepsilon_N{}^2 \bullet \varepsilon_{1/G}{}^2 + \varepsilon_N{}^2 + \varepsilon_{1/G}{}^2} , \tag{18}$$

where ε_N is the average local error in the number of measured photoevents presented in Table 22 and $\varepsilon_{1/G}$ is the error in the gain conversion factor tabulated in Table 23.

For the case of M averaged images, an upper bound estimate of the total error is given by

$$\varepsilon_T = \sqrt{\varepsilon_\mu^2 \cdot \varepsilon_{1/G}^2 + \varepsilon_\mu^2 + \varepsilon_{1/G}^2} \, . \tag{19}$$

Notice that ε_T can never be smaller than $\varepsilon_{1/G}$ no matter how many images are averaged together.

Table 24 summarizes the overall error analysis results for the plume central region radiant intensities for each of the data intervals. The first column identifies the data interval. The second column contains the number of images within the data interval. The column under the K heading contains the ratio of the average standard deviation of photoevents to the square root of the average number of photoevents, i.e.,

$$K = \frac{1}{N} \Sigma_i \left(\frac{\sigma_i}{\sqrt{\mu_i}} \right). \tag{20}$$

Under the assumption that the signal is not changing rapidly in time, K relates the measured noise to the theoretical performance of a background-limited system, where the dominant source of noise is shot noise. A ratio of $K=1$ implies pure background-limited performance. Hence, the values obtained indicate that although UVPI is close to background-limited performance, other sources of sensor noise are present.

Table 24 - Plume Central Region Radiometric Percent Errors for Plume Camera

Interval	M	K	ε_F	ε_T
1	157	1.38	18.7	13.6
2	41	1.03	49.2	15.3
3	48	1.14	49.1	16.1
4	44	1.40	46.3	14.4
5	108	1.48	44.1	12.0
6	36	1.07	50.2	18.9
7	153	1.26	61.9	13.2

The fourth and fifth columns show, respectively, the total percent error on an image-by-image basis and the total percent error resulting after averaging all M images available within the appropriate data interval.

Similar to Table 24, Tables 25 and 26 show, respectively, the radiant intensity errors for the total plume camera field of view and those for the 19 by 19 tracker camera pixels that overlay the plume-camera field of view.

For those intervals in which there were too few frames to calculate K and ε_F, the gain conversion factor error $\varepsilon_{1/G}$, is given as a lower bound for ε_T.

Table 27 lists ε_T for each of the seven data intervals for the plume camera observing the central region only, the plume camera observing the central region and the outer region, and the 19 by 19 pixel field in the tracker camera that corresponds to the full plume camera field of view.

Table 25 – Central Region Plus Outer Region Radiometric Percent Errors for Plume Camera

Interval	M	K	ε_F	ε_T
1	157	1.67	19.5	13.6
2	41	1.00	42.3	13.2
3	48	1.61	48.9	16.2
4	44	1.42	43.2	14.4
5	108	1.53	40.2	11.7
6	36	0.88	31.6	16.8
7	153	1.37	54.7	11.9

Table 26 – Radiometric Percent Errors: Tracker Camera Over 19 x 19 Pixel Window

Interval	M	K^*	ε_F^*	ε_T^*
1	40	1.9	16.7	15.6
2	11	–	–	$\geq$15.6
3	12	–	–	$\geq$15.6
4	10	–	–	$\geq$15.6
5	26	1.8	16.2	18.3
6	8	–	–	$\geq$15.6
7	38	2.7	16.4	15.6

*Not redleak corrected

Table 27 – Total Radiometric Percent Errors, ε_T

Interval	Plume Camera Central Region	Plume Camera Central Region + Outer Region	Tracker Camera 19 x 19*
1	13.6	13.6	15.6
2	15.3	13.2	$\geq$15.6
3	16.1	16.2	$\geq$15.6
4	14.4	14.4	$\geq$15.6
5	12.0	11.7	18.3
6	18.9	16.8	$\geq$15.6
7	13.2	11.9	15.6

*Not redleak corrected

4.7 Noise Equivalent Radiance

Following the noise equivalent radiance (NER) definition given in the *Infrared Handbook* [16], the UVPI NER is defined as the source radiance level that will result in a signal-to-noise ratio of 1 at the output of a single pixel. The NER can be interpreted as the sensitivity limit for an imaging system. For UVPI, a single NER number does not fully characterize the sensitivity of the system since this is a function of integration time, spectral filter, camera gain level, number of images superposed, and the assumed source spectrum.

The following discussion is based on empirical estimates of the signal and noise within the UVPI cameras as opposed to a theoretical discussion. Reference 17 provides theoretical expression for the signal power to noise power ratio that is applicable to the microchannel plate image intensifier

of the UVPI. A single pixel in the plume or tracker camera can be treated as a photoevent counting device. The signal-to-noise ratio (SNR) definition from which the empirical UVPI NER is derived is

$$(SNR)^2 = \frac{M^2 \bullet S^2}{\left(M \bullet N^2 + M \bullet N_s^2\right)} \tag{21}$$

where:

M is the number of images superposed. This affects the effective integration time.

S is the mean number of signal-related photoevents collected in a pixel during the integration time.

N is the signal-independent noise standard deviation for a single pixel in a single image expressed in photoevents/pixel-image. This noise source is constant. When expressed in photoevents/pixel-image, its level depends on the camera gain setting used.

N_s is the signal-dependent photon shot noise standard deviation, in a pixel during the integration time, expressed in photoevents/pixel-image. Based on extensive measurements made on UVPI data, the signal-dependent noise can be expressed in terms of the mean number of signal-related photoevents by using the equation:

$$N_s = 2S^{1/2}. \tag{22}$$

Note that this is two times higher than the photon shot noise prediction.

From the SNR expression above, the mean number of signal-related photoevents/pixel-image in a pixel that will result in a SNR of 1 is

$$S' = \frac{2\left[1+\left(1+M \bullet N^2/4\right)^{1/2}\right]}{M}. \tag{23}$$

Notice that for the case of only one superposed image, $M=1$, and a negligible level of sensor noise N, the resulting sensitivity limit is 4 photoevents/pixel-image. The NER is related to S' by a multiplicative constant K, i.e.,

$$NER = K \bullet S' = \frac{2K\left[1+\left(1+M \bullet N^2/4\right)^{1/2}\right]}{M}, \tag{24}$$

where K is the radiometric calibration constant that converts from photoevents/pixel-image to $\mu W/sr$-cm^2. K is a function of the spectral filter used, the single image exposure time, and the assumed source spectrum.

The radiometric sensitivity could also be improved by performing spatial averaging but at the expense of a lower spatial resolution.

Table 28 summarizes the estimated NERs, or sensitivity levels, for the seven data intervals for the plume camera under the assumption of the reference spectrum. Since, for the plume camera, the signal-independent noise is negligible compared to the signal-dependent noise, image superposition provided an increase in sensitivity that is linear with the number of superposed images.

Table 28 – Plume Camera NER Per Pixel for Data Intervals

Data Interval	Stage	Filter	UVPI Gain Step	NER for Single Image (W/sr-cm^2)	No. of Images Superposed	NER for Data Interval (W/sr-cm^2)
1	3	PC-4	11	2.3×10^{-6}	157	1.5×10^{-8}
2	3	PC-3	13	1.6×10^{-5}	41	4.0×10^{-7}
3	3	PC-2	13	7.8×10^{-6}	48	1.6×10^{-7}
4	3	PC-1	13	1.2×10^{-5}	44	2.8×10^{-7}
5	4	PC-1	13	1.2×10^{-5}	108	1.2×10^{-7}
6	4	PC-2	12	7.8×10^{-6}	36	2.2×10^{-7}
7	4	PC-3	13	1.6×10^{-5}	153	1.1×10^{-7}

Table 29 summarizes the estimated NERs, or sensitivity levels, for the seven data intervals for the tracker camera under the assumption of the reference spectrum. The last column expresses the sensitivity level in photoevents/s. As opposed to the plume camera, in the tracker camera the signal-independent noise is not negligible, and the improvement in sensitivity is not linear with the number of images superposed.

Table 29 – Tracker Camera NER Per Pixel for Data Intervals

Data Interval	Stage	NER for Single Image (W/sr-cm^2)*	No. of Images Superposed	UVPI Gain Step	NER for Data Interval (W/sr- cm^2)*	Minimum Detectable No. of Photoevents/s for Superposed Images*
1	3	8.5×10^{-9}	40	9	5.2×10^{-10}	31.3
2	3	7.2×10^{-9}	11	8	1.4×10^{-9}	81.8
3	3	7.2×10^{-9}	12	8	1.3×10^{-9}	77.5
4	3	7.2×10^{-9}	10	8	1.4×10^{-9}	86.7
5	4	8.7×10^{-9}	26	7	1.3×10^{-9}	78.7
6	4	8.7×10^{-9}	8	7	2.5×10^{-9}	150
7	4	8.7×10^{-9}	38	7	1.1×10^{-9}	64.3

*Not redleak corrected

5.0 SPATIAL FEATURES

This section concentrates on the spatial characterization of the measured plumes. First, definitions for the plume central region and outer region are presented. Second, the plume's spatial extent is discussed with consideration for the UVPI's point spread function (PSF). Finally, the observed plume is compared to the CHARM 1.3 model predictions.

5.1 Delineation of Plume Central and Outer Regions

Because of the generally low signal statistics in a single image, the plume central or outer region cannot be accurately delineated from a single image. Hence, an average of superposed images (a composite image) is used to define the plume central region extent for each of the seven intervals.

Definition of the central region was begun by selecting all pixels in the composite image for which the radiance was at least 25% of the brightest pixel radiance. The resulting region was expanded further by performing a dilation with a square window of 5 by 5 pixels. Using this criterion, the region defining the plume central region is depicted in Figs. 57 and 58. The images on the left are the composite images, and in the images on the right, the corresponding central region is

overlaid as a completely white region. Figure 57 shows the four intervals for the Starbird third-stage burn; Fig. 58 shows the three intervals for the Starbird fourth stage burn.

Table 30 summarizes the central region extent in pixels for each of the seven data intervals considered.

Table 30 – Central Region Extent in Plume Camera

Interval	Stage	Filter	Central Region Extent (pixels)	Central Region Extent (m^2)
1	3	PC-4	203	9232
2	3	PC-3	196	8004
3	3	PC-2	150	5875
4	3	PC-1	245	8973
5	4	PC-1	205	6523
6	4	PC-2	173	5263
7	4	PC-3	228	6796

For the tracker camera, the central region was defined as all those pixels that overlap the plume-camera field of view. Hence, in this report, the central region for the tracker camera is not defined over the same area as for the plume camera.

From the point of view of phenomenology, an argument can be made that the central region definition above does not fully contain the plume core. To validate the definition of the plume central region, additional consecutive dilation operations were performed to force the defined central region to become larger. As an example, Fig. 59 shows the number of photoevents per image in the central and outer regions as a function of central region size for the Starbird third stage for data interval 1. A vertical dashed line illustrates the central region size used in this report. This plot can be used to scale the results presented in the report if a different central region size is desired.

Although these figures show that the outer region contributes somewhat to the total signal measured during each interval, the composite images clearly show that the outer region signal is not localized to the area behind the rocket. For this reason, it is concluded that the outer region component of the total signal is not attributable to plume-induced far-field emissions and that central region results most accurately represent the true plume radiance.

5.2 Plume Extent and Point Spread Function

The effective UVPI point spread function (PSF) is defined as the response of the instrument to a point source, e.g., a star or a ground-based beacon. An understanding of the UVPI plume camera's PSF is critical in establishing the maximum size of the observed Starbird third- and fourth-stage plumes. Table 31 summarizes the estimated plume central region axial length, as defined from peak to either 50% or 10% of peak brightness, for each data interval. These plume length estimates do not incorporate corrections for the aspect angle or for the plume camera's PSF.

PC 4

PC 3

PC 2

PC 1
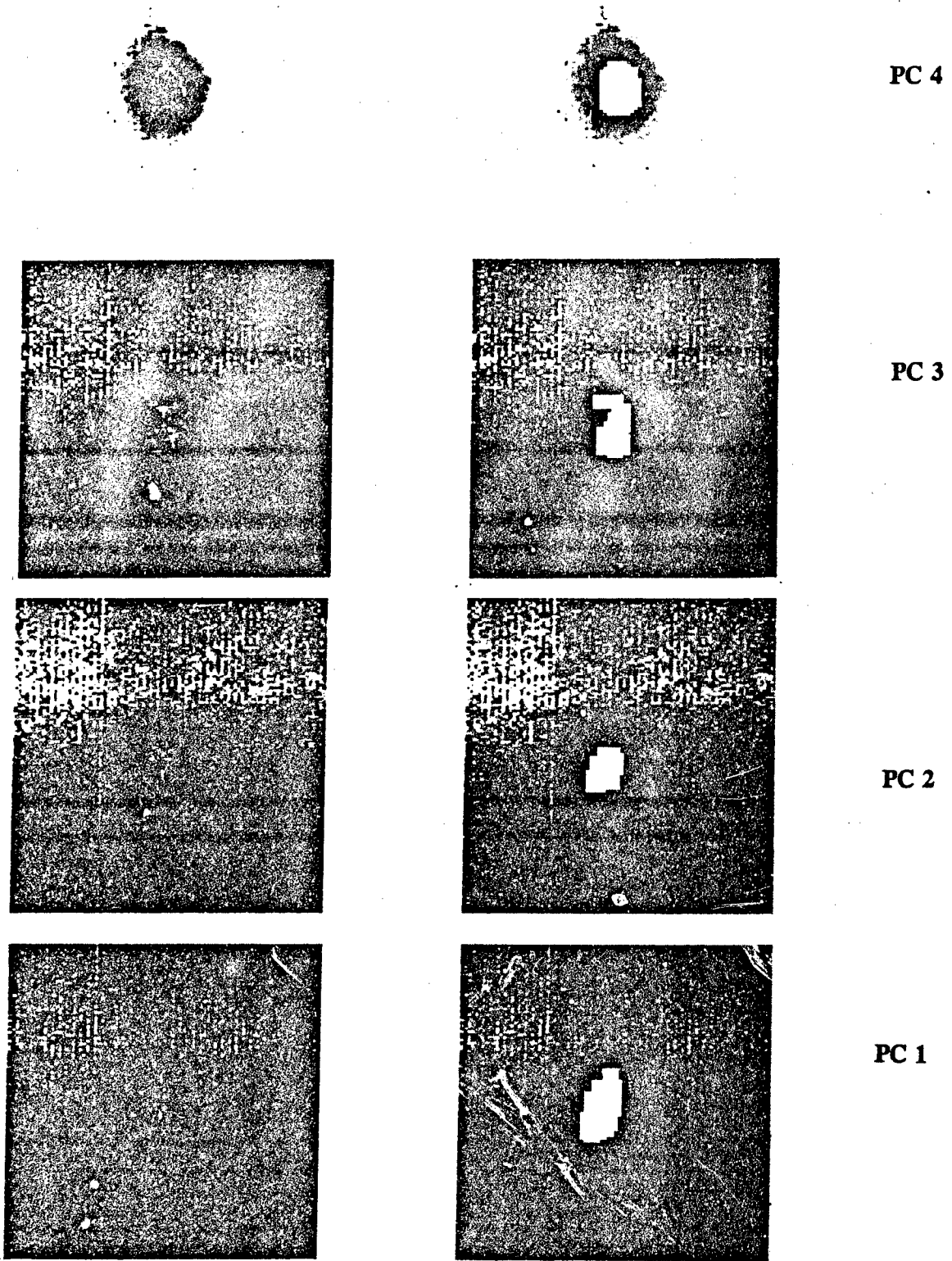
Fig. 57 - Highlighted plume central regions for Starbird third stage

PC 1

PC 2

PC 3
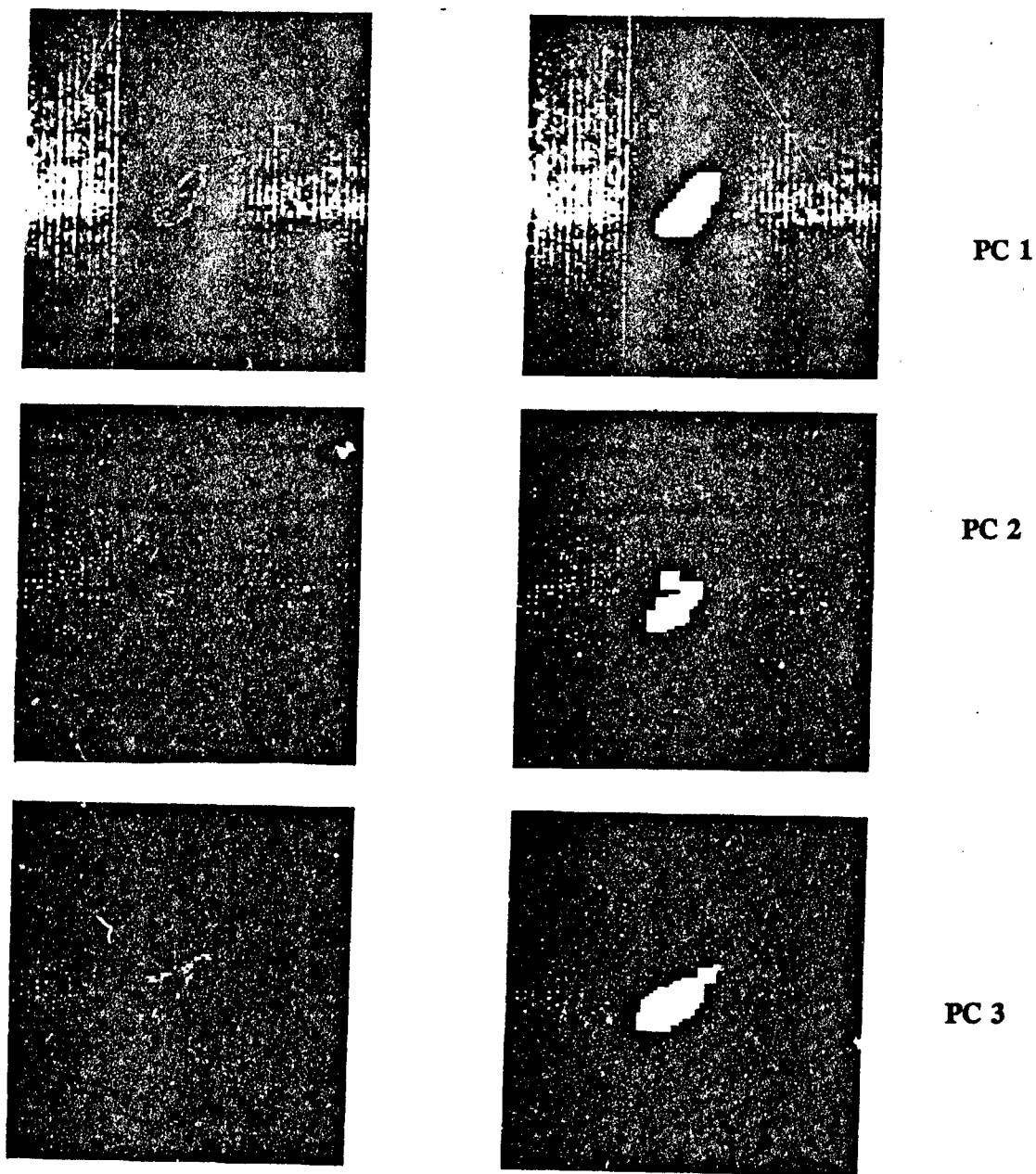
Fig. 58 - Highlighted plume central regions for Starbird fourth stage
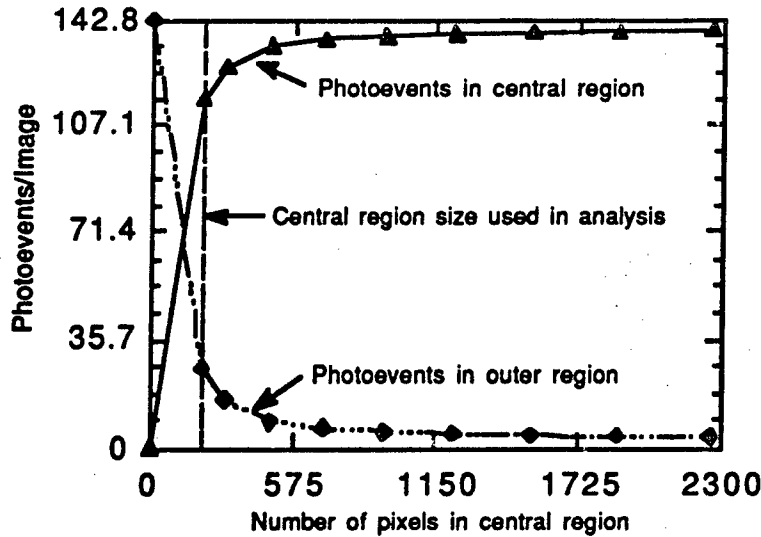
Fig. 59 - Photoevents as a function of defined central region size, Starbird third stage, interval 1

Table 31 - Observed Axial Length of Plume Central Region

Interval	Stage	Filter	Peak to 50% Maximum (m)	Peak to 10% Maximum (m)
1	3	PC-4	54	108
2	3	PC-3	22	116
3	3	PC-2	14	78
4	3	PC-1	7	96
5	4	PC-1	32	83
6	4	PC-2	13	50
7	4	PC-3	31	89

Based on review of UVPI data from many observations, one may conclude that the plume camera's PSF depends on the observation modality, i.e., downward looking vs sideward looking. Sideward-looking observations use the door-mounted mirror but downward-looking do not. The observation of the Starbird third- and fourth- stage plumes did not use the door-mounted mirror. The existing data for point sources indicate that the PSF is less circularly symmetric when using the door-mounted mirror. This could be the result of jitter in the door mirror.

Figure 61 shows a plume-camera image of a ground-based beacon. Reference 1 gives a scaled version of the plume camera's PSF for the beacon. Figure 60 shows a three-dimensional plot of the PSF that results from observation of the ground-based beacon. For the ground-based beacon, the axial length of the PSF from peak to 50% of the peak along the major axis is about 4 pixels, or 20 meters at a range of 450 km, as shown in Fig. 61. The full-width-half-maximum length is about 40 m.

Figures 62 through 68 show profiles of the radiance along the major axis of the plume, as measured by the plume camera, for each of the data intervals. The horizontal line in each figure corresponds to the NER sensitivity limit after image superposition. It is evident from these figures that, after image superposition, a good SNR was achieved for intervals 1, 3, 5, and 7. The SNR for intervals 2, 4, and 6 was marginal.

Figure 69 shows a tracker-camera image of a ground-based beacon. Reference 1 gives a scaled version of the tracker camera's PSF for the beacon. Figure 69 shows a three-dimensional plot of the PSF that results from observation of the ground-based beacon; Fig. 70 is an axial profile of the beacon as seen by the tracker camera.
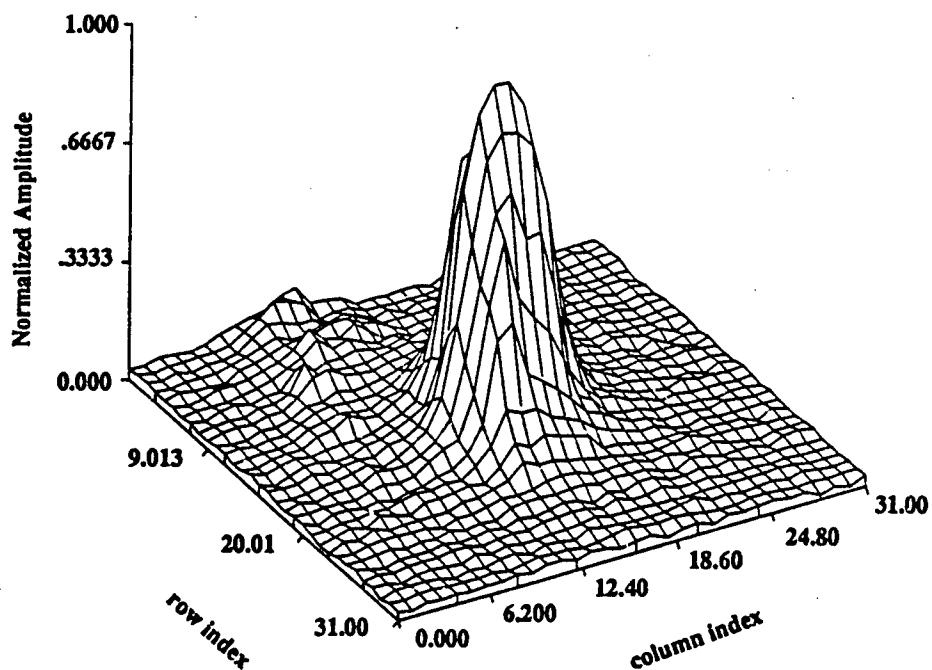
Fig. 60 - Plume-camera PSF for ground-based beacon
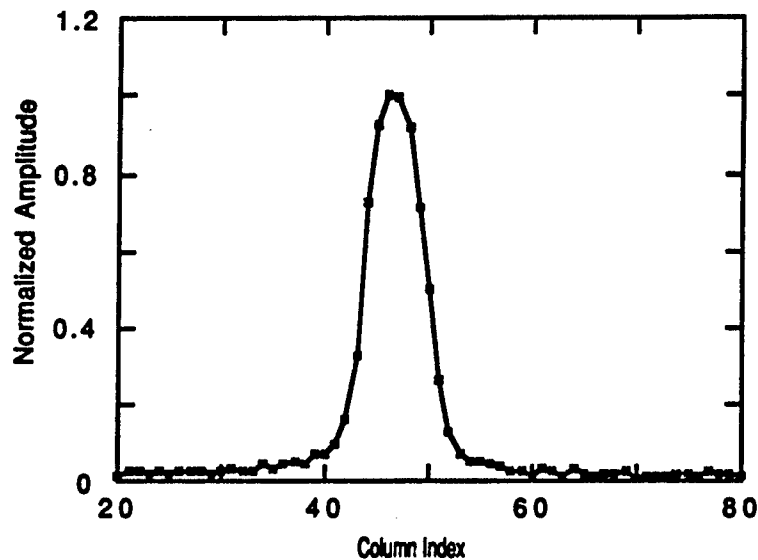
Fig. 61 - Axial profile through plume-camera PSF for ground-based beacon
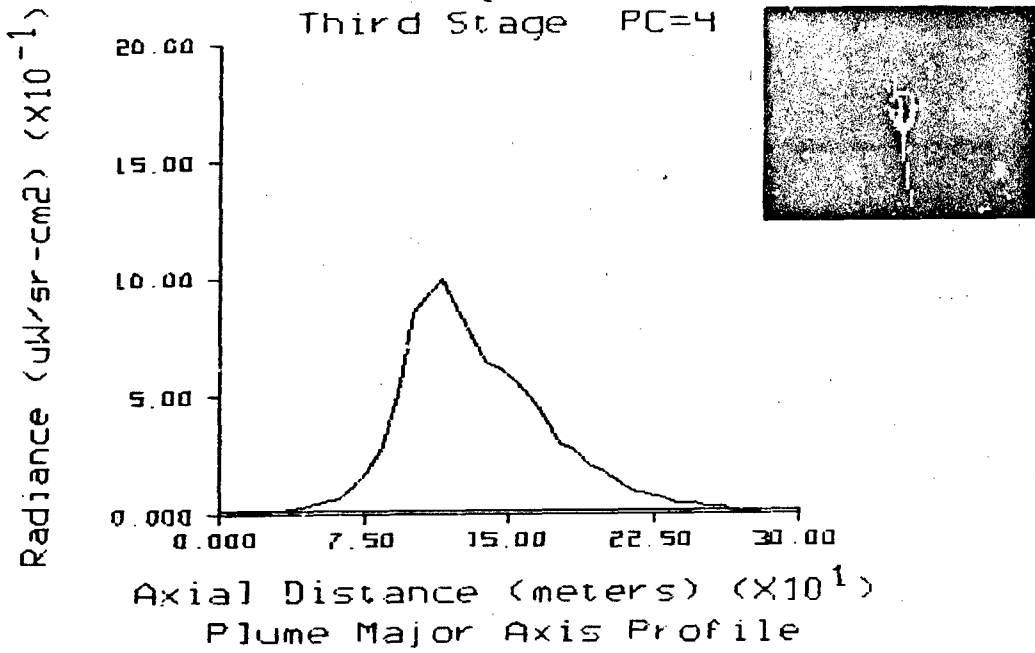
Fig. 62 - Axial profile along plume central region for data interval 1, plume camera
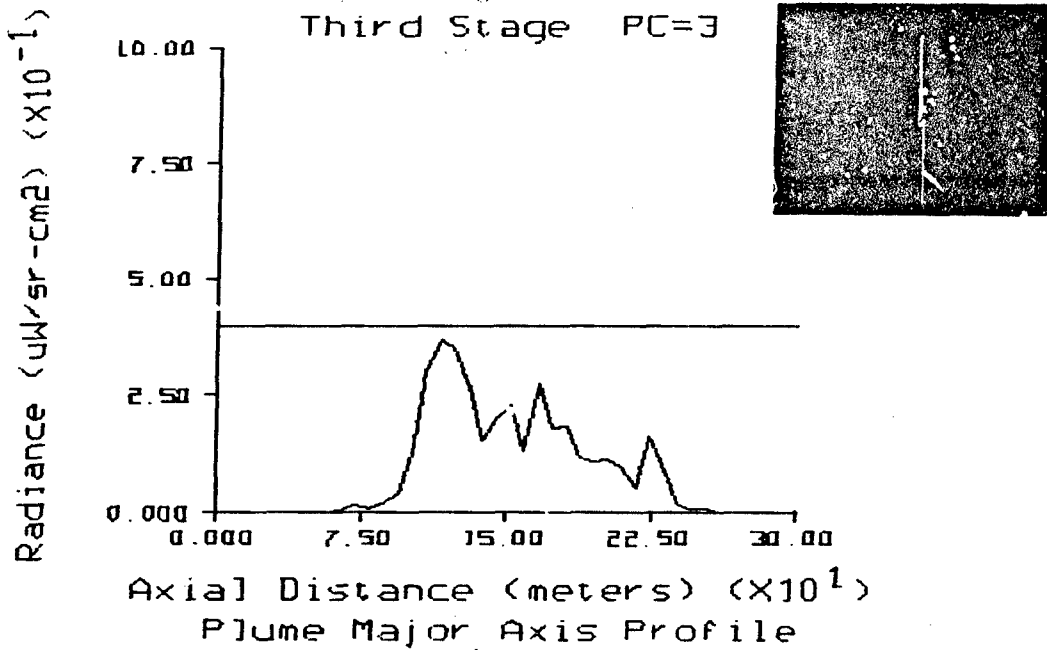
Fig. 63 - Axial profile along plume central region for data interval 2, plume camera
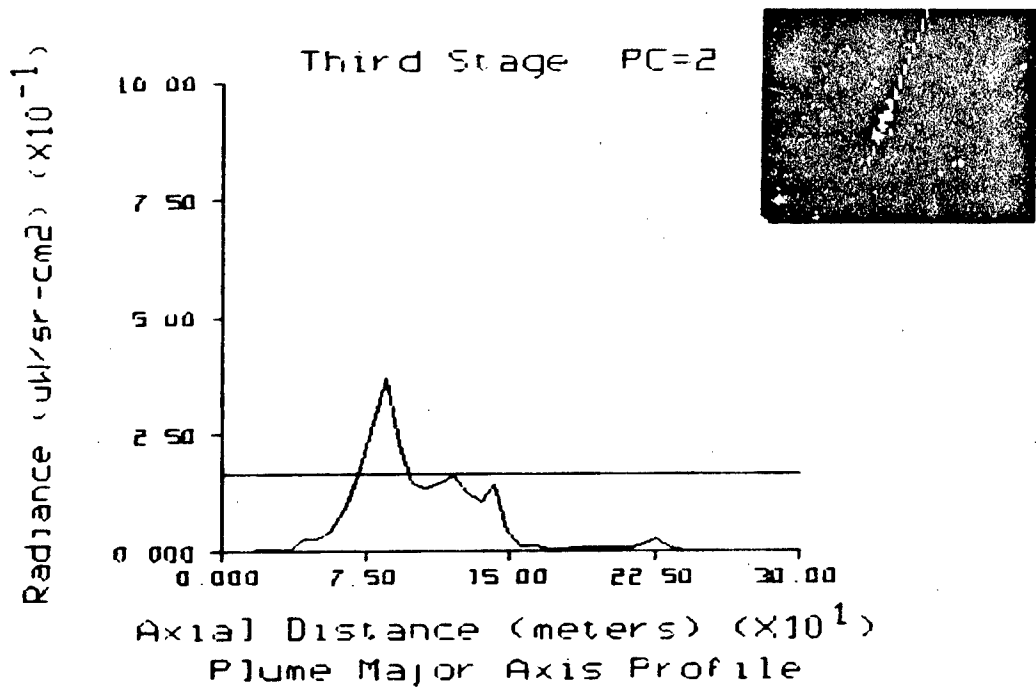
Fig. 64 - Axial profile along plume central region for data interval 3, plume camera
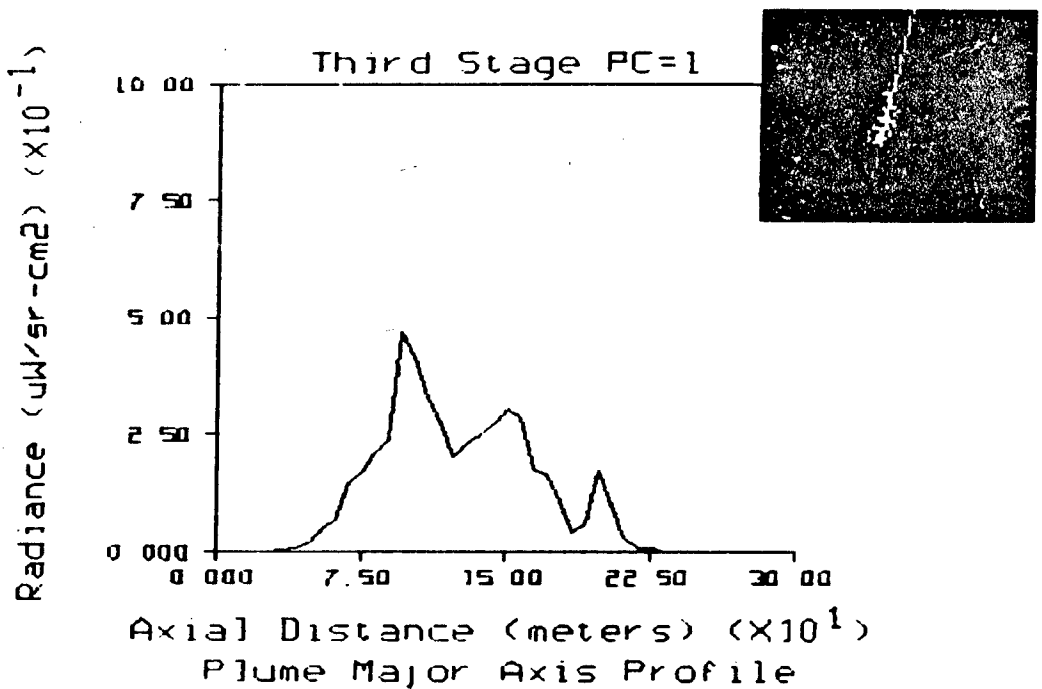
Fig. 65 - Axial profile along plume central region for data interval 4, plume camera
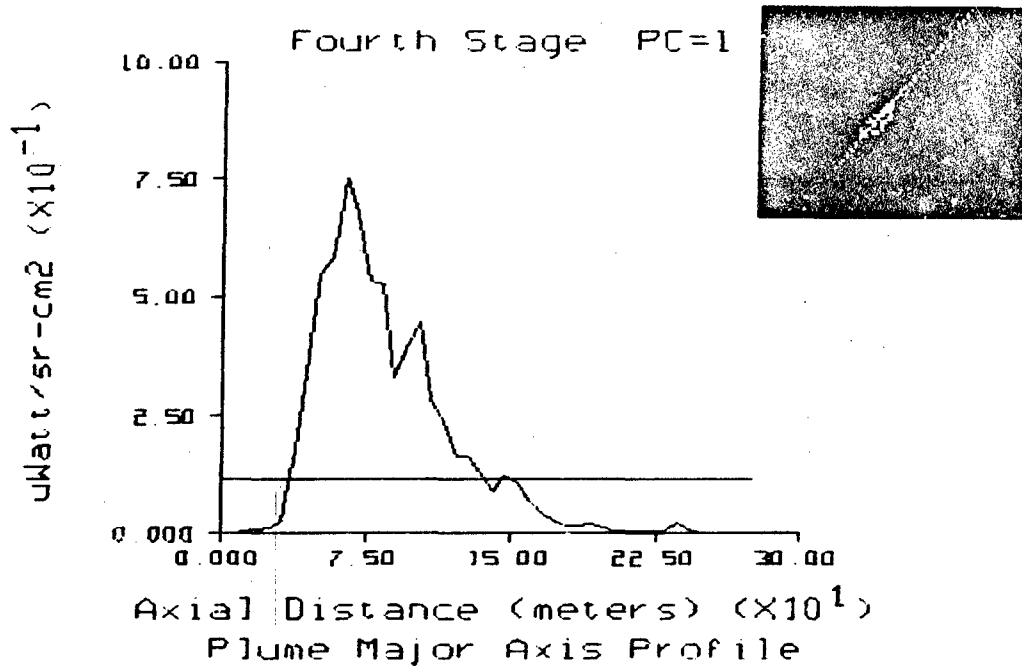
Fig. 66 - Axial profile along plume central region for data interval 5, plume camera
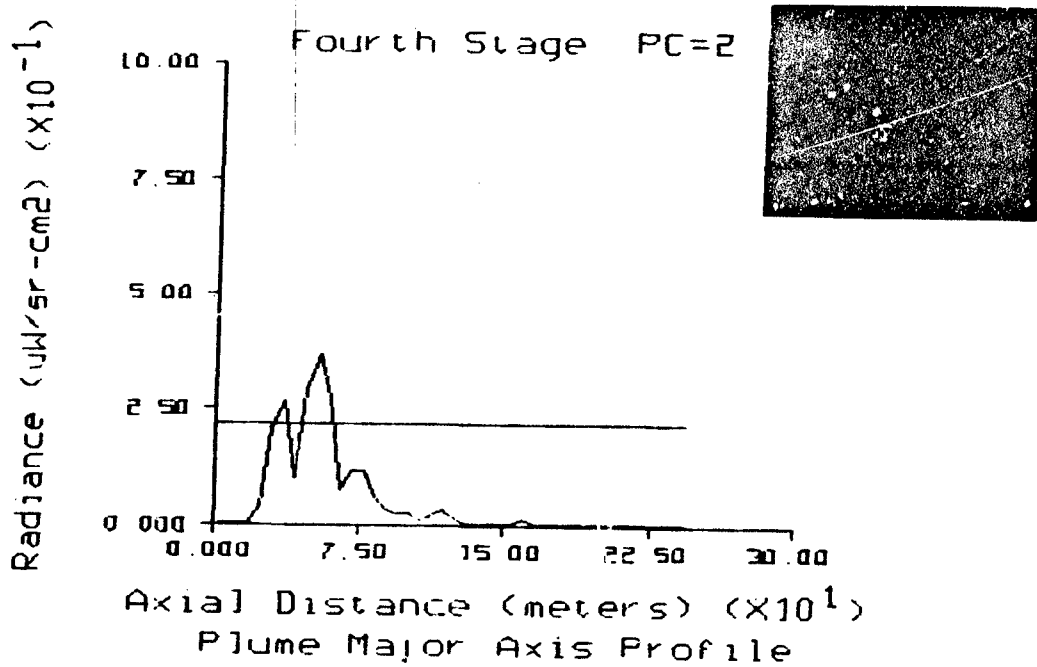
Fig. 67 - Axial profile along plume central region for data interval 6, plume camera
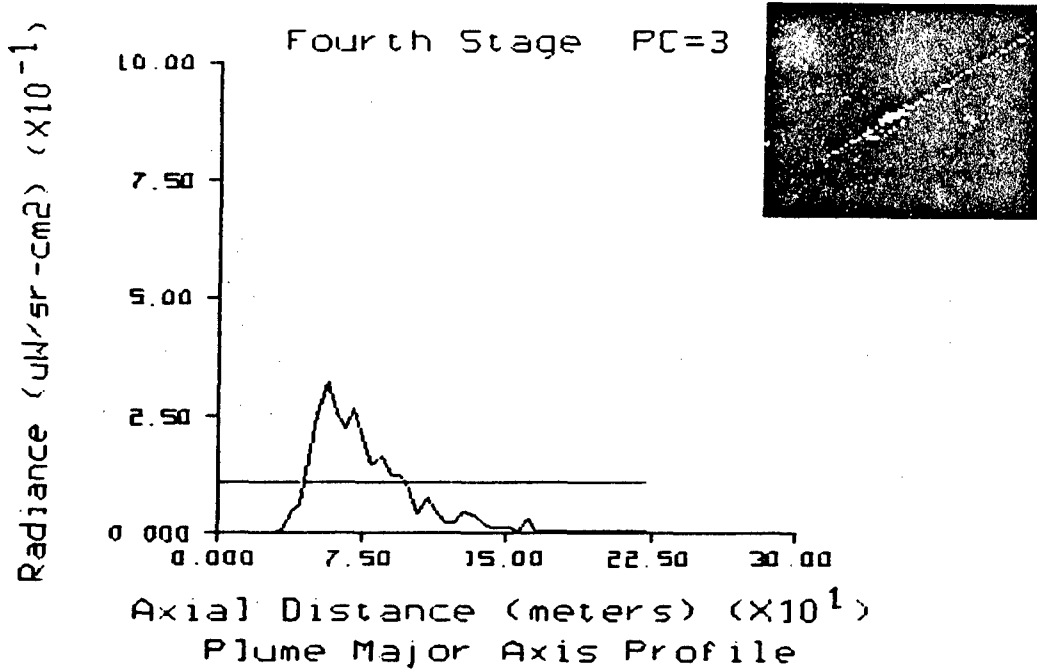
Fig. 68 - Axial profile along plume central region for data interval 7, plume camera
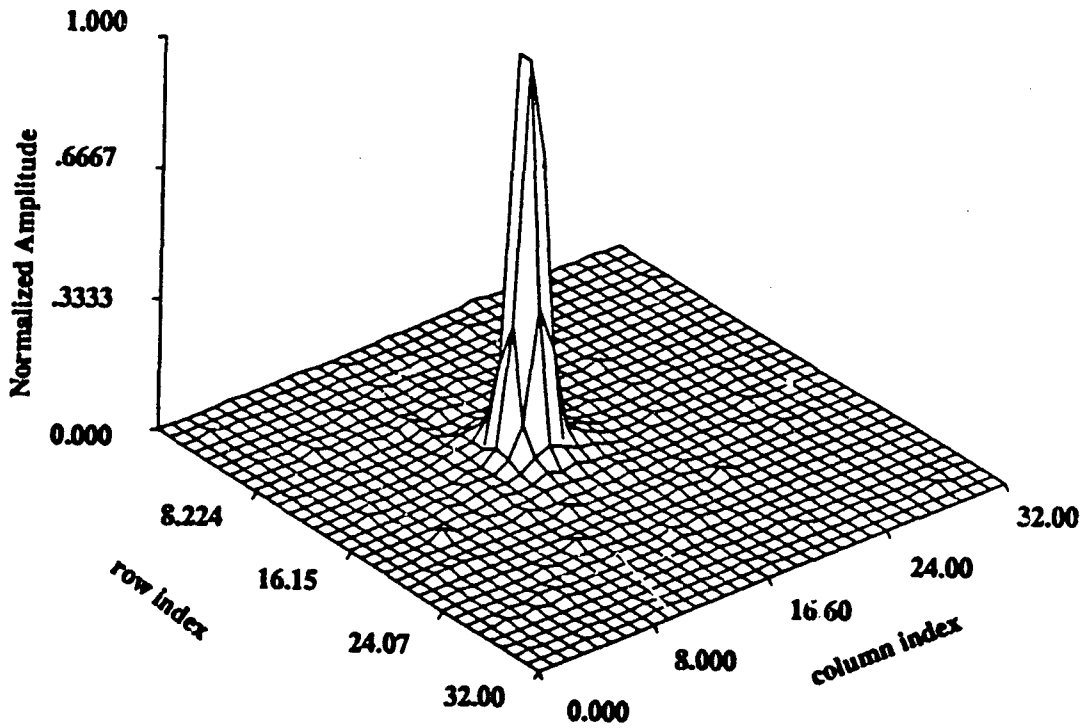
Fig. 69 - Tracker camera PSF for ground-based beacon
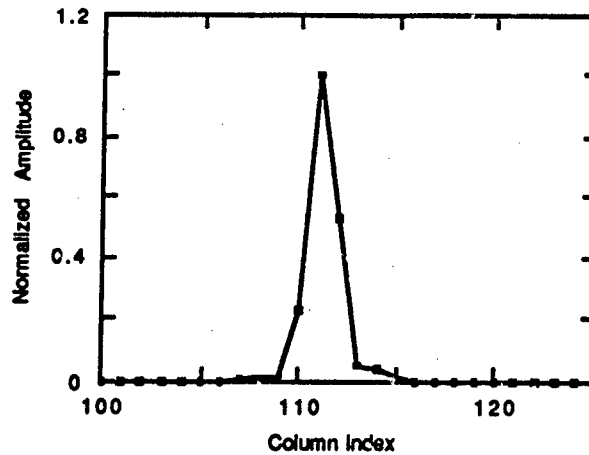
Fig. 70 - Axial profile through tracker camera PSF for ground-based beacon

5.3 Comparison of Results to CHARM 1.3 Predictions

This subsection compares the UVPI measurements to the predictions provided by a theoretical plume model. Grumman Corp. generated a number of CHARM 1.3 runs in which both the Starbird third and fourth stages were modeled [18], using each of the UVPI's plume-camera filter bandpasses. The following parameters were common to all the runs:

Model: CHARM 1.3
Object modeled: Intrinsic core
Aspect for seven data intervals: 45.6, 46.8, 47.7, 50.9, 54.4, 83.7, 91.7
Horizontal resolution: 5.0 m
Vertical resolution: 5.0 m

In all of Grumman's runs, a 5 by 5 m pixel resolution was used. To get a comparison between the CHARM 1.3 predictions and the UVPI measurement, the CHARM 1.3 predictions were convolved with an estimate of the UVPI's PSF. A normalized version of the ground beacon image, Frame 12778, Orbit 1173, was used as the best UVPI plume-camera PSF estimate.

Figures 71 and 72 are examples of the CHARM 1.3 prediction convolved with the UVPI PSF. The left image in Fig. 71 shows a false-color CHARM 1.3 image prediction with 5-m resolution for an Orbus motor, assuming it is being observed with PC-4. The right image shows the same CHARM 1.3 prediction, except that it is convolved with the UVPI PSF. Figure 72 is the corresponding contour plot for the image prediction, again assuming UVPI PC-4 and convolution with UVPI PSF. The CHARM 1.3 plume predictions and contour plots for the other UVPI filter positions are qualitatively similar to those shown in Figs. 71 and 72.

For each of the seven data intervals, Figs. 73-79 show: (a) the CHARM 1.3 high-resolution prediction of the plume radiance as a function of axial distance, (b) the CHARM 1.3 prediction convolved with the UVPI plume-camera PSF, and (c) a horizontal line depicting the interval noise equivalent radiance (NER) of the plume camera.

The peak radiances and the plume lengths for the CHARM 1.3 image predictions are listed in Tables 32 and 33. These tables list computed results for both the Starbird third and fourth stages and for UVPI filters used for the observation of these stages.

Plume Prediction Using PC-4

CHARM1.3 Prediction
Using 5 Meter Resolution

CHARM 1.3 Prediction
Using UVPI's PSF

max=22 uW/sr-cm2

| =0.095*max | =0.50*max | =0.95*max

NRL/ACT 6/15/92

Fig. 71 - CHARM 1.3 image prediction before and after smearing for PC-4

Column Axis(meters) $(\times 10^1)$
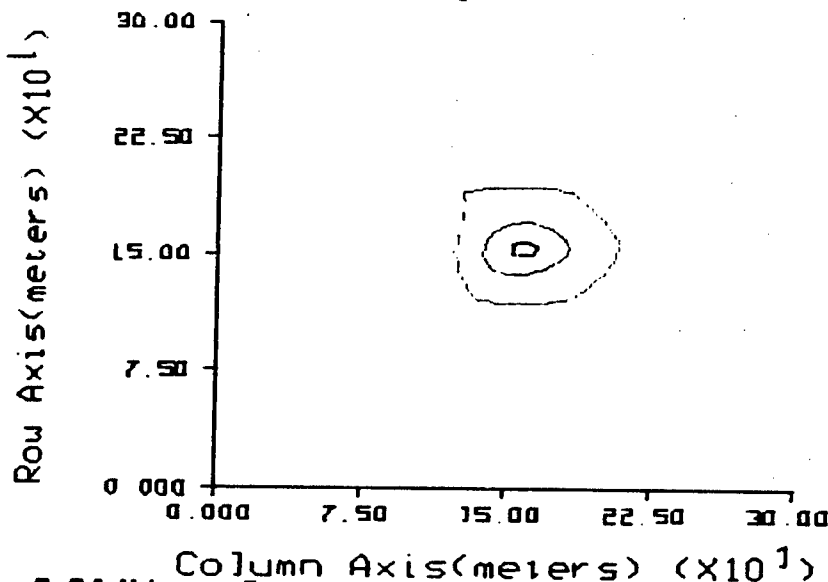
max=2.24uW/sr-cm2

| =0.095*max | =0.50*max | =0.95*max

NRL/ACT 6/3/91

Fig. 72 - CHARM 1.3 contour plot prediction for PC-4 after smearing
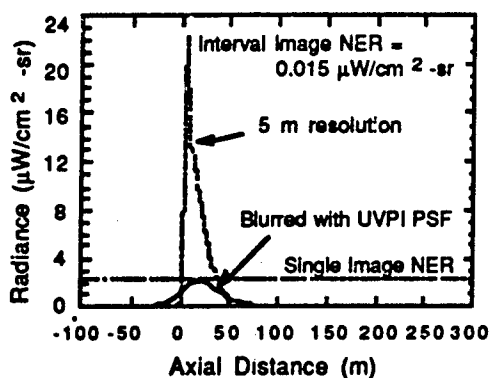
Fig. 73 - CHARM 1.3 predicted axial profile before and after smearing, interval 1
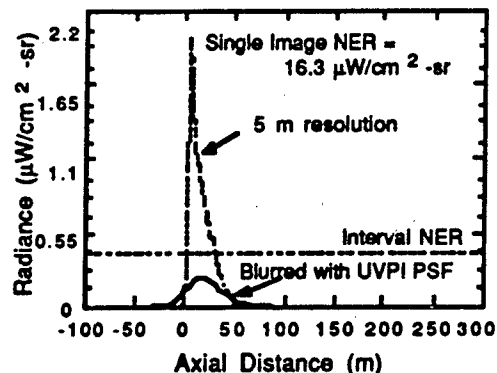
Fig. 74 - CHARM 1.3 predicted axial profile before and after smearing, interval 2
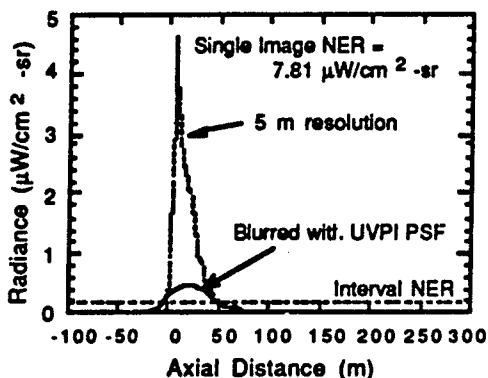
Fig. 75 - CHARM 1.3 predicted axial profile before and after smearing, interval 3
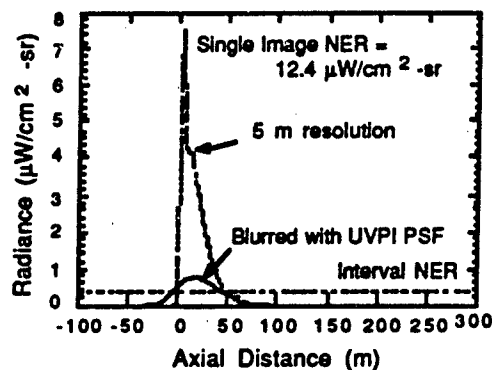
Fig. 76 - CHARM 1.3 predicted axial profile before and after smearing, interval 4
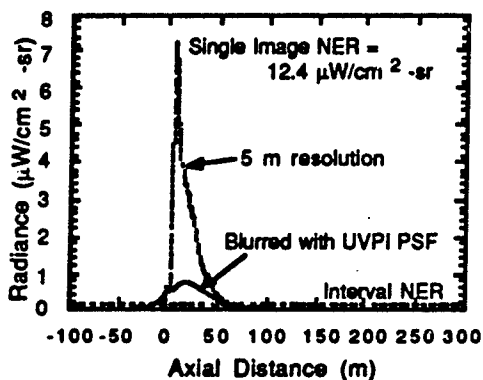
Fig. 77 - CHARM 1.3 predicted axial profile before and after smearing, interval 5
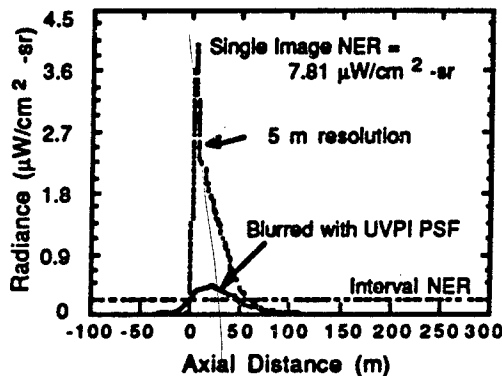
Fig. 78 - CHARM 1.3 predicted axial profile before and after smearing, interval 6
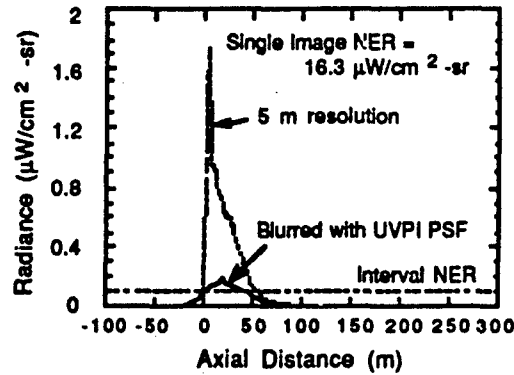
Fig. 79 - CHARM 1.3 predicted axial profile before and after smearing, interval 7

Table 32 – Peak Radiance Comparison

Interval	Stage	Filter	CHARM 1.3 @ 5 m Resolution Peak Radiance (μW/sr-cm^2)	CHARM 1.3 Convolved Peak Radiance (μW/sr-cm^2)	UVPI Measured Peak Radiance (μW/sr-cm^2)
1	3	PC-4	2.20×10^1	2.24	9.97×10^{-1}
2	3	PC-3	1.99	2.01×10^{-1}	5.35×10^{-1}
3	3	PC-2	4.61	4.89×10^{-1}	3.70×10^{-1}
4	3	PC-1	7.47	7.52×10^{-1}	5.14×10^{-1}
5	4	PC-1	7.27	7.37×10^{-1}	7.50×10^{-1}
6	4	PC-2	3.99	4.10×10^{-1}	3.69×10^{-1}
7	4	PC-3	1.75	1.72×10^{-1}	3.24×10^{-1}

Table 33 – Comparison of Measured to Predicted Plume Length

Interval	Stage	Filter	Plume Length (m) Peak to 50% and Peak to 10%					
			CHARM 1.3 @-5-m Resolution		CHARM 1.3 Using UVPI's PSF		UVPI Measured	
			50%	10%	50%	10%	50%	10%
1	3	PC-4	10	35	40	65	54	108
2	3	PC-3	10	35	40	60	22	116
3	3	PC-2	15	35	40	65	14	78
4	3	PC-1	10	35	40	65	6.8	96
5	4	PC-1	10	40	40	65	32	83
6	4	PC-2	10	45	45	80	13	50
7	4	PC-3	10	45	45	75	31	89

6.0 TEMPORAL FEATURES

This section presents calibrated photoevents per image and radiant intensity values for each of the seven data intervals selected. The calibration procedure used is described in Section 3. The conversion to radiant intensity is performed by using a reference emission spectrum for incandescent alumina particles that is typical of the emission spectrum produced by solid-fuel rocket motors containing ammonium perchlorate/aluminur . The latter is similar to the model used in the CHARM 1.3 code. The bandpasses of each of the plume camera filters are also shown in Section 1.2. Section 6.1 presents the plume-camera observations and 6.2 presents the tracker-camera observations.

6.1 Plume Camera Intensity Plots

This section presents the number of photoevents observed in the plume camera, both central region and total, for each image of the seven analyzed data intervals. Table 34 lists the figures contained in this section.

Table 34 - Radiant Intensity Figures

Interval	Stage	Total	Central Region
1	3	80	81
2	3	82	83
3	3	84	85
4	3	86	87
5	4	88	89
6	4	90	91
7	4	92	93

The separation of plume central region from total FOV is described in Section 5.1. During the telemetry frame ranges depicted in each plot, the plume-to-tracker image ratio was 8:2. Consequently, the plots show repeated groups consisting of eight consecutive plume-camera images followed by a gap where the two tracker-camera images occurred.

In addition to the intensities, the figures include the estimated local mean, which is a running average of the intensity, and a threshold of 3.1 standard deviations above the local mean, which flags intensity values that are highly unlikely (probability less than .001), based on local statistics. The local statistics are computed by using a running window of 15 frames for plume-camera data. Section 4.6 contains a more complete discussion of the computations of local statistics.

Figures 80-93 convey information useful for indexing those frames or times at which a significant statistical deviation in the intensity is observed, based on the local statistics, and for showing the intensity variation over both the plume central region and the total plume.

Figures 84, 92, and 93 show instances in which the measured number of photoevents exceeds the local mean by more than 3.1 standard deviations. The probability of such an event is less than 0.001. Therefore, all instances in which the measured number of photoevents exceeded the threshold were investigated in great detail. No significant difference was observed in the composite images after disregarding the images where the measured number of photoevents exceeded the threshold.

Table 35 summarizes the average radiant intensities (ARI) for the plume camera observations over the seven data intervals. The average radiant intensity reported for each of the data intervals is based on the reference spectral energy distribution assumption. It represents the average of all images in the interval. Table 35 includes reference spectrum predictions of ARI for the sake of completeness.

When operating in the zoom image transmission rate, each telemetry frame contains one image.

Table 35 - Summary of Plume Camera Average Radiant Intensities

			Measured ARI*		Measured ASRI**		Reference Model
Interval	Filter	Band (nm)	Central Region ARI (W/sr)	Total ARI (W/sr)	Centroid wavelength (nm)	Total ASRI (W/sr- μm)	Predicted ARI (W/sr)
1	PC-4	235-350	28.7	35.3	305	334	44.2
2	PC-3	195-295	7.7	9.5	265	90.6	3.8
3	PC-2	300-320	4.5	9.5	310	465	9.6
4	PC-1	220-320	10.5	12.2	280	81.3	15.0
5	PC-1	220-320	12.0	15.6	280	104	15.0
6	PC-2	300-320	3.1	6.0	310	296	9.4
7	PC-3	195-295	5.4	8.6	265	81.9	3.8

* Average Radiant Intensity
** Average Spectral Radiant Intensity
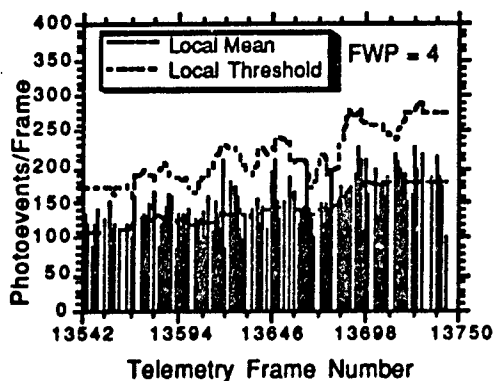
Fig. 80 - Third stage, plume camera, total intensity for interval 1
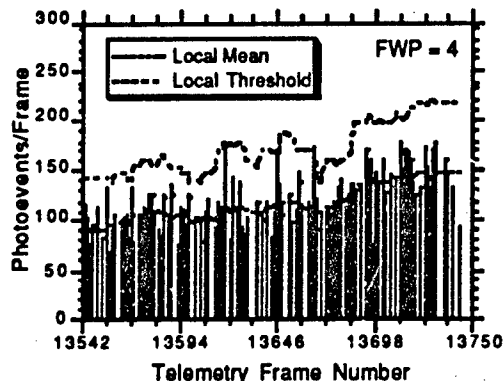
Fig. 81 - Third stage, plume camera, central region intensity for interval 1
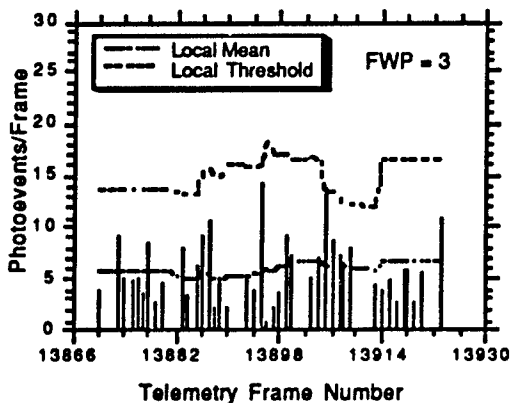
Fig. 82 - Third stage, plume camera, total intensity for interval 2
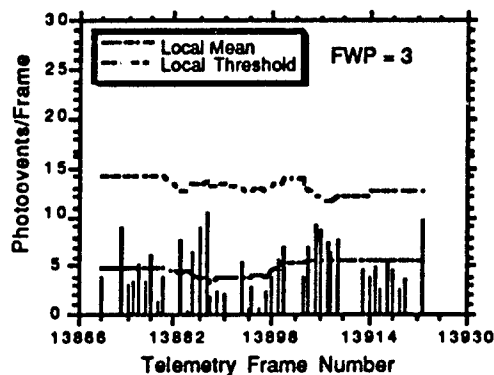
Fig. 83 - Third stage, plume camera, central region intensity for interval 2
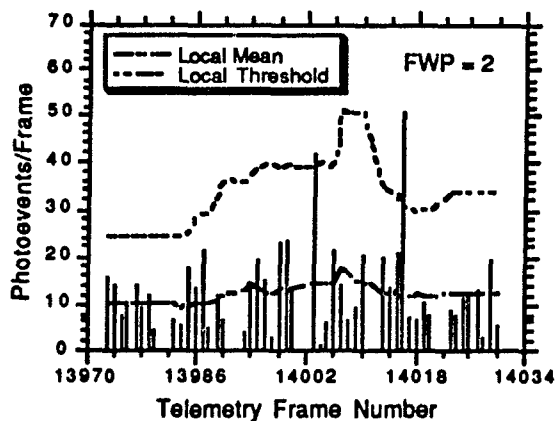
Fig. 84 - Third stage, plume camera, total intensity for interval 3
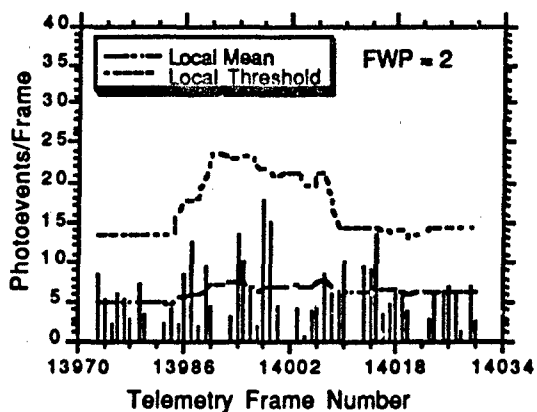
Fig. 85 - Third stage, plume camera, central region intensity for interval 3
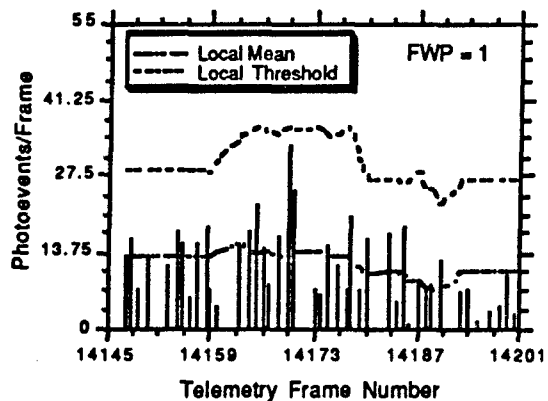
Fig. 86 - Third stage, plume camera, total intensity for interval 4
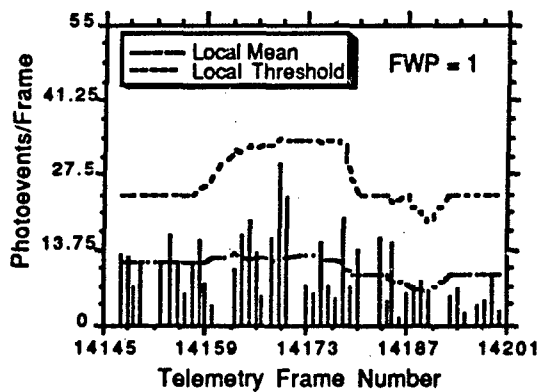
Fig. 87 - Third stage, plume camera, central region intensity for interval 4
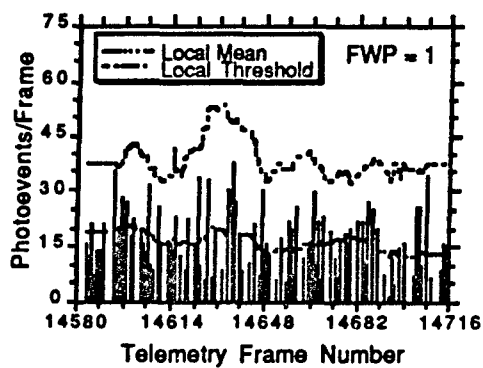
Fig. 88 - Fourth stage, plume camera, total intensity for interval 5
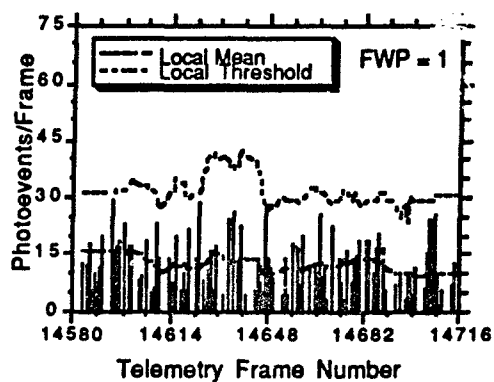
Fig. 89 - Fourth stage, plume camera, central region intensity for interval 5
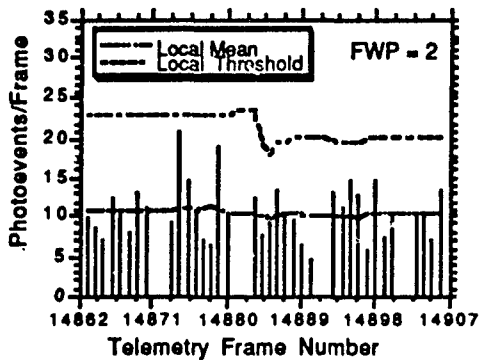
Fig. 90 - Fourth stage, plume camera, total intensity for interval 6
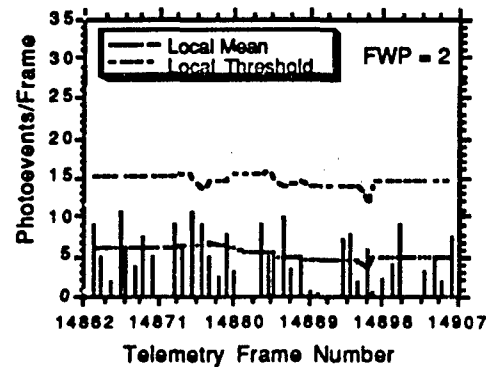
Fig. 91 - Fourth stage, plume camera, central region intensity for interval 6
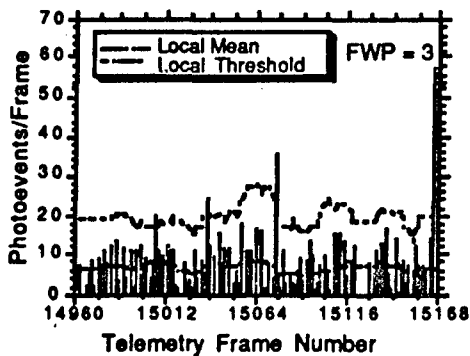
Fig. 92 - Fourth stage, plume camera, total intensity for interval 7
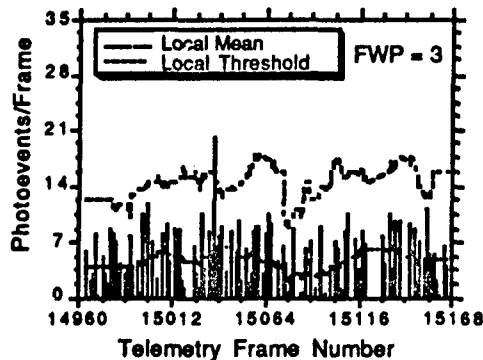
Fig. 93 - Fourth stage, plume camera, central region intensity for interval 7

6.2 Tracker Camera Intensity Plots

Figures 94-100 present total photoevents per image for the seven data intervals analyzed throughout this report. The figures in this section are based on a 19 by 19 pixel section of the tracker camera, which corresponds approximately to the total field of view of the plume camera. This field of view contains plume central region and a portion of the outer region. To provide an estimate of the average radiant intensity, values based on reference spectral energy distribution assumptions are reported in Table 36 for the tracker-camera observations. These results have been reduced by 16.3% to account for redleakage in the tracker-camera filter.

Figures 94-100 are primarily intended to show image-to-image variations in the number of photoevents per image after redleak correction.

For the telemetry frame ranges depicted in each plot, the plume-to-tracker image ratio was 8:2. Consequently, the plots show repeated groups consisting of two consecutive tracker-camera images followed by a gap where the eight plume-camera images occurred.

In addition to the intensities, the figures include the estimated local mean, which is a running average of the intensity, and a threshold of 3.1 standard deviations above the local mean, which flags intensity values that are highly unlikely (probability less than .001), based on the local statistics. The local statistics are computed by using a running window of 15 frames for tracker-camera data. A

more complete discussion of the computations of local statistics is contained in Section 4.6. The greater than 3.1 standard deviation events appear uncorrelated between the plume and tracker cameras suggesting that, if they represent real events, they last less than $1/30$th of a second.

Table 36 - Summary of Tracker-Camera Average Radiant Intensities

Interval	Stage	Filter	Band (nm)	ARI* in 19 x 19 Pixel Region (W/sr)	ASRI** in 19 x 19 Pixel Region @ 390 nm (W/sr-μm)
1	?	PC-4	255-450	163	1300
2	3	PC-3	255-450	169	1350
3	3	PC-2	255-450	166	1320
4	3	PC-1	255-450	101	809
5	4	PC-1	255-450	106	846
6	4	PC-2	255-450	134	1070
7	4	PC-3	255-450	160	1280

* Average Radiant Intensity
** Average Spectral Radiant Intensity
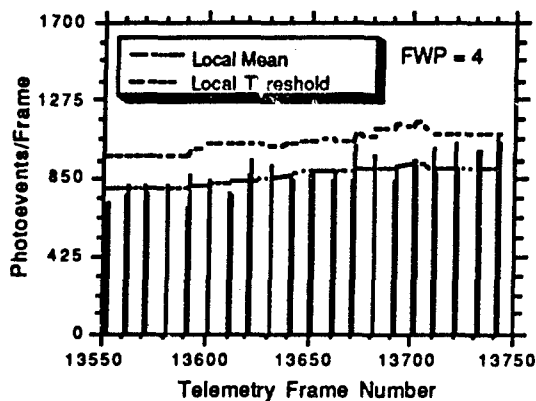
Fig. 94 - Third stage, tracker camera total intensity for interval 1
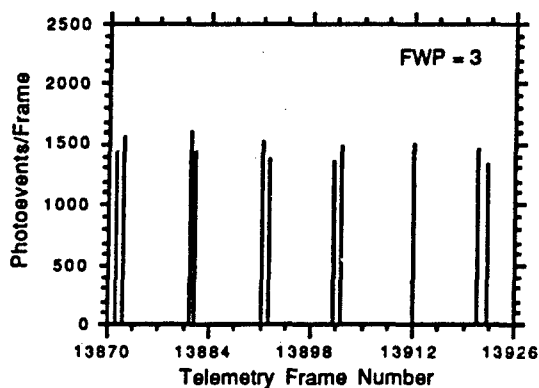
Fig. 95 - Third stage, tracker camera total intensity for interval 2
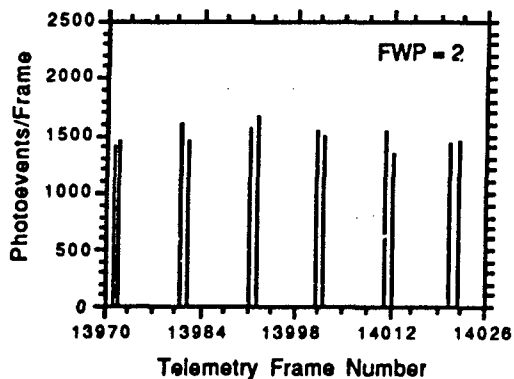
Fig. 96 - Third stage, tracker camera total intensity for interval 3
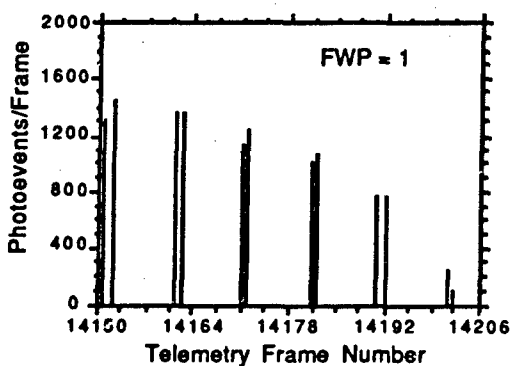
Fig. 97 - Third stage, tracker camera total intensity for interval 4
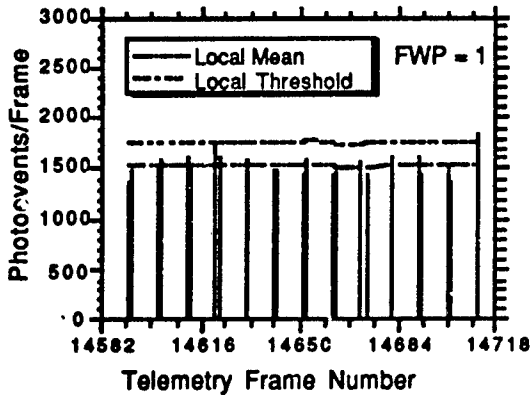
Fig. 98 - Fourth stage, tracker camera total intensity for interval 5
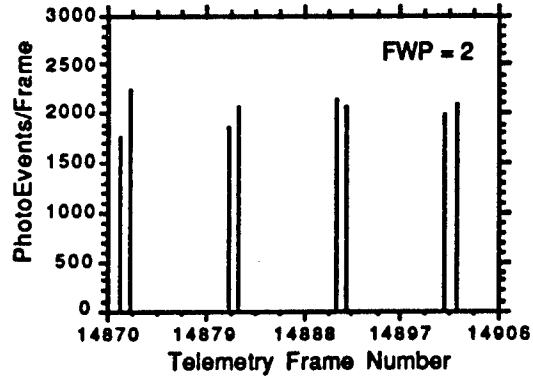
Fig. 99 - Fourth stage, tracker camera total intensity for interval 6
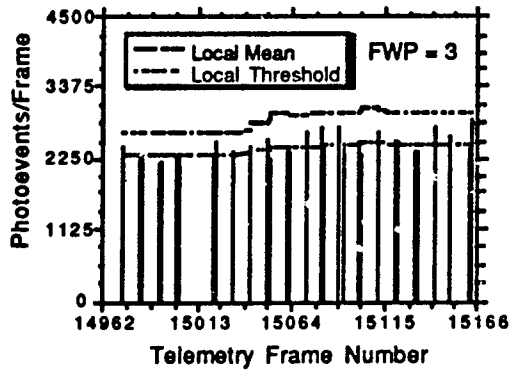
Fig. 100 - Fourth stage, tracker camera total intensity for interval 7

7.0 SPECTRAL ANALYSIS OF PLUMES

This section presents the spectral analysis of the emission from the Starbird third- and fourth-stage plumes' central region and from the outer region. As discussed in Section 2, the UVPI plume and tracker cameras observed the Starbird third and fourth stages at a range of approximately 530 km by using a sequence of bandpasses. The figures and tables in this section show the computed spectral radiant intensity in W/sr-µm of the plume central region, and the spectral radiant intensity measured over the entire plume camera field of view. The results from the UVPI observations of the central region show that the ratio of the spectral radiant intensity at the longer wavelengths, relative to the spectral radiant intensity at the shorter wavelengths, is smaller than predicted by the reference spectrum. The results for the entire plume camera field of view shows a similar relative deficit at the longer wavelengths.

7.1 Observed Spectral Radiant Intensities

The conversion of the plume- and tracker-camera data to radiometric values requires the assumption of a source spectrum, as described in Section 3.5. The reference spectral shape was used in the analysis of the camera data presented in this section. The wavelength for which the spectral radiant intensity is reported for each filter bandpass is the centroid wavelength when the assumed

source spectrum is convolved with the UVPI net quantum efficiency function, as described in Section 3.6.

In selecting the reference spectrum scaling factor, an effort was made to find a good fit for all bands. This method is less sensitive to single band signals but instead compares overall spectral shapes.

The plume camera observations of the third and fourth stage were made between 115 and 170 seconds after liftoff. The range from UVPI to the rocket was between 483 and 596 km over this time period. The spectral radiant intensities of the plume central region, as measured by UVPI in the four plume camera bands, are plotted in Fig. 101. In addition, Fig. 101 shows the reference spectral shape, scaled arbitrarily to pass through the data points, and for comparison shows a blackbody spectrum chosen to coincide with the reference spectral shape at short wavelengths. The data and scaled reference-based values are also listed in Table 37. Note that the average radiant intensities of the plume changed with time during the seven intervals. Consequently, the relative spectral intensities must be compared with caution.

Figure 102 shows that the reference spectral shape is in good agreement with the 275 to 390-nm trend. It also shows that the reference model predicts a more rapid decrease with decreasing wavelength below 275 nm than the data show. These results are similar to those found for the plume central region analysis.
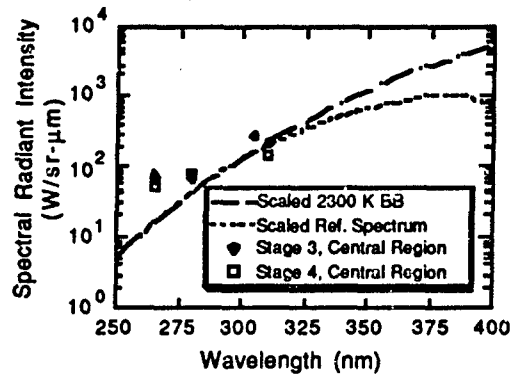
Fig. 101 - Measured spectral radiant intensity for the Standard plume central region

Table 37 - Measured and Scaled Spectral Radiant Intensity in Units of W/sr-μm

Wavelength (nm)	Stage	Filter	Observed Central Region	Plume Camera Field of View	Central Region: Scaled Reference Comparison
265	3	PC-3	7.33×10^1	9.06×10^1	1.58×10^1
280	3	PC-1	6.99×10^1	8.13×10^1	4.24×10^1
305	3	PC-4	2.72×10^2	3.34×10^2	1.65×10^2
310	3	PC-2	2.21×10^2	4.65×10^2	2.02×10^2
265	4	PC-3	5.19×10^1	8.19×10^1	1.58×10^1
280	4	PC-1	7.99×10^1	1.04×10^2	4.24×10^1
310	4	PC-2	1.51×10^2	2.96×10^2	2.02×10^2

Figure 101 shows that the ratio of the spectral radiant intensity measured by UVPI for the third- and fourth-stage central regions at the shorter wavelengths, relative to that at the longer wavelengths, is larger than predicted by the reference spectral shape. The relative intensity increase

for the 265-nm data point is a factor of almost five, well beyond the instrument uncertainty discussed in Section 4.6.

The spectral radiant intensity for the third and fourth stages, measured by UVPI over the entire plume camera field of view, is shown in Fig. 102. These measurements were made by the plume camera operating in the four plume-camera bands and by the tracker camera. Note that the tracker-camera pixels analyzed in this section correspond to the full field of view of the plume camera. Figure 102 also shows a scaled reference spectral shape and blackbody spectrum. The data are also listed in Table 37.
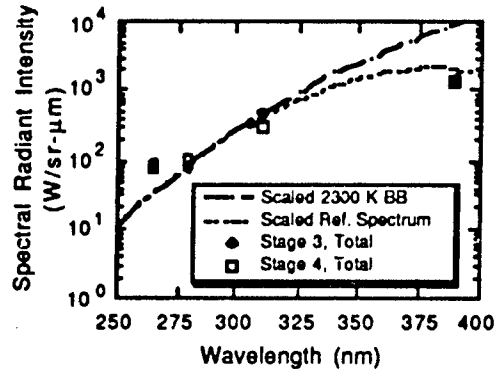
Fig. 102 - Measured spectral radiant intensity for the Starbird plume camera field of view

It should be noted that the Starbird total and central region spectral data are almost identical, both showing the short wavelength excess. In contrast, the Strypi Antares stage total field of view results, shown in Fig. 103, show a short wavelength excess, but the central region results shown in Fig. 104 showed a much reduced excess. The UV luminous outer region seen in Strypi appeared to be associated with the far-UV excess, whereas in the Starbird data the plume central region displays the same marked excess as the total. Thus, the greatest contrast between the Starbird and Strypi plume data is the apparent difference in PC-3, or far-UV data, for which the Starbird plumes' central regions showed a stronger relative signal.
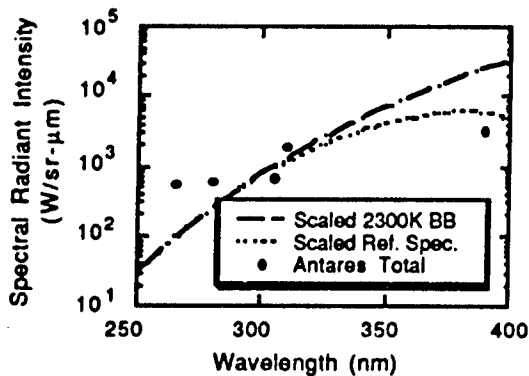
Fig. 103 - Measured spectral radiant intensity for the plume camera field of view for Antares
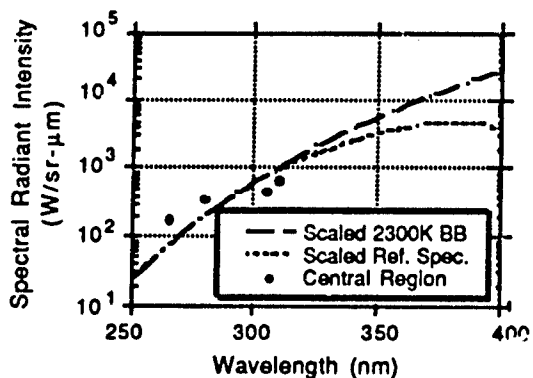
Fig. 104 - Measured spectral radiant intensity for the Antares central region

7.2 Discussion

The reference model hypothesizes that the principal source of UV radiation is thermal emission from alumina particles at the fusion temperature of alumina, 2320 K. The spectral shape

departs from that of a blackbody because of the decreasing effective emissivity of the particles with increasing wavelength. No obvious modification to this model will yield the far-UV excess evident in the UVPI data. A plausible hypothesis is that an additional emission mechanism is producing the excess UV emission. Spectral line emission by exhaust gases and by the mesospheric atmosphere disturbed by the rocket, e.g., CO cameron and NOγ bands, are possible sources. The possibility of a far-UV excess due to luminous gases was discussed briefly in the Starbird preflight document [7].

8.0 SUMMARY AND CONCLUSIONS

8.1 Summary

The goal of the Starbird mission was the acquisition from space of radiometric UV plume data, using the UVPI onboard the LACE satellite. The UVPI plume camera is an imaging radiometer with four filters, centered at 250, 270, 280, and 305 nm (Table 9). This instrument was designed to obtain radiometric data in a spectral region that is especially favorable for missile detection because of the very low solar background. Operation from space is necessary because the atmosphere is practically opaque to wavelengths below 300 nm. From 500-km range, the plume camera has a resolution of approximately 45 m.

The Starbird, a four-stage solid-propellant missile system, was obtained for this observation. The first stage (a Talos motor) and the second stage (a Sergeant motor) operated at too low an altitude to be observed from space. The mission was designed for observing the third- and fourth-stage plumes, both of which were produced by identical Orbus rocket motors. The rocket trajectory was selected to permit simultaneous observation from the LACE satellite and from the Air Force Malabar (Florida) tracking site.

The Starbird was launched from the Kennedy Space Center before sunrise on 17 December 1990. The third and fourth stages were successfully tracked by the UVPI camera from a range of 596 to 483 km. The third-stage plume was tracked for about 20 seconds, and plume data were acquired with all four plume camera filters. The weaker plume from the fourth stage was also tracked. Its weaker plume signal is attributed to its less-than-nominal thrust level for the fourth-stage Orbus motor. Plume data were obtained with three of the four plume-camera filters. The observation intervals are summarized in Tables 16 and 17.

The 290 images of the third-stage plume and 297 images of the fourth-stage plume from the plume camera were of sufficient quality and tracking accuracy to permit the superposition of images for increased radiometric accuracy.

The superposed images were analyzed to obtain the spectral radiance, evaluating the plume as a spatially resolved source, and the spectral radiant intensity, summing over space to treat the plume as a point source. The radiometric analysis requires a model spectral shape, for which a reference model is taken. The analysis procedure is described in Section 3. The spectral values were also integrated over the nominal filter bandwidths to obtain radiance and radiant intensity values.

The odd numbered Figs. 33 through 45 are false-color maps of the spatial distributions of the time-averaged radiant intensities of the third-stage and fourth-stage plumes. Contour plots of the plume radiance were also generated from the superposed images and are presented in the even-numbered Figs. 34 through 46.

Figure 31 shows the image and Fig. 32 the contour plot of the NRL ground-based UV beacon, which well represents a point source under these conditions. This image indicates the resolution limit of the instrument at 450-km range. The lengths of the rocket plumes observed during this mission are less than, or comparable to, the 45-m resolution limit (Table 33). The consequent smearing of the source over an increased effective area significantly reduces the observed peak radiance of the plumes. The observed radiances are thereby denoted "apparent" values to distinguish between the observed radiance values and those that would be obtained from an instrument with

higher spatial resolution. An adjustment of the CHARM predicted peak radiances for this effect yields approximately factor-of-two agreement between prediction and observation (Table 32).

Radiant intensity values, obtained by summing over the plume central region and over the plume camera field of view, are not affected by this resolution effect. For these computations, the plume central region was defined as the region in which the radiance exceeded 25% of the peak apparent value, with the addition of the area defined by a 5 by 5 pixel dilation of this region. The projected area of the central region so defined was approximately 5000 to 9000 m² (Table 30). The remainder of the plume-camera images is denoted the outer region.

The outer region data from the Starbird showed weak radiances and suffered from poor signal-to-noise ratio. Unlike the Strypi test at higher altitude, no identifiable shock or mixing layer structure could be found in the Starbird outer region data and, thus, the outer region radiance cannot be causally connected to the Starbird third or fourth stage. The central region and total radiant intensities measured by the plume camera are summarized in Table 35. The temporal behavior of the plume central region and total spectral radiant intensities measured by the plume camera are shown in Figs. 26 and 27.

The UVPI tracker camera provides wideband (255 to 450 nm) data, which may complement the plume camera data. The wide field of view of the tracker camera clearly prevents resolution of the plume, but radiant intensity values can be obtained. A 19 by 19 pixel region of the tracker camera images, matching the total field of view of the plume camera, was taken for computing radiant intensities. The values so obtained are summarized in Table 36, and the spectral radiant intensity time dependence is shown in Fig. 28.

The spectral radiant intensities deduced from the UVPI observations can be compared to the reference model of plume emission. The plume central region spectral radiant intensities show a reference spectrum-like dependence over the 250 to 300-nm range. The data suggest that the 250 to 270-nm values are higher, relative to the 280 to 300-nm values, than the reference spectrum predicts (Fig. 101). However, the greatest contract between the Starbird and Strypi [2] plume data is the apparent difference in the PC-3 filter bandpass for which the Starbird plumes' central regions showed a stronger relative signal. The spectral radiant intensities summed over the plume camera field of view show a similar ultraviolet excess. The full field values from the plume camera can be complemented by the tracker camera data over the same area (Fig. 102). The 390-nm value so obtained adds support to the tentative conclusion that the decrease in plume spectral radiant intensity, as the wavelength decreases below 300 nm, is less than expected on the basis of the reference model. This is similar to trends in data seen in the Strypi plume data [2].

The Starbird vehicle carried two identical solid-fuel motors of the Orbus type to power its third and fourth stages. The performance of the two motors in terms of thrust was slightly different. The third stage performed nominally but the fourth stage was less than nominal, causing the rocket to reach only 90-km altitude rather than the planned 105 km. This difference in performance was reflected in the plume radiances measured by the UVPI, which detected a lower radiance for the fourth stage than was seen in the nominal third stage. This can be seen clearly in Figs. 26 - 28. These data suggest that observation in the UV can distinguish rocket motor performance rather than design type.

8.2 Achievement of Objectives

The results of the UVPI observation of the Starbird missile can be compared to the objectives listed in Section 1.3.

8.2.1 General Objectives

- *Obtain isoradiance contours for the third stage and fourth stage plumes.* Spatially resolved images of the third stage and fourth stage plumes were obtained for seven data intervals, corresponding to imaging with all four plume-camera filters for the third stage

and three of the four filters for the fourth stage. These images were scaled to radiance maps and contours, as illustrated in Sections 4 and 5.

- *Obtain radiant intensity measurements based on the entire field of view of the plume camera and on a subregion corresponding approximately to a plume core.* Radiant intensity measurements for the plume camera FOV and for a plume central region defined in Section 5.1 were extracted from the images for the seven data intervals. These results are presented in Section 6.

- *Compare radiometric measurements for the third stage and fourth stage plumes with those generated by the CHARM computer codes.* The preliminary comparison undertaken here suggests that the UVPI data present a spectral shape somewhat different from that of the reference spectrum. The experimental results indicate that the emission at wavelengths shorter than 300 nm is greater, relative to the emission at longer wavelengths, than is predicted by the reference model. These results are described in Section 7. Detailed comparison of CHARM predictions to UVPI observations is a task for the modelers.

- *Provide radiometric measurements for nonplume, transient phenomena, if any.* No clouds or other notable transients were seen in the Starbird data.

8.2.2 *Specific Objectives Related to Spatial Features*

- *Obtain the length of the third-stage and fourth-stage plume central regions.* The resolution limit of the PSF-corrected UVPI corresponds, at this range, to about 40 meters, which is comparable to the expected plume length. Thus, a close measurement of the plume length was not possible, but (as described in Section 5.3) the observations are consistent with the predicted plume length.

- *Determine the shape of the shock boundary/mixing layer for different rocket velocities.* The very weak radiance of the outer region and the absence of any apparent shock or mixing layer structure in the radiance suggests that, in contrast to the Strypi tests, no UV luminous outer region formed as a result of the Starbird.

- *Identify asymmetries in plume shape and investigate possible causes.* No plume shape asymmetries were observed. The resolution limit of the UVPI at this range is such that only large asymmetries could have been detected.

8.2.3 *Specific Objectives Related to Temporal Features*

- *Identify temporal trends in radiometrics and investigate possible dependence on rocket velocity.* The time behavior of the radiant intensity of the third- and fourth-stage plumes is described in Section 6. No obvious correlation with rocket velocity was observed.

- *Investigate radiometric fluctuations to determine whether short-term variations in brightness are observed.* The statistics of the variations in plume radiant intensity are described in Section 6. Several peaks beyond the range of statistical likelihood were observed. The data were carefully analyzed and no reason was found to reject them.

- *Identify changes with time in the shape of the plumes' outer region.* No identifiable outer region was found.

- *Identify persistence and cumulative effects, if any, in plumes or nonplume phenomena.* No clouds or trails were observed in the Starbird test.

8.2.4 *Specific Objectives Related to Spectral Features*

- *Compare the shape of the plume central region's emission spectrum with the reference spectral shape, which is that of submicron alumina particles at the melting point, and spectral shape determinations based on other sensors.* As described in Section 7, the UVPI data indicate that the decrease in spectral radiance and radiant intensity, as the wavelength decreases below 300-nm, is less than indicated by the reference model. This is similar to data from the Strypi test.

- *Relate tracker-camera measurement to visible and infrared measurements made by other sensors.* The UVPI acquired plume radiometric data to 450 nm wavelength. These radiant intensity values can be compared to data at longer wavelengths from other sensors as those data become available.

- *Characterize the emission spectrum for the plumes' outer regions, if any.* No identifiable outer region was found in the Starbird test data, in contrast to the Strypi test.

It is clear from the above that most of the task objectives were achieved. However, the instrumental limitations in resolution, as well as the uncertainty in the reference spectral shape, complicate the extraction of precise values.

8.3 Conclusions

The UVPI observation of the Starbird launch again demonstrates the capability of the instrument for tracking and imaging missiles in flight from 550 km range. The bright plume of the third stage was successfully tracked throughout its burn. The weaker plume of the fourth stage was also tracked successfully.

The third stage was acquired for a total of 290 plume camera images distributed over all four UVPI filters. The fourth stage was tracked for a total of 297 images, and data were obtained for three of the four filters. The spectral radiance and spectral radiant intensities were extracted from these images. Absolute values are necessarily obtained on the basis of an assumed spectral shape, namely the reference spectrum, which is the spectrum of micron-sized alumina particles at their melting point of 2320 K. A comparison of the results for the four UVPI filters indicates that the reference shape is not inaccurate, but the new data indicate a stronger component in the far UV, $\lambda < 300$ nm, than the model predicts. This result is similar to that obtained in the Strypi test.

In contrast to the Strypi test, the images reveal a radiant plume but no identifiable outer region of UV radiance such as might be associated with a shock or mixing layer produced by the plume. The outer region radiances that are measured are generally weak, have poor signal-to-noise ratio, and exhibit no marked difference before or behind the rocket.

The time dependence of the third-stage plume central region radiant intensity within each filter interval showed no pronounced trends or variations. The fourth stage, however, showed an upward ramp in time from ignition, starting from below the third-stage radiant intensity level and rising to approximately the third-stage value. This lower average output, relative to the third stage, seemed correlated to the lower ballistic performance of the fourth stage. Momentary, single-frame peaks exceeding the range of normal statistical variation were detected. Whether these can be correlated with missile engine events or other sensors remains to be seen.

The tracker camera obtained radiant intensity data in the 255 to 450-nm wavelength range. These data, taken with the plume camera data in the 195 to 350-nm range, support the conclusion that the central region spectrum is quite close to the reference model with an enhancement of the emission in the far-UV between 250 and 280 nm. A similar enhancement was seen in the Strypi data, but it is associated with the outer region more than the central region. It has been suggested that the Strypi's higher altitude allows greater expansion of gaseous products (speculated to be the source of the short wavelength emission excess) into the far field.

This base of UV radiometric data will be a foundation for further analysis to provide refined interpretations and evaluation. Comparison with models, with data from sensors on other platforms, and with UVPI data from other tests will also yield improved radiometric results and an enhanced phenomenological understanding of UV emission by solid rocket motors in the upper atmosphere.

REFERENCES

1. H.W. Smathers, D.M. Horan, J.G. Cardon, E.R. Malaret, M.R. Corson, and J.E. Brandenburg, "Ultraviolet Plume Instrument Description and Plume Data Reduction Methodology Report," NRL Report 9531, May 1993.

2. H.W. Smathers, D.M. Horan, J.G. Cardon, E.R. Malaret, M. Singh, T. Sorensen, P.M. Laufer, M.R. Corson, J.E. Brandenburg, J.A. McKay and R.R. Strunce Jr., "UVPI Imaging From the Lace Satellite, The Strypi Rocket Plume" NRL Report 9526 July 1993.

3. J.T. Wright, "Ultraviolet Plume Instrument (UVPI) Subsystem Users Manual," SDRL 068, Loral EOS Document No. 3731 (26 Jan. 1989).

4. H.W. Smathers and D.M. Horan, L.H. Reynolds, W. Ramsey and H.D. Wolpert, "Design and Description of the Ultraviolet Plume Instrument (UVPI)," *SPIE* **1158**, 196 (1989).

5. H.W. Smathers, G.R. Carruthers, W. Ramsey, G. Steiner and W. Louissant "Calibration and Performance of the Ultraviolet Plume Instrument (UVPI)," *SPIE* **1158**, 212 (1989).

6. J. Nicholas, "Experiment Requirements Document for UVPI Observations of SDIO Special Projects (SPFE) Launches, Rev 3," The Analytic Sciences Corporation (1 Aug. 1990).

7. W.A. Jeffrey, M. Slack, and L. Laux, "Orbus Preflight Predictions," IDA document D-755, Institute for Defense Analyses (April, 1990).

8. J.A. Marqusee, "The State of Knowledge of UV/V Boost- and Post-Boost-Phase Phenomenology and a Preliminary Assessment of Its Utility to SDI," IDA Paper P-2232, Institute for Defense Analyses (July 1989).

9. R.A. Reed and V.S. Calia, "Review of Rocket Particle Properties Research," AEDC-TR-89-11 Arnold Engineering Development Center Final Report (Nov. 1989).

10. H.L. Fukunaga, *Introduction to Statistical Pattern Recognition*, (Academic Press, New York, New York, 1972).

11. C.L. Wyatt *Radiometric System Design* (MacMillan, New York, 1987).

12. F.E. Nicodemus "Normalization in Radiometry," *Applied Optics* **12**(12), 2960-2973 (1973).

13. J. Marqusee, Institute for Defense Analyses, private communication, 14 March, 1991.

14. P.W. Erdman, E. Zipf, P. Espy, C. Howlett, D.A. Levin, and G.V. Candler, "In-Situ Measurements of UV and VUV Radiation from a Rocket Plume and Re-entry Bow Shock," AIAA Paper No. 92-0124, January 1992.

15. A. Papoulis, *Probability, Random Variables, and Stochastic Processes*, 2nd ed. (McGraw-Hill, New York, 1984).

16. W.L. Wolfe and G.J. Zissis, ed. *The Infrared Handbook* (Environmental Research Institute of Michigan, 1978).

17. R.H. Kingston *Detection of Optical and Infrared Radiation* (Springer-Verlag, New York, 1978) pp. 43-51.

18. W. Jeffrey, Grumman Corp., private communication, May 1992.

Appendix A

STARBIRD TRAJECTORY PARAMETERS

The following tables present various Starbird trajectory-related parameters as a function of time. The first column in each table is TALO, time after lift-off, in seconds. Table A1 shows the rocket's position in Earth center-fixed (ECF) coordinates and the rocket's speed. Table A2 shows the aspect angle, the angle of attack, and the distance between the satellite and the rocket. The aspect angle is defined as the angle between the line-of-sight (LOS) vector from the satellite to the target point and the longitudinal axis of the rocket. The angle of attack is defined as the angle between the longitudinal axis of the rocket and its velocity vector. Table A3 shows the rocket's altitude, geodetic latitude, and longitude.

Table A1 - Rocket Position and Speed in ECF Coordinates

TALO (s)	XPOS (km)	YPOS (km)	ZPOS (km)	Speed (km/s)
0.0	920.3427	-5532.9531	3026.2971	0.0472
1.0	920.3597	-5532.9912	3026.3191	0.1002
2.0	920.3980	-5533.0713	3026.3655	0.1599
3.0	920.4615	-5533.1982	3026.4390	0.2236
4.0	920.5586	-5533.3721	3026.5408	0.2849
5.0	920.6888	-5533.5903	3026.6694	0.3084
6.0	920.8338	-5533.8247	3026.8079	0.2959
7.0	920.9769	-5534.0474	3026.9402	0.2843
8.0	921.1175	-5534.2598	3027.0664	0.2725
9.0	921.2556	-5534.4614	3027.1868	0.2610
10.0	921.3912	-5534.6528	3027.3013	0.2508
11.0	921.5252	-5534.8345	3027.4106	0.2384
12.0	921.6531	-5535.0068	3027.5144	0.2450
13.0	921.7801	-5535.1865	3027.6221	0.2697
14.0	921.9122	-5535.3887	3027.7422	0.2938
15.0	922.0487	-5535.6128	3027.8743	0.3166
16.0	922.1889	-5535.8589	3028.0156	0.3395
17.0	922.3374	-5536.1313	3028.1533	0.3604
18.0	922.4926	-5536.4214	3028.3005	0.3812
19.0	922.6545	-5536.7290	3028.4570	0.4025
20.0	922.8238	-5537.0542	3028.6230	0.4236
21.0	923.0007	-5537.3970	3028.7981	0.4453
22.0	923.1830	-5537.7588	3028.9829	0.4690
23.0	923.3746	-5538.1401	3029.1775	0.4926
24.0	923.5728	-5538.5420	3029.3821	0.5186
25.0	923.7792	-5538.9663	3029.5974	0.5446
26.0	923.9911	-5539.4136	3029.8245	0.5731
27.0	924.2087	-5539.8862	3030.0647	0.6028

Table A1 - Rocket Position and Speed in ECF Coordinates (Cont'd.)

TALO (s)	XPOS (km)	YPOS (km)	ZPOS (km)	Speed (km/s)
28.0	924.4293	-5540.3862	3030.3191	0.6341
29.0	924.6569	-5540.9136	3030.5879	0.6687
30.0	924.8911	-5541.4722	3030.8713	0.7046
31.0	925.1338	-5542.0630	3031.1689	0.7438
32.0	925.3863	-5542.6890	3031.4814	0.7857
33.0	925.6518	-5543.3521	3031.8088	0.8293
34.0	925.9306	-5544.0537	3032.1519	0.8766
35.0	926.2253	-5544.7964	3032.5125	0.9223
36.0	926.5369	-5545.5752	3032.8960	0.9473
37.0	925.8599	-5546.3726	3033.2925	0.9550
38.0	927.1877	-5547.1758	3033.6917	0.9569
39.0	927.5161	-5547.9814	3034.0901	0.9555
40.0	927.8444	-5548.7866	3034.4861	0.9510
41.0	928.1705	-5549.5879	3034.8809	0.9448
42.0	928.4958	-5550.3833	3035.2734	0.9368
43.0	928.8199	-5551.1719	3035.6616	0.9280
44.0	929.1443	-5551.9521	3036.0452	0.9181
45.0	929.4658	-5552.7241	3036.4241	0.9078
46.0	929.7872	-5553.4863	3036.7981	0.8971
47.0	930.1085	-5554.2383	3037.1670	0.8859
48.0	930.4282	-5554.9805	3037.5300	0.8744
49.0	930.7469	-5555.7119	3037.8879	0.8632
50.0	931.0634	-5556.4336	3038.2402	0.8524
51.0	931.3796	-5557.1450	3038.5874	0.8413
52.0	931.6935	-5557.8467	3038.9292	0.8306
53.0	932.0066	-5558.5386	3039.2656	0.8199
54.0	932.3181	-5559.2207	3039.5972	0.8099
55.0	932.6282	-5559.8940	3039.9233	0.7993
56.0	932.9359	-5560.5581	3040.2446	0.7896
57.0	933.2444	-5561.2124	3040.5610	0.7794
58.0	933.5508	-5561.8579	3040.8723	0.7693
59.0	933.8549	-5562.4946	3041.1790	0.7594
60.0	934.1583	-5563.1221	3041.4805	0.7498
61.0	934.4602	-5563.7407	3041.7776	0.7403
62.0	934.7607	-5564.3511	3042.0693	0.7303
63.0	935.0598	-5564.9521	3042.3567	0.7210
64.0	935.3575	-5565.5449	3042.6392	0.7113
65.0	935.6539	-5566.1289	3042.9167	0.7014
66.0	935.9480	-5566.7041	3043.1899	0.6923
67.0	936.2414	-5567.2710	3043.4580	0.6829
68.0	936.5343	-5567.8286	3043.7219	0.6737
69.0	936.8249	-5568.3784	3043.9810	0.6635
70.0	937.1127	-5568.9194	3044.2354	0.6548
71.0	937.4013	-5569.4517	3044.4849	0.6454
72.0	937.6879	-5569.9756	3044.7297	0.6358

Table A1 - Rocket Position and Speed in ECF Coordinates (Cont'd.)

TALO (s)	XPOS (km)	YPOS (km)	ZPOS (km)	Speed (km/s)
73.0	937.9714	-5570.4912	3044.9705	0.6270
74.0	938.2559	-5570.9980	3045.2058	0.6175
75.0	938.5367	-5571.4971	3045.4368	0.6087
76.0	938.8184	-5571.9868	3045.6633	0.5989
77.0	939.0964	-5572.4688	3045.8850	0.5906
78.0	939.3746	-5572.9424	3046.1021	0.5808
79.0	939.6507	-5573.4072	3046.3145	0.5719
80.0	939.9254	-5573.8638	3046.5222	0.5630
81.0	940.1987	-5574.3120	3046.7256	0.5539
82.0	940.4713	-5574.7515	3046.9238	0.5450
83.0	940.7419	-5575.1831	3047.1177	0.5354
84.0	941.0103	-5575.6060	3047.3066	0.5273
85.0	941.2780	-5576.0210	3047.4912	0.5180
86.0	941.5444	-5576.4272	3047.6711	0.5085
87.0	941.8079	-5576.8252	3047.8467	0.5003
88.0	942.0715	-5577.2148	3048.0171	0.4915
89.0	942.3338	-5577.5957	3048.1833	0.4824
90.0	942.5939	-5577.9688	3048.3445	0.4742
91.0	942.8533	-5578.3335	3048.5012	0.4651
92.0	943.1107	-5578.6895	3048.6538	0.4564
93.0	943.3666	-5579.0376	3048.8010	0.4478
94.0	943.6212	-5579.3770	3048.9441	0.4394
95.0	943.8745	-5579.7085	3049.0823	0.4306
96.0	944.1263	-5580.0312	3049.2158	0.4227
97.0	944.3768	-5580.3462	3049.3452	0.4166
98.0	944.6270	-5580.6548	3049.4707	0.4228
99.0	944.8838	-5580.9663	3049.5962	0.4304
100.0	945.1481	-5581.2817	3049.7224	0.4372
101.0	945.4193	-5581.6006	3049.8486	0.4452
102.0	945.6980	-5581.9238	3049.9753	0.4516
103.0	945.9835	-5582.2500	3050.1013	0.4586
104.0	946.2757	-5582.5801	3050.2283	0.4656
105.0	946.5760	-5582.9126	3050.3547	0.4711
106.0	946.8822	-5583.2476	3050.4810	0.4782
107.0	947.1965	-5583.5854	3050.6062	0.4846
108.0	947.5181	-5583.9258	3050.7310	0.4923
109.0	947.8486	-5584.2686	3050.8557	0.4994
110.0	948.1860	-5584.6152	3050.9800	0.5093
111.0	948.5339	-5584.9658	3051.1040	0.5182
112.0	948.8911	-5585.3203	3051.2275	0.5285
113.0	949.2589	-5585.6792	3051.3511	0.5389
114.0	949.6368	-5586.0430	3051.4744	0.5498
115.0	950.0255	-5586.4116	3051.5979	0.5623
116.0	950.4273	-5586.7852	3051.7214	0.5744
117.0	950.8409	-5587.1641	3051.8450	0.5872

Table A1 - Rocket Position and Speed in ECF Coordinates (Cont'd.)

TALO (s)	XPOS (km)	YPOS (km)	ZPOS (km)	Speed (km/s)
118.0	951.2670	-5587.5488	3051.9683	0.6008
119.0	951.7071	-5587.9390	3052.0911	0.6144
120.0	952.1605	-5588.3350	3052.2139	0.6304
121.0	952.6309	-5588.7363	3052.3362	0.6438
122.0	953.1146	-5589.1436	3052.4580	0.6605
123.0	953.6161	-5589.5562	3052.5786	0.6755
124.0	954.1333	-5589.9736	3052.6990	0.6918
125.0	954.6674	-5590.3970	3052.8176	0.7085
126.0	955.2195	-5590.8252	3052.9353	0.7259
127.0	955.7900	-5591.2588	3053.0513	0.7427
128.0	956.3792	-5591.6963	3053.1655	0.7599
129.0	956.9867	-5592.1387	3053.2778	0.7771
130.0	957.6133	-5592.5850	3053.3877	0.7932
131.0	958.2584	-5593.0342	3053.4946	0.8075
132.0	958.9199	-5593.4854	3053.5991	0.8230
133.0	959.5994	-5593.9385	3053.7000	0.8368
134.0	960.2961	-5594.3916	3053.7976	0.8498
135.0	961.0082	-5594.8457	3053.8911	0.8602
136.0	961.7342	-5595.2983	3053.9807	0.8711
137.0	962.4751	-5595.7485	3054.0652	0.8712
138.0	963.2205	-5596.1924	3054.1453	0.8645
139.0	963.9632	-5596.6284	3054.2207	0.8588
140.0	964.7045	-5597.0562	3054.2915	0.8541
141.0	965.4453	-5597.4761	3054.3579	0.8481
142.0	966.1842	-5597.8877	3054.4197	0.8438
143.0	966.9232	-5598.2910	3054.4768	0.8513
144.0	967.6738	-5598.6895	3054.5281	0.8677
145.0	968.4448	-5599.0850	3054.5730	0.8861
146.0	969.2378	-5599.4785	3054.6108	0.9046
147.0	970.0534	-5599.8687	3054.6416	0.9226
148.0	970.8907	-5600.2554	3054.6655	0.9412
149.0	971.7506	-5600.6377	3054.6816	0.9591
150.0	972.6321	-5601.0156	3054.6897	0.9770
151.0	973.5352	-5601.3887	3054.6895	0.9947
152.0	974.4596	-5601.7559	3054.6814	1.0125
153.0	975.4055	-5602.1167	3054.6643	1.0305
154.0	976.3727	-5602.4712	3054.6382	1.0503
155.0	977.3633	-5602.8184	3054.6028	1.0693
156.0	978.3768	-5603.1582	3054.5569	1.0924
157.0	979.4160	-5603.4902	3054.5010	1.1139
158.0	980.4798	-5603.8135	3054.4336	1.1372
159.0	981.5699	-5604.1274	3054.3545	1.1629
160.0	982.6886	-5604.4316	3054.2629	1.1870
161.0	983.8340	-5604.7251	3054.1587	1.2150
162.0	985.0098	-5605.0073	3054.0405	1.2410

Table A1 -   t Position and Speed in ECF Coordinates (Cont'd.)

TALO (s)	XPOS (km)	YPOS (km)	ZPOS (km)	Speed (km/s)
163.0	986.2138	-5605.2773	3053.9084	1.2699
164.0	987.4487	-5605.5342	3053.7612	1.2994
165.0	988.7141	-5605.7832	3053.6016	1.3293
166.0	990.0113	-5606.0117	3053.4226	1.3604
167.0	991.3406	-5606.2241	3053.2263	1.3912
168.0	992.7012	-5606.4209	3053.0127	1.4257
169.0	994.0965	-5606.5996	3052.7810	1.4584
170.0	995.5242	-5606.7598	3052.5300	1.4924
171.0	996.9849	-5606.9014	3052.2595	1.5285
172.0	998.4808	-5607.0229	3051.9695	1.5648
173.0	1000.0110	-5607.1235	3051.6582	1.5995
174.0	1001.5737	-5607.2026	3051.3264	1.6363
175.0	1003.1703	-5607.2603	3050.9731	1.6711
176.0	1004.7986	-5607.2949	3050.5991	1.7048
177.0	1006.4571	-5607.3076	3050.2041	1.7366
178.0	1008.1432	-5607.2979	3049.7888	1.7710
179.0	1009.8595	-5607.2651	3049.3530	1.8003
180.0	1011.5999	-5607.2075	3048.8962	1.8283
181.0	1013.3640	-5607.1318	3048.4224	1.8559
182.0	1015.1500	-5607.0303	3047.9280	1.8686
183.0	1016.9449	-5606.9146	3047.4216	1.8698

Table A2 - Rocket Aspect Angle, Attack Angle, and Range from Satellite

TALO (s)	Attack Angle (deg)	Aspect Angle (deg)	Target Range (km)
0.0	0.458	76.130	1254.188
1.0	0.594	75.710	1248.018
2.0	0.721	77.220	1241.847
3.0	3.218	79.060	1235.675
4.0	4.135	80.340	1229.505
5.0	1.804	77.770	1223.337
6.0	2.017	79.910	1217.177
7.0	1.387	79.690	1211.027
8.0	1.497	80.100	1204.889
9.0	2.027	80.500	1198.762
10.0	2.008	80.800	1192.646
11.0	5.466	75.930	1186.542
12.0	13.190	70.420	1180.447
13.0	10.524	69.670	1174.357
14.0	10.328	69.170	1168.266
15.0	7.682	69.460	1162.174
16.0	4.850	69.000	1156.079
17.0	4.425	68.310	1149.974
18.0	4.199	68.100	1143.871

Table A2 - Rocket Aspect Angle, Attack Angle, and Range from Satellite (Cont'd.)

TALO (s)	Attack Angle (deg)	Aspect Angle (deg)	Target Range (km)
19.0	3.878	67.910	1137.771
20.0	3.775	67.650	1131.672
21.0	3.524	67.490	1125.576
22.0	3.323	67.310	1119.480
23.0	3.104	67.230	1113.386
24.0	3.276	67.070	1107.292
25.0	3.425	67.010	1101.197
26.0	4.316	66.930	1095.100
27.0	4.228	66.800	1088.999
28.0	3.715	66.430	1082.894
29.0	3.440	66.190	1076.784
30.0	2.751	66.030	1070.668
31.0	2.502	65.840	1064.544
32.0	1.862	65.770	1058.412
33.0	1.372	65.750	1052.270
34.0	1.274	65.770	1046.117
35.0	1.737	65.750	1039.954
36.0	1.469	65.540	1033.786
37.0	0.313	65.040	1027.623
38.0	1.616	64.840	1021.465
39.0	1.344	64.730	1015.312
40.0	1.376	64.620	1009.168
41.0	0.618	64.420	1003.033
42.0	0.232	64.330	996.910
43.0	0.727	64.150	990.799
44.0	0.462	64.000	984.702
45.0	1.430	63.890	978.618
46.0	3.112	63.790	972.549
47.0	2.087	63.600	966.495
48.0	1.986	63.440	960.457
49.0	2.206	63.230	954.435
50.0	2.173	63.060	948.429
51.0	2.162	62.870	942.439
52.0	1.665	62.650	936.466
53.0	1.729	62.580	930.510
54.0	1.770	62.440	924.571
55.0	1.623	62.230	918.648
56.0	1.596	62.030	912.743
57.0	1.655	61.780	906.857
58.0	1.610	61.330	900.989
59.0	1.508	61.350	895.139
60.0	1.638	61.140	889.308
61.0	1.379	60.680	883.496
62.0	1.355	60.800	877.703
63.0	1.665	60.340	871.931

Table A2 - Rocket Aspect Angle, Attack Angle, and Range from Satellite (Cont'd.)

TALO (s)	Attack Angle (deg)	Aspect Angle (deg)	Target Range (km)
64.0	1.234	60.090	866.179
65.0	1.030	60.110	860.448
66.0	1.195	59.850	854.737
67.0	1.694	59.240	849.049
68.0	1.595	59.420	843.383
69.0	1.023	58.740	837.739
70.0	0.716	57.990	832.117
71.0	0.833	58.260	826.520
72.0	0.966	58.570	820.946
73.0	0.884	58.130	815.397
74.0	0.557	57.110	809.873
75.0	0.249	56.870	804.374
76.0	0.234	56.860	798.902
77.0	0.174	56.730	793.455
78.0	0.271	56.350	788.036
79.0	0.347	55.750	782.645
80.0	0.701	55.600	777.282
81.0	1.084	55.910	771.948
82.0	1.110	56.280	766.643
83.0	0.824	55.730	761.369
84.0	0.532	54.720	756.125
85.0	0.417	53.830	750.913
86.0	0.512	53.990	745.733
87.0	0.611	53.970	740.586
88.0	0.740	53.700	735.473
89.0	0.887	53.220	730.394
90.0	1.069	52.590	725.350
91.0	1.286	52.030	720.342
92.0	1.544	51.900	715.371
93.0	1.738	51.690	710.436
94.0	1.936	51.340	705.540
95.0	2.138	50.840	700.683
96.0	2.411	50.840	695.866
97.0	2.650	51.320	691.090
98.0	4.497	50.460	686.353
99.0	4.879	49.160	681.652
100.0	4.665	48.750	676.984
101.0	4.442	48.460	672.351
102.0	4.246	48.210	667.754
103.0	4.068	47.980	663.193
104.0	3.900	47.780	658.669
105.0	3.738	47.610	654.184
106.0	3.604	47.460	649.737
107.0	3.323	47.360	645.331
108.0	3.104	47.110	640.965

Table A2 - Rocket Aspect Angle, Attack Angle, and Range from Satellite (Cont'd.)

TALO (s)	Attack Angle (deg)	Aspect Angle (deg)	Target Range (km)
109.0	2.953	46.850	636.640
110.0	2.791	46.620	632.356
111.0	2.631	46.400	628.115
112.0	2.471	46.210	623.915
113.0	2.308	46.050	619.757
114.0	2.152	45.900	615.643
115.0	1.971	45.710	611.572
116.0	1.655	45.580	607.546
117.0	0.954	45.610	603.564
118.0	0.333	45.530	599.627
119.0	0.475	45.450	595.735
120.0	1.077	45.430	591.889
121.0	1.701	45.470	588.091
122.0	2.307	45.570	584.339
123.0	2.894	45.770	580.636
124.0	3.475	46.060	576.982
125.0	4.044	46.370	573.377
126.0	4.609	46.540	569.823
127.0	5.138	46.740	566.319
128.0	5.673	47.000	562.867
129.0	6.192	47.190	559.468
130.0	6.710	47.430	556.122
131.0	7.228	47.760	552.832
132.0	7.746	48.050	549.598
133.0	8.270	48.340	546.422
134.0	8.808	48.670	543.306
135.0	11.312	50.230	540.251
136.0	12.778	50.680	537.259
137.0	13.303	51.030	534.332
138.0	14.086	51.490	531.477
139.0	15.288	51.990	528.697
140.0	16.033	52.290	525.994
141.0	16.104	52.390	523.370
142.0	16.457	52.480	520.824
143.0	17.199	52.860	518.359
144.0	15.982	52.430	515.969
145.0	15.866	52.640	513.650
146.0	16.373	53.210	511.403
147.0	16.821	53.700	509.228
148.0	17.261	54.020	507.126
149.0	17.699	54.060	505.098
150.0	18.134	54.050	503.146
151.0	18.588	54.100	501.270
152.0	19.039	54.230	499.470
153.0	19.520	54.090	497.749

Table A2 - Rocket Aspect Angle, Attack Angle, and Range from Satellite (Cont'd.)

TALO (s)	Attack Angle (deg)	Aspect Angle (deg)	Target Range (km)
154.0	19.983	54.130	496.107
155.0	20.427	54.850	494.543
156.0	20.867	57.040	493.059
157.0	21.284	61.680	491.655
158.0	21.695	68.710	490.331
159.0	22.083	75.760	489.087
160.0	22.733	82.620	487.924
161.C	23.148	86.780	486.842
162.0	23.530	89.510	485.841
163.0	22.018	91.200	484.922
164.0	24.846	92.050	484.085
165.0	25.187	92.720	483.326
166.0	25.488	92.850	482.655
167.0	25.634	92.900	482.066
168.0	25.776	92.630	481.562
169.0	25.943	92.480	481.140
170.0	26.090	92.200	480.803
171.0	26.244	91.730	480.549
172.0	26.423	91.350	480.379
173.0	26.599	90.940	480.293
174.0	26.811	90.390	480.292
175.0	27.054	89.880	480.375
176.0	27.336	89.340	480.543
177.0	27.646	88.730	480.796
178.0	28.894	88.070	481.134
179.0	31.336	87.320	481.557
180.0	31.645	84.530	482.067
181.0	32.123	83.610	482.659
182.0	33.012	82.920	483.340
183.0	33.587	82.310	484.105

Table A3 - Rocket Altitude, Geodetic Latitude, and Longitude

TALO (s)	Altitude (km)	Longitude (deg)	Latitude (deg)
0.0	0.023	279.444	28.510
1.0	0.069	279.444	28.510
2.0	0.166	279.444	28.510
3.0	0.321	279.445	28.510
4.0	0.534	279.446	28.510
5.0	0.803	279.446	28.510
6.0	1.093	279.448	28.510
7.0	1.370	279.449	28.510

Table A3 - Rocket Altitude, Geodetic Latitude, and Longitude (Cont.'d)

TALO (s)	Altitude (km)	Longitude (deg)	Latitude (deg)
8.0	1.635	279.450	28.510
9.0	1.887	279.451	28.510
10.0	2.127	279.452	28.510
11.0	2.356	279.453	28.510
12.0	2.574	279.454	28.510
13.0	2.799	279.455	28.510
14.0	3.051	279.456	28.510
15.0	3.328	279.457	28.510
16.0	3.629	279.458	28.510
17.0	3.952	279.459	28.510
18.0	4.296	279.460	28.510
19.0	4.661	279.461	28.509
20.0	5.046	279.462	28.509
21.0	5.453	279.463	28.509
22.0	5.881	279.465	28.509
23.0	6.332	279.466	28.509
24.0	6.807	279.467	28.508
25.0	7.307	279.469	28.508
26.0	7.834	279.470	28.508
27.0	8.389	279.471	28.508
28.0	8.976	279.473	28.507
29.0	9.595	279.474	28.507
30.0	10.248	279.476	28.507
31.0	10.937	279.477	28.507
32.0	11.665	279.479	28.506
33.0	12.434	279.480	28.506
34.0	13.247	279.482	28.505
35.0	14.105	279.483	28.505
36.0	15.009	279.485	28.504
37.0	15.936	279.487	28.504
38.0	16.870	279.489	28.503
39.0	17.806	279.491	28.503
40.0	18.740	279.493	28.502
41.0	19.671	279.495	28.502
42.0	20.594	279.497	28.501
43.0	21.510	279.499	28.501
44.0	22.417	279.501	28.500
45.0	23.313	279.503	28.500
46.0	24.199	279.505	28.499
47.0	25.073	279.507	28.499
48.0	25.936	279.509	28.498
49.0	26.787	279.510	28.498
50.0	27.627	279.512	28.497
51.0	28.455	279.514	28.497
52.0	29.272	279.516	28.496

Table A3 - Rocket Altitude, Geodetic Latitude, and Longitude (Cont.'d)

TALO (s)	Altitude (km)	Longitude (deg)	Latitude (deg)
53.0	30.077	279.518	28.496
54.0	30.872	279.520	28.495
55.0	31.656	279.522	28.495
56.0	32.430	279.524	28.495
57.0	33.193	279.526	28.494
58.0	33.946	279.528	28.494
59.0	34.688	279.530	28.493
60.0	35.420	279.532	28.493
61.0	36.142	279.534	28.492
62.0	36.854	279.536	28.492
63.0	37.555	279.538	28.491
64.0	38.247	279.540	28.491
65.0	38.929	279.542	28.490
66.0	39.601	279.544	28.490
67.0	40.262	279.546	28.489
68.0	40.915	279.548	28.489
69.0	41.557	279.550	28.488
70.0	42.189	279.552	28.488
71.0	42.812	279.554	28.487
72.0	43.424	279.556	28.487
73.0	44.027	279.558	28.486
74.0	44.621	279.560	28.486
75.0	45.204	279.562	28.485
76.0	45.778	279.564	28.485
77.0	46.342	279.566	28.484
78.0	46.896	279.568	28.484
79.0	47.441	279.570	28.483
80.0	47.976	279.572	28.483
81.0	48.501	279.574	28.482
82.0	49.017	279.576	28.482
83.0	49.523	279.578	28.481
84.0	50.019	279.580	28.481
85.0	50.505	279.582	28.480
86.0	50.982	279.584	28.480
87.0	51.449	279.586	28.480
88.0	51.907	279.588	28.479
89.0	52.355	279.590	28.479
90.0	52.793	279.592	28.478
91.0	53.222	279.594	28.478
92.0	53.641	279.596	28.477
93.0	54.050	279.597	28.477
94.0	54.450	279.599	28.476
95.0	54.840	279.601	28.476
96.0	55.221	279.603	28.475
97.0	55.592	279.605	28.475

Table A3 - Rocket Altitude, Geodetic Latitude, and Longitude (Cont.'d)

TALO (s)	Altitude (km)	Longitude (deg)	Latitude (deg)
98.0	55.956	279.607	28.474
99.0	56.324	279.609	28.474
100.0	56.696	279.611	28.473
101.0	57.072	279.614	28.473
102.0	57.454	279.616	28.472
103.0	57.839	279.618	28.471
104.0	58.228	279.621	28.471
105.0	58.620	279.623	28.470
106.0	59.016	279.625	28.470
107.0	59.415	279.628	28.469
108.0	59.816	279.631	28.468
109.0	60.222	279.633	28.468
110.0	60.631	279.636	28.467
111.0	61.045	279.639	28.466
112.0	61.464	279.642	28.465
113.0	61.888	279.645	28.465
114.0	62.318	279.648	28.464
115.0	62.753	279.651	28.463
116.0	63.195	279.655	28.462
117.0	63.643	279.658	28.461
118.0	64.098	279.662	28.460
119.0	64.560	279.666	28.459
120.0	65.029	279.669	28.458
121.0	65.504	279.673	28.457
122.0	65.987	279.678	28.456
123.0	66.476	279.682	28.455
124.0	66.972	279.686	28.454
125.0	67.474	279.691	28.452
126.0	67.983	279.696	28.451
127.0	68.498	279.701	28.450
128.0	69.020	279.706	28.448
129.0	69.547	279.711	28.447
130.0	70.078	279.717	28.446
131.0	70.614	279.722	28.444
132.0	71.154	279.728	28.443
133.0	71.695	279.734	28.441
134.0	72.238	279.740	28.439
135.0	72.782	279.746	28.438
136.0	73.325	279.753	28.436
137.0	73.866	279.759	28.434
138.0	74.400	279.766	28.432
139.0	74.924	279.773	28.431
140.0	75.440	279.779	28.429
141.0	75.946	279.786	28.427
142.0	76.442	279.793	28.425

Table A3 - Rocket Altitude, Geodetic Latitude, and Longitude (Cont.'d)

TALO (s)	Altitude (km)	Longitude (deg)	Latitude (deg)
143.0	76.930	279.799	28.424
144.0	77.412	279.806	28.422
145.0	77.892	279.813	28.420
146.0	78.370	279.820	28.418
147.0	78.845	279.828	28.416
148.0	79.317	279.835	28.414
149.0	79.785	279.843	28.412
150.0	80.249	279.851	28.410
151.0	80.708	279.860	28.407
152.0	81.162	279.868	28.405
153.0	81.609	279.877	28.403
154.0	82.050	279.886	28.401
155.0	82.484	279.895	28.398
156.0	82.910	279.905	28.396
157.0	83.328	279.914	28.393
158.0	83.737	279.924	28.390
159.0	84.137	279.935	28.388
160.0	84.527	279.945	28.385
161.0	84.906	279.956	28.382
162.0	85.273	279.967	28.379
163.0	85.628	279.979	28.376
164.0	85.969	279.991	28.373
165.0	86.302	280.003	28.370
166.0	86.613	280.015	28.366
167.0	86.908	280.028	28.363
168.0	87.185	280.041	28.359
169.0	87.444	280.055	28.356
170.0	87.684	280.068	28.352
171.0	87.903	280.083	28.348
172.0	88.101	280.097	28.344
173.0	88.277	280.112	28.340
174.0	88.429	280.128	28.336
175.0	88.559	280.143	28.332
176.0	88.664	280.159	28.328
177.0	88.745	280.176	28.323
178.0	88.802	280.192	28.319
179.0	88.835	280.209	28.314
180.0	88.840	280.227	28.310
181.0	88.826	280.244	28.305
182.0	88.783	280.262	28.300
183.0	88.725	280.280	28.295

Appendix B

UVPI PARAMETERS

This appendix collects parameters and information that are useful to analyze the data by using different assumptions for the source spectrum. The average number of photoevents per second for each of the intervals analyzed in this report is recorded in Table B1. Table B2 lists the net quantum efficiency in 5-nm steps for the tracker camera, and Table B3 lists plume-camera net quantum efficiency for each of the four filters.

Tables B4 and B5 list the digital number per photoevent values for the tracker and plume cameras, respectively.

A scaled version of the beacon's point spread function (PSF) for the plume camera is presented in Table B6 in the form of a 16 by 16 pixel array. The intensity values are scaled such that the brightest pixel will map to 1. A row representative of the full-width-half-maximum is highlighted by a bold box. For the ground-based beacon, the equivalent full-width-half-maximum of the PSF along the major axis is about 40 m at a range of 450 km. A similar array for the tracker camera's PSF is presented in Table B7.

Finally, Table B8 is a list of all frames recorded for this encounter. The time and frame number are recorded in the first two columns. Note that the frame number carries a trailing P if it is a plume-camera frame and a trailing T if it is a tracker-camera frame. The third column lists the filter wheel position if it is a plume-camera frame. A filter wheel position of 0 denotes a tracker-camera frame. The next two columns indicate the exposure time for the frame. For the plume camera this is fixed at $^1/_{30}$th of a second, but for the tracker camera it is variable, with a maximum allowed value of $^1/_{30}$th second. The next two columns list the tracker camera and plume camera gain steps.

For the zoom image transmission rate, 30 Hz, each telemetry frame carries one image. For the normal image transmission rate, 5 Hz, six telemetry frames carry one image.

UVPI mission time (UMT) is related to GMT at launch for the Starbird observation pass by the equation

$$UMT = GMT + (0.26 + Frame \times 1.23 \times 10^{-5}) \text{ s}$$

Table B1 - Average Number of Photoevents/s

Interval	Stage	Filter	Plume Camera		Tracker Camera	
			Bandpass (nm)	Photoevents/s	Bandpass (nm)	Photoevents/s*
1	3	PC-4	235-350	4.29×10^3	255-450	1.07×10^5
2	3	PC-3	195-295	1.78×10^2	255-450	1.23×10^5
3	3	PC-2	300-320	3.89×10^2	255-450	1.26×10^5
4	3	PC-1	200-320	3.36×10^2	255-450	8.22×10^4
5	4	PC-1	200-320	4.94×10^2	255-450	9.89×10^4
6	4	PC-2	300-320	3.19×10^2	255-450	1.30×10^5
7	4	PC-3	195-295	2.21×10^2	255-450	1.59×10^5

* For central 19 x 19 pixels

Table B2 - Net Quantum Efficiency for Tracker Camera

Wavelength (nm)	Tracker NQE	Wavelength (nm)	Tracker NQE
255	.00001	355	.020003
260	.000588	360	.018705
265	.00181	365	.018683
270	.003983	370	.018225
275	.005878	375	.01797
280	.0073	380	.018615
285	.008858	385	.019058
290	.008895	390	.018285
295	.010898	395	.01881
300	.01209	400	.018833
305	.014025	405	.017865
310	.014978	410	.018083
315	.012263	415	.016418
320	.01428	420	.016418
325	.017858	425	.016148
330	.017355	430	.016148
335	.015248	435	.013883
340	.011235	440	.010988
345	.014745	445	.00179
350	.017145	450	8.75E-5

Table B3 - Net Quantum Efficiency for Plume Camera

Wavelength (nm)	PC-1	PC-2	PC-3	PC-4
195	0	0	6.16E-05	0
200	0	0	0.000129	0
205	0	0	0.000217	0
210	0	0	0.000328	0
215	0	0	0.000464	0
220	0.000015	0	0.00071	0
225	3.75E-05	0	0.001079	0
230	0.000075	0	0.001547	0
235	9.25E-05	0	0.002091	0.000119
240	0.0002	0	0.00247	0.000676
245	0.000385	0	0.002735	0.00198
250	0.00088	0	0.002842	0.003519
255	0.001873	0	0.002696	0.004933
260	0.003798	0	0.002415	0.006923
265	0.00546	0	0.00168	0.007535
270	0.006063	0	0.001124	0.009322
275	0.005303	0	0.000638	0.012336
280	0.003808	0	0.000345	0.013118
285	0.00211	0	0.000183	0.013089
290	0.001028	0	0.000123	0.01192
295	0.00048	0	5.13E-05	0.010684
300	0.000208	5.33E-05	0	0.009051

Table B3 - Net Quantum Efficiency for Plume Camera (Cont'd.)

Wavelength (nm)	PC-1	PC-2	PC-3	PC-4
305	0.000095	0.001816	0	0.007641
310	5.25E-05	0.001597	0	0.006131
315	0.000015	0.000906	0	0.004956
320	0.000005	2.08E-05	0	0.003767
325	0	0	0	0.002663
330	0	0	0	0.001745
335	0	0	0	0.000985
340	0	0	0	0.000412
345	0	0	0	0.000119
350	0	0	0	3.22E-06

Table B4 - Gain Conversion Factor G_g for Tracker Camera

Gain Step g	Gain Conversion Factor G_g (digital number per photoevent)
0	.001904
1	.00366
2	.007906
3	.016691
4	.034848
5	.079651
6	.149346
7	.279667
8	.612008
9	1.194808
10	2.298668
11	4.875681
12	10.15084
13	25.43053
14	45.58302
15	120.795

Table B5 - Gain Conversion Factor G_g for Plume Camera

Gain Step g	Gain Conversion Factor G_g (digital number per photoevent)
0	.026987
1	.037107
2	.067467
3	.104575
4	.168667
5	.377868
6	.951453
7	2.285832
8	5.129954
9	10.80777
10	23.19167
11	39.75714
12	77.57491
13	143.6387
14	221.3121
15	292.9474

Table B6 - Scaled Version of Plume Camera PSF Based on Ground Beacon

0.139	0.153	0.125	0.116	0.111	0.125	0.130	0.134	0.144	0.167	0.134	0.111	0.102	0.093	0.074	0.074
0.093	0.111	0.102	0.106	0.111	0.125	0.139	0.148	0.200	0.237	0.209	0.158	0.116	0.097	0.097	0.069
0.106	0.102	0.102	0.102	0.116	0.144	0.186	0.213	0.246	0.251	0.241	0.195	0.158	0.125	0.097	0.079
0.106	0.097	0.093	0.111	0.120	0.167	0.241	0.316	0.404	0.395	0.386	0.293	0.200	0.116	0.102	0.069
0.120	0.102	0.097	0.120	0.144	0.204	0.367	0.525	0.534	0.581	0.67	0.469	0.237	0.134	0.116	0.097
0.074	0.083	0.097	0.111	0.134	0.241	0.511	0.762	0.730	0.804	0.800	0.613	0.376	0.181	0.111	0.083
0.083	0.088	0.102	0.120	0.144	0.260	0.627	0.804	0.869	0.958	0.855	0.623	0.506	0.265	0.148	0.111
0.069	0.093	0.097	0.120	0.181	0.344	0.734	0.925	1.000	0.995	0.920	0.720	0.511	0.283	0.153	0.097
0.065	0.079	0.102	0.130	0.209	0.400	0.609	0.823	0.888	0.874	0.827	0.660	0.367	0.209	0.120	0.097
0.079	0.079	0.093	0.120	0.172	0.316	0.516	0.697	0.744	0.609	0.613	0.437	0.209	0.148	0.111	0.106
0.065	0.069	0.097	0.120	0.134	0.246	0.479	0.651	0.479	0.413	0.362	0.274	0.162	0.139	0.093	0.083
0.060	0.065	0.079	0.088	0.116	0.186	0.404	0.441	0.288	0.260	0.223	0.186	0.139	0.125	0.097	0.079
0.079	0.074	0.083	0.079	0.106	0.148	0.237	0.218	0.218	0.181	0.167	0.148	0.116	0.097	0.088	0.069
0.074	0.074	0.079	0.088	0.079	0.111	0.167	0.144	0.167	0.153	0.139	0.130	0.083	0.083	0.069	0.065
0.060	0.060	0.074	0.074	0.088	0.097	0.134	0.116	0.116	0.106	0.097	0.088	0.083	0.069	0.065	0.065
0.046	0.065	0.065	0.069	0.083	0.079	0.083	0.093	0.097	0.093	0.079	0.079	0.079	0.079	0.065	0.069

Table B7 - Scaled Version of Tracker Camera PSF Based on Ground Beacon

0.036	0.041	0.036	0.023	0.037	0.039	0.034	0.056	0.030	0.024	0.036	0.001	0.036	0.008	0.047	0.021
0.012	0.035	0.017	0.026	0.037	0.034	0.039	0.019	0.032	0.008	0.051	0.003	0.042	0.000	0.029	0.025
0.047	0.016	0.018	0.027	0.043	0.026	0.036	0.033	0.022	0.013	0.058	0.034	0.024	0.035	0.027	0.032
0.044	0.024	0.028	0.052	0.035	0.052	0.054	0.024	0.034	0.016	0.037	0.032	0.028	0.061	0.037	0.041
0.045	0.033	0.034	0.038	0.029	0.047	0.015	0.064	0.049	0.036	0.082	0.028	0.042	0.028	0.068	0.015
0.045	0.001	0.061	0.028	0.063	0.059	0.054	0.057	0.083	0.056	0.061	0.017	0.042	0.029	0.036	0.026
0.036	0.058	0.043	0.060	0.047	0.050	0.074	0.126	0.108	0.042	0.027	0.036	0.043	0.026	0.046	0.033
0.037	0.028	0.026	0.041	0.055	0.049	0.212	0.986	0.511	0.081	0.069	0.051	0.033	0.026	0.027	0.015
0.050	0.032	0.037	0.052	0.037	0.087	0.227	1.000	0.535	0.092	0.076	0.034	0.016	0.044	0.010	0.030
0.053	0.017	0.036	0.027	0.021	0.051	0.055	0.141	0.105	0.055	0.067	0.040	0.026	0.032	0.021	0.097
0.010	0.032	0.032	0.059	0.025	0.049	0.070	0.075	0.039	0.040	0.035	0.032	0.036	0.036	0.021	0.032
0.030	0.030	0.036	0.016	0.027	0.050	0.034	0.042	0.039	0.022	0.046	0.031	0.037	0.017	0.029	0.015
0.028	0.025	0.034	0.020	0.053	0.033	0.059	0.029	0.039	0.042	0.053	0.052	0.036	0.043	0.045	0.026
0.046	0.034	0.042	0.042	0.042	0.025	0.045	0.051	0.056	0.018	0.036	0.018	0.013	0.029	0.037	0.041
0.043	0.027	0.026	0.023	0.044	0.041	0.036	0.028	0.006	0.027	0.033	0.035	0.053	0.035	0.053	0.040
0.042	0.031	0.027	0.056	0.061	0.024	0.055	0.027	0.040	0.015	0.040	0.027	0.028	0.028	0.037	0.017

Table B8 - Telemetry Frames and Camera Parameters

UMT	Telemetry Frame	Filter	Tracker Exp. Time (ms)	Plume Exp. Time (ms)	Tracker Gain Step	Plume Gain Step	Comments
3:39:21.07	13543P	4	8.600	33.3	9	11	Begin data interval 1, PC 4
3:39:21.10	13544P	4	8.600	33.3	9	11	
3:39:21.14	13545P	4	8.600	33.3	9	11	
3:39:21.17	13546P	4	8.600	33.3	9	11	
3:39:21.20	13547P	4	8.600	33.3	9	11	
3:39:21.24	13548P	4	8.600	33.3	9	11	
3:39:21.27	13549P	4	8.600	33.3	9	11	
3:39:21.30	13550P	4	8.600	33.3	9	11	
3:39:21.34	13551T	0	8.600	33.3	9	11	
3:39:21.37	13552T	0	8.600	33.3	9	11	
3:39:21.40	13553P	4	8.600	33.3	9	11	
3:39:21.44	13554P	4	8.600	33.3	9	11	
3:39:21.47	13555P	4	8.600	33.3	9	11	
3:39:21.50	13556P	4	8.600	33.3	9	11	
3:39:21.54	13557P	4	8.600	33.3	9	11	
3:39:21.57	13558P	4	8.600	33.3	9	11	
3:39:21.60	13559P	4	8.600	33.3	9	11	
3:39:21.64	13560P	4	8.600	33.3	9	11	
3:39:21.67	13561T	0	8.600	33.3	9	11	
3:39:21.71	13562T	0	8.600	33.3	9	11	

Table B8 - Telemetry Frames and Camera Parameters (Cont.'d)

UMT	Telemetry Frame	Filter	Tracker Exp. Time (ms)	Plume Exp. Time (ms)	Tracker Gain Step	Plume Gain Step	Comments
3:39:21.74	13563P	4	8.600	33.3	9	11	
3:39:21.77	13564P	4	8.600	33.3	9	11	
3:39:21.81	13565P	4	8.600	33.3	9	11	
3:39:21.84	13566P	4	8.600	33.3	9	11	
3:39:21.87	13567P	4	8.600	33.3	9	11	
3:39:21.91	13568P	4	8.600	33.3	9	11	
3:39:21.94	13569P	4	8.600	33.3	9	11	
3:39:21.97	13570P	4	8.600	33.3	9	11	
3:39:22.01	13571T	0	8.600	33.3	9	11	
3:39:22.04	13572T	0	8.600	33.3	9	11	
3:39:22.07	13573P	4	8.600	33.3	9	11	
3:39:22.11	13574P	4	8.600	33.3	9	11	
3:39:22.14	13575P	4	8.600	33.3	9	11	
3:39:22.17	13576P	4	8.600	33.3	9	11	
3:39:22.21	13577P	4	8.600	33.3	9	11	
3:39:22.24	13578P	4	8.600	33.3	9	11	
3:39:22.27	13579P	4	8.600	33.3	9	11	
3:39:22.31	13580P	4	8.600	33.3	9	11	
3:39:22.34	13581T	0	8.600	33.3	9	11	
3:39:22.37	13582T	0	8.600	33.3	9	11	
3:39:22.41	13583P	4	8.600	33.3	9	11	
3:39:22.44	13584P	4	8.600	33.3	9	11	
3:39:22.47	13585P	4	8.600	33.3	9	11	
3:39:22.51	13586P	4	8.600	33.3	9	11	
3:39:22.54	13587P	4	8.600	33.3	9	11	
3:39:22.57	13588P	4	8.600	33.3	9	11	
3:39:22.61	13589P	4	8.600	33.3	9	11	
3:39:22.64	13590P	4	8.600	33.3	9	11	
3:39:22.67	13591T	0	8.600	33.3	9	11	
3:39:22.71	13592T	0	8.600	33.3	9	11	
3:39:22.74	13593P	4	8.600	33.3	9	11	
3:39:22.77	13594P	4	8.600	33.3	9	11	
3:39:22.81	13595P	4	8.600	33.3	9	11	
3:39:22.84	13596P	4	8.600	33.3	9	11	
3:39:22.87	13597P	4	8.600	33.3	9	11	
3:39:22.91	13598P	4	8.600	33.3	9	11	
3:39:22.94	13599P	4	8.600	33.3	9	11	
3:39:22.97	13600P	4	8.600	33.3	9	11	
3:39:23.01	13601T	0	8.600	33.3	9	11	
3:39:23.04	13602T	0	8.600	33.3	9	11	
3:39:23.07	13603P	4	8.600	33.3	9	11	

Table B8 - Telemetry Frames and Camera Parameters (Cont.'d)

UMT	Telemetry Frame	Filter	Tracker Exp. Time (ms)	Plume Exp. Time (ms)	Tracker Gain Step	Plume Gain Step	Comments
3:39:23.11	13604P	4	8.600	33.3	9	11	
3:39:23.14	13605P	4	8.600	33.3	9	11	
3:39:23.17	13606P	4	8.600	33.3	9	11	
3:39:23.21	13607P	4	8.600	33.3	9	11	
3:39:23.24	13608P	4	8.600	33.3	9	11	
3:39:23.27	13609P	4	8.600	33.3	9	11	
3:39:23.31	13610P	4	8.600	33.3	9	11	
3:39:23.34	13611T	0	8.600	33.3	9	11	
3:39:23.37	13612T	0	8.600	33.3	9	11	
3:39:23.41	13613P	4	8.600	33.3	9	11	
3:39:23.44	13614P	4	8.600	33.3	9	11	
3:39:23.47	13615P	4	8.600	33.3	9	11	
3:39:23.51	13616P	4	8.600	33.3	9	11	
3:39:23.54	13617P	4	8.600	33.3	9	11	
3:39:23.57	13618P	4	8.600	33.3	9	11	
3:39:23.61	13619P	4	8.600	33.3	9	11	
3:39:23.64	13620P	4	8.600	33.3	9	11	
3:39:23.67	13621T	0	8.600	33.3	9	11	
3:39:23.71	13622T	0	8.600	33.3	9	11	
3:39:23.74	13623P	4	8.600	33.3	9	11	
3:39:23.77	13624P	4	8.600	33.3	9	11	
3:39:23.81	13625P	4	8.600	33.3	9	11	
3:39:23.84	13626P	4	8.600	33.3	9	11	
3:39:23.87	13627P	4	8.600	33.3	9	11	
3:39:23.91	13628P	4	8.600	33.3	9	11	
3:39:23.94	13629P	4	8.600	33.3	9	11	
3:39:23.97	13630P	4	8.600	33.3	9	11	
3:39:24.01	13631T	0	8.600	33.3	9	11	
3:39:24.04	13632T	0	8.600	33.3	9	11	
3:39:24.07	13633P	4	8.600	33.3	9	11	
3:39:24.11	13634P	4	8.600	33.3	9	11	
3:39:24.14	13635P	4	8.600	33.3	9	11	
3:39:24.17	13636P	4	8.600	33.3	9	11	
3:39:24.21	13637P	4	8.600	33.3	9	11	
3:39:24.24	13638P	4	8.600	33.3	9	11	
3:39:24.28	13639P	4	8.600	33.3	9	11	
3:39:24.31	13640P	4	8.600	33.3	9	11	
3:39:24.34	13641T	0	8.600	33.3	9	11	
3:39:24.37	13642T	0	8.600	33.3	9	11	
3:39:24.41	13643P	4	8.600	33.3	9	11	
3:39:24.44	13644P	4	8.600	33.3	9	11	

Table B8 - Telemetry Frames and Camera Parameters (Cont.'d)

UMT	Telemetry Frame	Filter	Tracker Exp. Time (ms)	Plume Exp. Time (ms)	Tracker Gain Step	Plume Gain Step	Comments
3:39:24.48	13645P	4	8.600	33.3	9	11	
3:39:24.51	13646P	4	8.600	33.3	9	11	
3:39:24.54	13647P	4	8.600	33.3	9	11	
3:39:24.57	13648P	4	8.600	33.3	9	11	
3:39:24.61	13649P	4	8.600	33.3	9	11	
3:39:24.64	13650P	4	8.600	33.3	9	11	
3:39:24.68	13651T	0	8.600	33.3	9	11	
3:39:24.71	13652T	0	8.600	33.3	9	11	
3:39:24.74	13653P	4	8.600	33.3	9	11	
3:39:24.78	13654P	4	8.600	33.3	9	11	
3:39:24.81	13655P	4	8.600	33.3	9	11	
3:39:24.84	13656P	4	8.600	33.3	9	11	
3:39:24.88	13657P	4	8.600	33.3	9	11	
3:39:24.91	13658P	4	8.600	33.3	9	11	
3:39:24.94	13659P	4	8.600	33.3	9	11	
3:39:24.98	13660P	4	8.600	33.3	9	11	
3:39:25.01	13661T	0	8.600	33.3	9	11	
3:39:25.04	13662T	0	8.600	33.3	9	11	
3:39:25.08	13663P	4	8.600	33.3	9	11	
3:39:25.11	13664P	4	8.600	33.3	9	11	
3:39:25.14	13665P	4	8.600	33.3	9	11	
3:39:25.18	13666P	4	8.600	33.3	9	11	
3:39:25.21	13667P	4	8.600	33.3	9	11	
3:39:25.24	13668P	4	8.600	33.3	9	11	
3:39:25.28	13669P	4	8.600	33.3	9	11	
3:39:25.31	13670P	4	8.600	33.3	9	11	
3:39:25.34	13671T	0	8.600	33.3	9	11	
3:39:25.38	13672T	0	8.600	33.3	9	11	
3:39:25.41	13673P	4	8.600	33.3	9	11	
3:39:25.44	13674P	4	8.600	33.3	9	11	
3:39:25.48	13675P	4	8.600	33.3	9	11	
3:39:25.51	13676P	4	8.600	33.3	9	11	
3:39:25.54	13677P	4	8.600	33.3	9	11	
3:39:25.58	13678P	4	8.600	33.3	9	11	
3:39:25.61	13679P	4	8.600	33.3	9	11	
3:39:25.64	13680P	4	8.600	33.3	9	11	
3:39:25.68	13681T	0	8.600	33.3	9	11	
3:39:25.71	13682T	0	8.600	33.3	9	11	
3:39:25.74	13683P	4	8.600	33.3	9	11	
3:39:25.78	13684P	4	8.600	33.3	9	11	
3:39:25.81	13685P	4	8.600	33.3	9	11	

Table B8 - Telemetry Frames and Camera Parameters (Cont.'d)

UMT	Telemetry Frame	Filter	Tracker Exp. Time (ms)	Plume Exp. Time (ms)	Tracker Gain Step	Plume Gain Step	Comments
3:39:25.84	13686P	4	8.600	33.3	9	11	
3:39:25.88	13687P	4	8.600	33.3	9	11	
3:39:25.91	13688P	4	8.600	33.3	9	11	
3:39:25.94	13689P	4	8.600	33.3	9	11	
3:39:25.98	13690P	4	8.600	33.3	9	11	
3:39:26.01	13691T	0	8.600	33.3	9	11	
3:39:26.04	13692T	0	8.600	33.3	9	11	
3:39:26.08	13693P	4	8.600	33.3	9	11	
3:39:26.11	13694P	4	8.600	33.3	9	11	
3:39:26.14	13695P	4	8.600	33.3	9	11	
3:39:26.18	13696P	4	8.600	33.3	9	11	
3:39:26.21	13697P	4	8.600	33.3	9	11	
3:39:26.24	13698P	4	8.600	33.3	9	11	
3:39:26.28	13699P	4	8.600	33.3	9	11	
3:39:26.31	13700P	4	8.600	33.3	9	11	
3:39:26.34	13701T	0	8.600	33.3	9	11	
3:39:26.38	13702T	0	8.600	33.3	9	11	
3:39:26.41	13703P	4	8.600	33.3	9	11	
3:39:26.44	13704P	4	8.600	33.3	9	11	
3:39:26.48	13705P	4	8.600	33.3	9	11	
3:39:26.51	13706P	4	8.600	33.3	9	11	
3:39:26.54	13707P	4	8.600	33.3	9	11	
3:39:26.58	13708P	4	8.600	33.3	9	11	
3:39:26.61	13709P	4	8.600	33.3	9	11	
3:39:26.64	13710P	4	8.600	33.3	9	11	
3:39:26.68	13711T	0	8.600	33.3	9	11	
3:39:26.71	13712T	0	8.600	33.3	9	11	
3:39:26.74	13713P	4	8.600	33.3	9	11	
3:39:26.78	13714P	4	8.600	33.3	9	11	
3:39:26.81	13715P	4	8.600	33.3	9	11	
3:39:26.84	13716P	4	8.600	33.3	9	11	
3:39:26.88	13717P	4	8.600	33.3	9	11	
3:39:26.91	13718P	4	8.600	33.3	9	11	
3:39:26.94	13719P	4	8.600	33.3	9	11	
3:39:26.98	13720P	4	8.600	33.3	9	11	
3:39:27.01	13721T	0	8.600	33.3	9	11	
3:39:27.04	13722T	0	8.600	33.3	9	11	
3:39:27.08	13723P	4	8.600	33.3	9	11	
3:39:27.11	13724P	4	8.600	33.3	9	11	
3:39:27.14	13725P	4	8.600	33.3	9	11	
3:39:27.18	13726P	4	8.600	33.3	9	11	

Table B8 - Telemetry Frames and Camera Parameters (Cont.'d)

UMT	Telemetry Frame	Filter	Tracker Exp. Time (ms)	Plume Exp. Time (ms)	Tracker Gain Step	Plume Gain Step	Comments
3:39:27.21	13727P	4	8.600	33.3	9	11	
3:39:27.24	13728P	4	8.600	33.3	9	11	
3:39:27.28	13729P	4	8.600	33.3	9	11	
3:39:27.31	13730P	4	8.600	33.3	9	11	
3:39:27.34	13731T	0	8.600	33.3	9	11	
3:39:27.38	13732T	0	8.600	33.3	9	11	
3:39:27.48	13735P	4	8.600	33.3	9	11	
3:39:27.51	13736P	4	8.600	33.3	9	11	
3:39:27.54	13737P	4	8.600	33.3	9	11	
3:39:27.58	13738P	4	8.600	33.3	9	11	
3:39:27.61	13739P	4	8.600	33.3	9	11	
3:39:27.64	13740P	4	8.600	33.3	9	11	
3:39:27.68	13741T	0	8.600	33.3	9	11	
3:39:27.71	13742T	0	8.600	33.3	9	11	
3:39:27.75	13743P	4	8.600	33.3	9	11	End data interval 1, PC-4
3:39:31.98	13870P	3	15.402	33.3	8	13	Begin data interval 2, PC 3
3:39:32.02	13871T	0	15.402	33.3	8	13	
3:39:32.05	13872T	0	15.402	33.3	8	13	
3:39:32.08	13873P	3	12.200	33.3	8	13	
3:39:32.12	13874P	3	12.200	33.3	8	13	
3:39:32.15	13875P	3	12.200	33.3	8	13	
3:39:32.18	13876P	3	12.200	33.3	8	13	
3:39:32.22	13877P	3	12.200	33.3	8	13	
3:39:32.25	13878P	3	12.200	33.3	8	13	
3:39:32.28	13879P	3	12.200	33.3	8	13	
3:39:32.32	13880P	3	12.200	33.3	8	13	
3:39:32.35	13881T	0	12.200	33.3	8	13	
3:39:32.38	13882T	0	12.200	33.3	8	13	
3:39:32.42	13883P	3	12.200	33.3	8	13	
3:39:32.45	13884P	3	12.200	33.3	8	13	
3:39:32.48	13885P	3	12.200	33.3	8	13	
3:39:32.52	13886P	3	12.200	33.3	8	13	
3:39:32.55	13887P	3	12.200	33.3	8	13	
3:39:32.58	13888P	3	12.200	33.3	8	13	
3:39:32.62	13889P	3	12.200	33.3	8	13	
3:39:32.65	13890P	3	12.200	33.3	8	13	
3:39:32.68	13891T	0	12.200	33.3	8	13	
3:39:32.72	13892T	0	12.200	33.3	8	13	
3:39:32.75	13893P	3	12.200	33.3	8	13	

Table B8 - Telemetry Frames and Camera Parameters (Cont.'d)

UMT	Telemetry Frame	Filter	Tracker Exp. Time (ms)	Plume Exp. Time (ms)	Tracker Gain Step	Plume Gain Step	Comments
3:39:32.78	13894P	3	12.200	33.3	8	13	
3:39:32.82	13895P	3	12.200	33.3	8	13	
3:39:32.85	13896P	3	12.200	33.3	8	13	
3:39:32.88	13897P	3	12.200	33.3	8	13	
3:39:32.92	13898P	3	12.200	33.3	8	13	
3:39:32.95	13899P	3	12.200	33.3	8	13	
3:39:32.98	13900P	3	12.200	33.3	8	13	
3:39:33.02	13901T	0	12.200	33.3	8	13	
3:39:33.05	13902T	0	12.200	33.3	8	13	
3:39:33.08	13903P	3	12.200	33.3	8	13	
3:39:33.12	13904P	3	12.200	33.3	8	13	
3:39:33.15	13905P	3	12.200	33.3	8	13	
3:39:33.18	13906P	3	12.200	33.3	8	13	
3:39:33.22	13907P	3	12.200	33.3	8	13	
3:39:33.25	13908P	3	12.200	33.3	8	13	
3:39:33.28	13909P	3	12.200	33.3	8	13	
3:39.33.32	13910P	3	12.200	33.3	8	13	
3:39:33.35	13911T	0	12.200	33.3	8	13	
3:39:33.39	13912T	0	12.200	33.3	8	13	
3:39:33.42	13913P	3	12.200	33.3	8	13	
3:39:33.45	13914P	3	12.200	33.3	8	13	
3:39:33.49	13915P	3	12.200	33.3	8	13	
3:39:33.52	13916P	3	12.200	33.3	8	13	
3:39:33.55	13917P	3	12.200	33.3	8	13	
3:39:33.59	13918P	3	12.200	33.3	8	13	
3:39:33.62	13919P	3	12.200	33.3	8	13	
3:39:33.65	13920P	3	12.200	33.3	8	13	
3:39:33.69	13921T	0	12.200	33.3	8	13	
3:39:33.72	13922T	0	12.200	33.3	8	13	
3:39:33.75	13923P	3	12.200	33.3	8	13	End data interval 2, PC-3
3:39:35.35	13971T	0	12.200	33.3	8	13	Begin data interval 3, PC 2
3:39:35.39	13972T	0	12.200	33.3	8	13	
3:39:35.42	13973P	2	12.200	33.3	8	13	
3:39:35.45	13974P	2	12.200	33.3	8	13	
3:39:35.49	13975P	2	12.200	33.3	8	13	
3:39:35.52	13976P	2	12.200	33.3	8	13	
3:39:35.55	13977P	2	12.200	33.3	8	13	
3:39:35.59	13978P	2	12.200	33.3	8	13	
3:39:35.62	13979P	2	12.200	33.3	8	13	

Table B8 - Telemetry Frames and Camera Parameters (Cont.'d)

UMT	Telemetry Frame	Filter	Tracker Exp. Time (ms)	Plume Exp. Time (ms)	Tracker Gain Step	Plume Gain Step	Comments
3:39:35.65	13980P	2	12.200	33.3	8	13	
3:39:35.69	13981T	0	12.200	33.3	8	13	
3:39:35.72	13982T	0	12.200	33.3	8	13	
3:39:35.75	13983P	2	12.200	33.3	8	13	
3:39:35.79	13984P	2	12.200	33.3	8	13	
3:39:35.82	13985P	2	12.200	33.3	8	13	
3:39:35.85	13986P	2	12.200	33.3	8	13	
3:39:35.89	13987P	2	12.200	33.3	8	13	
3:39:35.92	13988P	2	12.200	33.3	8	13	
3:39:35.95	13989P	2	12.200	33.3	8	13	
3:39:35.99	13990P	2	12.200	33.3	8	13	
3:39:36.02	13991T	0	12.200	33.3	8	13	
3:39:36.05	13992T	0	12.200	33.3	8	13	
3:39:36.09	13993P	2	12.200	33.3	8	13	
3:39:36.12	13994P	2	12.200	33.3	8	13	
3:39:36.15	13995P	2	12.200	33.3	8	13	
3:39:36.19	13996P	2	12.200	33.3	8	13	
3:39:36.22	13997P	2	12.200	33.3	8	13	
3:39:36.25	13998P	2	12.200	33.3	8	13	
3:39:36.29	13999P	2	12.200	33.3	8	13	
3:39:36.32	14000P	2	12.200	33.3	8	13	
3:39:36.35	14001T	0	12.200	33.3	8	13	
3:39:36.39	14002T	0	12.200	33.3	8	13	
3:39:36.42	14003P	2	12.200	33.3	8	13	
3:39:36.45	14004P	2	12.200	33.3	8	13	
3:39:36.49	14005P	2	12.200	33.3	8	13	
3:39:36.52	14006P	2	12.200	33.3	8	13	
3:39:36.56	14007P	2	12.200	33.3	8	13	
3:39:36.59	14008P	2	12.200	33.3	8	13	
3:39:36.62	14009P	2	12.200	33.3	8	13	
3:39:36.66	14010P	2	12.200	33.3	8	13	
3:39:36.69	14011T	0	12.200	33.3	8	13	
3:39:36.72	14012T	0	12.200	33.3	8	13	
3:39:36.76	14013P	2	12.200	33.3	8	13	
3:39:36.79	14014P	2	12.200	33.3	8	13	
3:39:36.82	14015P	2	12.200	33.3	8	13	
3:39:36.86	14016P	2	12.200	33.3	8	13	
3:39:36.89	14017P	2	12.200	33.3	8	13	
3:39:36.92	14018P	2	12.200	33.3	8	13	
3:39:36.96	14019P	2	12.200	33.3	8	13	
3:39:36.99	14020P	2	12.200	33.3	8	13	

Table B8 - Telemetry Frames and Camera Parameters (Cont.'d)

UMT	Telemetry Frame	Filter	Tracker Exp. Time (ms)	Plume Exp. Time (ms)	Tracker Gain Step	Plume Gain Step	Comments
3:39:37.02	14021T	0	12.200	33.3	8	13	
3:39:37.06	14022T	0	12.200	33.3	8	13	
3:39:37.09	14023P	2	12.200	33.3	8	13	
3:39:37.12	14024P	2	12.200	33.3	8	13	
3:39:37.16	14025P	2	12.200	33.3	8	13	
3:39:37.19	14026P	2	12.200	33.3	8	13	
3:39:37.22	14027P	2	12.200	33.3	8	13	
3:39:37.26	14028P	2	12.200	33.3	8	13	
3:39:37.29	14029P	2	12.200	33.3	8	13	
3:39:37.32	14030P	2	12.200	33.3	8	13	End data interval 3, PC-2
3:39:41.23	14147P	1	12.200	33.3	8	13	Begin data interval 4, PC-1
3:39:41.26	14148P	1	12.200	33.3	8	13	
3:39:41.29	14149P	1	12.200	33.3	8	13	
3:39:41.33	14150P	1	12.200	33.3	8	13	
3:39:41.36	14151T	0	12.200	33.3	8	13	
3:39:41.39	14152T	0	12.200	33.3	8	13	
3:39:41.43	14153P	1	12.200	33.3	8	13	
3:39:41.46	14154P	1	12.200	33.3	8	13	
3:39:41.49	14155P	1	12.200	33.3	8	13	
3:39:41.53	14156P	1	12.200	33.3	8	13	
3:39:41.56	14157P	1	12.200	33.3	8	13	
3:39:41.59	14158P	1	12.200	33.3	8	13	
3:39:41.63	14159P	1	12.200	33.3	8	13	
3:39:41.66	14160P	1	12.200	33.3	8	13	
3:39:41.69	14161T	0	12.200	33.3	8	13	
3:39:41.73	14162T	0	12.200	33.3	8	13	
3:39:41.76	14163P	1	12.200	33.3	8	13	
3:39:41.79	14164P	1	12.200	33.3	8	13	
3:39:41.83	14165P	1	12.200	33.3	8	13	
3:39:41.86	14166P	1	12.200	33.3	8	13	
3:39:41.89	14167P	1	12.200	33.3	8	13	
3:39:41.93	14168P	1	12.200	33.3	8	13	
3:39:41.96	14169P	1	12.200	33.3	8	13	
3:39:41.99	14170P	1	12.200	33.3	8	13	
3:39:42.03	14171T	0	12.200	33.3	8	13	
3:39:42.06	14172T	0	12.200	33.3	8	13	
3:39:42.09	14173P	1	12.200	33.3	8	13	
3:39:42.13	14174P	1	12.200	33.3	8	13	
3:39:42.16	14175P	1	12.200	33.3	8	13	

Table B8 - Telemetry Frames and Camera Parameters (Cont.'d)

UMT	Telemetry Frame	Filter	Tracker Exp. Time (ms)	Plume Exp. Time (ms)	Tracker Gain Step	Plume Gain Step	Comments
3:39:42.19	14176P	1	12.200	33.3	8	13	
3:39:42.23	14177P	1	12.200	33.3	8	13	
3:39:42.26	14178P	1	12.200	33.3	8	13	
3:39:42.29	14179P	1	12.200	33.3	8	13	
3:39:42.33	14180P	1	12.200	33.3	8	13	
3:39:42.36	14181T	0	12.200	33.3	8	13	
3:39:42.40	14182T	0	12.200	33.3	8	13	
3:39:42.43	14183P	1	12.200	33.3	8	13	
3:39:42.46	14184P	1	12.200	33.3	8	13	
3:39:42.50	14185P	1	12.200	33.3	8	13	
3:39:42.53	14186P	1	12.200	33.3	8	13	
3:39:42.56	14187P	1	12.200	33.3	8	13	
3:39:42.60	14188P	1	12.200	33.3	8	13	
3:39:42.63	14189P	1	12.200	33.3	8	13	
3:39:42.66	14190P	1	12.200	33.3	8	13	
3:39:42.70	14191T	0	12.200	33.3	8	13	
3:39:42.73	14192T	0	12.200	33.3	8	13	
3:39:42.76	14193P	1	12.200	33.3	8	13	
3:39:42.80	14194P	1	12.200	33.3	8	13	
3:39:42.83	14195P	1	12.200	53.3	8	13	
3:39:42.86	14196P	1	12.200	33.3	8	13	
3:39:42.90	14197P	1	12.200	33.3	8	13	
3:39:42.93	14198P	1	12.200	33.3	8	13	
3:39:42.96	14199P	1	12.200	33.3	8	13	
3:39:43.00	14200P	1	12.200	33.3	8	13	End data interval 4, PC-1
3:39:43.03	14201T	0	12.200	33.3	8	13	
3:39:43.07	14202T	0	15.402	33.3	8	13	Third stage burnout
3:39:43.10	14203P	1	19.444	33.3	8	13	
3:39:43.13	14204P	1	19.444	33.3	8	13	
3:39:43.16	14205P	1	19.444	33.3	8	13	
3:39:43.20	14206P	1	19.444	33.3	8	13	
3:39:43.23	14207P	1	19.444	33.3	8	13	
3:39:43.26	14208P	1	19.444	33.3	·8	13	
3:39:55.78	14583P	1	15.402	33.3	7	13	Begin data interval 5, PC 1
3:39:55.81	14584P	1	15.402	33.3	7	13	
3:39:55.84	14585P	1	15.402	33.3	7	13	
3:39:55.88	14586P	1	15.402	33.3	7	13	.
3:39:55.91	14587P	1	15.402	33.3	7	13	
3:39:55.94	14588P	1	15.402	33.3	7	13	

Table B8 - Telemetry Frames and Camera Parameters (Cont.'d)

UMT	Telemetry Frame	Filter	Tracker Exp. Time (ms)	Plume Exp. Time (ms)	Tracker Gain Step	Plume Gain Step	Comments
3:39:55.98	14589P	1	15.402	33.3	7	13	
3:39:56.01	14590P	1	15.402	33.3	7	13	
3:39:56.04	14591T	0	15.402	33.3	7	13	
3:39:56.08	14592T	0	15.402	33.3	7	13	
3:39:56.11	14593P	1	15.402	33.3	7	13	
3:39:56.14	14594P	1	15.402	33.3	7	13	
3:39:56.18	14595P	1	15.402	33.3	7	13	
3:39:56.21	14596P	1	15.402	33.3	7	13	
3:39:56.24	14597P	1	15.402	33.3	7	13	
3:39:56.28	14598P	1	15.402	33.3	7	13	
3:39:56.31	14599P	1	15.402	33.3	7	13	
3:39:56.34	14600P	1	15.402	33.3	7	13	
3:39:56.38	14601T	0	15.402	33.3	7	13	
3:39:56.41	14602T	0	15.402	33.3	7	13	
3:39:56.44	14603P	1	15.402	33.3	7	13	
3:39:56.48	14604P	1	15.402	33.3	7	13	
3:39:56.51	14605P	1	15.402	33.3	7	13	
3:39:56.54	14606P	1	15.402	33.3	7	13	
3:39:56.58	14607P	1	15.402	33.3	7	13	
3:39:56.61	14608P	1	15.402	33.3	7	13	
3:39:56.64	14609P	1	15.402	33.3	7	13	
3:39:56.68	14610P	1	15.402	33.3	7	13	
3:39:56.71	14611T	0	15.402	33.3	7	13	
3:39:56.74	14612T	0	15.402	33.3	7	13	
3:39:56.78	14613P	1	15.402	33.3	7	13	
3:39:56.81	14614P	1	15.402	33.3	7	13	
3:39:56.84	14615P	1	15.402	33.3	7	13	
3:39:56.88	14616P	1	15.402	33.3	7	13	
3:39:56.91	14617P	1	15.402	33.3	7	13	
3:39:56.94	14618P	1	15.402	33.3	7	13	
3:39:56.98	14619P	1	15.402	33.3	7	13	
3:39:57.01	14620P	1	15.402	33.3	7	13	
3:39:57.04	14621T	0	15.402	33.3	7	13	
3:39:57.08	14622T	0	15.402	33.3	7	13	
3:39:57.11	14623P	1	15.402	33.3	7	13	
3:39:57.14	14624P	1	15.402	33.3	7	13	
3:39:57.18	14625P	1	15.402	33.3	7	13	
3:39:57.21	14626P	1	15.402	33.3	7	13	
3:39:57.24	14627P	1	15.402	33.3	7	13	
3:39:57.28	14628P	1	15.402	33.3	7	13	
3:39:57.31	14629P	1	15.402	33.3	7	13	

Table B8 - Telemetry Frames and Camera Parameters (Cont.'d)

UMT	Telemetry Frame	Filter	Tracker Exp. Time (ms)	Plume Exp. Time (ms)	Tracker Gain Step	Plume Gain Step	Comments
3:39:57.35	14630P	1	15.402	33.3	7	13	
3:39:57.38	14631T	0	15.402	33.3	7	13	
3:39:57.41	14632T	0	15.402	33.3	7	13	
3:39:57.45	14633P	1	15.402	33.3	7	13	
3:39:57.48	14634P	1	15.402	33.3	7	13	
3:39:57.51	14635P	1	15.402	33.3	7	13	
3:39:57.55	14636P	1	15.402	33.3	7	13	
3:39:57.58	14637P	1	15.402	33.3	7	13	
3:39:57.61	14638P	1	15.402	33.3	7	13	
3:39:57.65	14639P	1	15.402	33.3	7	13	
3:39:57.68	14640P	1	15.402	33.3	7	13	
3:39:57.71	14641T	0	15.402	33.3	7	13	
3:39:57.75	14642T	0	15.402	33.3	7	13	
3:39:57.78	14643P	1	15.402	33.3	7	13	
3:39:57.81	14644P	1	15.402	33.3	7	13	
3:39:57.85	14645P	1	15.402	33.3	7	13	
3:39:57.88	14646P	1	15.402	33.3	7	13	
3:39:57.91	14647P	1	15.402	33.3	7	13	
3:39:57.95	14648P	1	15.402	33.3	7	13	
3:39:57.98	14649P	1	15.402	33.3	7	13	
3:39:58.01	14650P	1	15.402	33.3	7	13	
3:39:58.05	14651T	0	15.402	33.3	7	13	
3:39:58.08	14652T	0	15.402	33.3	7	13	
3:39:58.11	14653P	1	15.402	33.3	7	13	
3:39:58.15	14654P	1	15.402	33.3	7	13	
3:39:58.18	14655P	1	15.402	33.3	7	13	
3:39:58.21	14656P	1	15.402	33.3	7	13	
3:39:58.25	14657F	1	15.402	33.3	7	13	
3:39:58.28	14658P	1	15.402	33.3	7	13	
3:39:58.31	14659P	1	15.402	33.3	7	13	
3:39:58.35	14660P	1	15.402	33.3	7	13	
3:39:58.38	14661T	0	15.402	33.3	7	13	
3:39:58.41	14662T	0	15.402	33.3	7	13	
3:39:58.45	14663P	1	15.402	33.3	7	13	
3:39:58.48	14664P	1	15.402	33.3	7	13	
3:39:58.51	14665P	1	15.402	33.3	7	13	
3:39:58.55	14666P	1	15.402	33.3	7	13	
3:39:58.58	14667P	1	15.402	33.3	7	13	
3:39:58.61	14668P	1	15.402	33.3	7	13	
3:39:58.65	14669P	1	15.402	33.3	7	13	
3:39:58.68	14670P	1	15.402	33.3	7	13	

Table B8 - Telemetry Frames and Camera Parameters (Cont.'d)

UMT	Telemetry Frame	Filter	Tracker Exp. Time (ms)	Plume Exp. Time (ms)	Tracker Gain Step	Plume Gain Step	Comments
3:39:58.71	14671T	0	15.402	33.3	7	13	
3:39:58.75	14672T	0	15.402	33.3	7	13	
3:39:58.78	14673P	1	15.402	33.3	7	13	
3:39:58.81	14674P	1	15.402	33.3	7	13	
3:39:58.85	14675P	1	15.402	33.3	7	13	
3:39:58.88	14676P	1	15.402	33.3	7	13	
3:39:58.91	14677P	1	15.402	33.3	7	13	
3:39:58.95	14678P	1	15.402	33.3	7	13	
3:39:58.98	14679P	1	15.402	33.3	7	13	
3:39:59.01	14680P	1	15.402	33.3	7	13	
3:39:59.05	14681T	0	15.402	33.3	7	13	
3:39:59.08	14682T	0	15.402	33.3	7	13	
3:39:59.11	14683P	1	15.402	33.3	7	13	
3:39:59.15	14684P	1	15.402	33.3	7	13	
3:39:59.18	14685P	1	15.402	33.3	7	13	
3:39:59.21	14686P	1	15.402	33.3	7	13	
3:39:59.25	14687P	1	15.402	33.3	7	13	
3:39:59.28	14688P	1	15.402	33.3	7	13	
3:39:59.31	14689P	1	15.402	33.3	7	13	
3:39:59.35	14690P	1	15.402	33.3	7	13	
3:39:59.38	14691T	0	15.402	33.3	7	13	
3:39:59.41	14692T	0	15.402	33.3	7	13	
3:39:59.45	14693P	1	15.402	33.3	7	13	
3:39:59.48	14694P	1	15.402	33.3	7	13	
3:39:59.51	14695P	1	15.402	33.3	7	13	
3:39:59.55	14696P	1	15.402	33.3	7	13	
3:39:59.58	14697P	1	15.402	33.3	7	13	
3:39:59.61	14698P	1	15.402	33.3	7	13	
3:39:59.65	14699P	1	15.402	33.3	7	13	
3:39:59.68	14700P	1	15.402	33.3	7	13	
3:39:59.71	14701T	0	15.402	33.3	7	13	
3:39:59.75	14702T	0	15.402	33.3	7	13	
3:39:59.78	14703P	1	15.402	33.3	7	13	
3:39:59.81	14704P	1	15.402	33.3	7	13	
3:39:59.85	14705P	1	15.402	33.3	7	13	
3:39:59.88	14706P	1	15.402	33.3	7	13	
3:39:59.91	14707P	1	15.402	33.3	7	13	
3:39:59.95	14708P	1	15.402	33.3	7	13	
3:39:59.98	14709P	1	15.402	33.3	7	13	
3:40:0.01	14710P	1	15.402	33.3	7	13	
3:40:0.05	14711T	0	15.402	33.3	7	13	

Table B8 - Telemetry Frames and Camera Parameters (Cont.'d)

UMT	Telemetry Frame	Filter	Tracker Exp. Time (ms)	Plume Exp. Time (ms)	Tracker Gain Step	Plume Gain Step	Comments
3:40:0.08	14712T	0	15.402	33.3	7	13	
3:40:0.11	14713P	1	15.402	33.3	7	13	
3:40:0.15	14714P	1	15.402	33.3	7	13	
3:40:0.18	14715P	1	15.402	33.3	7	13	
3:40:0.22	14716P	1	15.402	33.3	7	13	End interval 5, PC-1
3:40:5.12	14863P	2	15.402	33.3	7	12	Begin interval 6, PC 2
3:40:5.15	14864P	2	15.402	33.3	7	12	
3:40:5.19	14865P	2	15.402	33.3	7	12	
3:40:5.22	14866P	2	15.402	33.3	7	12	
3:40:5.25	14867P	2	15.402	33.3	7	12	
3:40:5.29	14868P	2	15.402	33.3	7	12	
3:40:5.32	14869P	2	15.402	33.3	7	12	
3:40:5.35	14870P	2	15.402	33.3	7	12	
3:40:5.39	14871T	0	15.402	33.3	7	12	
3:40:5.42	14872T	0	15.402	33.3	7	12	
3:40:5.45	14873P	2	15.402	33.3	7	12	
3:40:5.49	14874P	2	15.402	33.3	7	12	
3:40:5.52	14875P	2	15.402	33.3	7	12	
3:40:5.55	14876P	2	15.402	33.3	7	12	
3:40:5.59	14877P	2	15.402	33.3	7	12	
3:40:5.62	14878P	2	15.402	33.3	7	12	
3:40:5.65	14879P	2	15.402	33.3	7	12	
3:40:5.69	14880P	2	15.402	33.3	7	12	
3:40:5.72	14881T	0	15.402	33.3	7	12	
3:40:5.75	14882T	0	15.402	33.3	7	12	
3:40:5.79	14883P	2	15.402	33.3	7	12	
3:40:5.82	14884P	2	15.402	33.3	7	12	
3:40:5.85	14885P	2	15.402	33.3	7	12	
3:40:5.89	14886P	2	15.402	33.3	7	12	
3:40:5.92	14887P	2	15.402	33.3	7	12	
3:40:5.95	14888P	2	15.402	33.3	7	12	
3:40:5.99	14889P	2	15.402	33.3	7	12	
3:40:6.02	14890P	2	15.402	33.3	7	12	
3:40:6.05	14891T	0	15.402	33.3	7	12	
3:40:6.09	14892T	0	15.402	33.3	7	12	
3:40:6.12	14893P	2	15.402	33.3	7	12	
3:40:6.16	14894P	2	15.402	33.3	7	12	
3:40:6.19	14895P	2	15.402	33.3	7	12	
3:40:6.22	14896P	2	15.402	33.3	7	12	
3:40:6.26	14897P	2	15.402	33.3	7	12	
3:40:6.29	14898P	2	15.402	33.3	7	12	

Table B8 - Telemetry Frames and Camera Parameters (Cont.'d)

UMT	Telemetry Frame	Filter	Tracker Exp. Time (ms)	Plume Exp. Time (ms)	Tracker Gain Step	Plume Gain Step	Comments
3:40:6.32	14899P	2	15.402	33.3	7	12	
3:40:6.36	14900P	2	15.402	33.3	7	12	
3:40:6.39	14901T	0	15.402	33.3	7	12	
3:40:6.42	14902T	0	15.402	33.3	7	12	
3:40:6.46	14903P	2	15.402	33.3	7	12	
3:40:6.49	14904P	2	15.402	33.3	7	12	
3:40:6.52	14905P	2	15.402	33.3	7	12	
3:40:6.56	14906P	2	15.402	33.3	7	12	End interval 6, PC-2
3:40:8.46	14963P	3	15.402	33.3	7	13	Begin interval 7, PC-3
3:40:8.56	14966P	3	15.402	33.3	7	13	
3:40:8.59	14967P	3	15.402	33.3	7	13	
3:40:8.62	14968P	3	15.402	33.3	7	13	
3:40:8.66	14969P	3	15.402	33.3	7	13	
3:40:8.69	14970P	3	15.402	33.3	7	13	
3:40:8.72	14971T	0	15.402	33.3	7	13	
3:40:8.76	14972T	0	15.402	33.3	7	13	
3:40:8.79	14973P	3	15.402	33.3	7	13	
3:40:8.82	14974P	3	15.402	33.3	7	13	
3:40:8.86	14975P	3	15.402	33.3	7	13	
3:40:8.89	14976P	3	15.402	33.3	7	13	
3:40:8.92	14977P	3	15.402	33.3	7	13	
3:40:8.96	14978P	3	15.402	33.3	7	13	
3:40:8.99	14979P	3	15.402	33.3	7	13	
3:40:9.02	14980P	3	15.402	33.3	7	13	
3:40:9.06	14981T	0	15.402	33.3	7	13	
3:40:9.09	14982T	0	15.402	33.3	7	13	
3:40:9.13	14983P	3	15.402	33.3	7	13	
3:40:9.16	14984P	3	15.402	33.3	7	13	
3:40:9.19	14985P	3	15.402	33.3	7	13	
3:40:9.23	14986P	3	15.402	33.3	7	13	
3:40:9.26	14987P	3	15.402	33.3	7	13	
3:40:9.29	14988P	3	15.402	33.3	7	13	
3:40:9.33	14989P	3	15.402	33.3	7	13	
3:40:9.36	14990P	3	15.402	33.3	7	13	
3:40:9.39	14991T	0	15.402	33.3	7	13	
3:40:9.43	14992T	0	15.402	33.3	7	13	
3:40:9.46	14993P	3	15.402	33.3	7	13	
3:40:9.49	14994P	3	15.402	33.3	7	13	
3:40:9.53	14995P	3	15.402	33.3	7	13	
3:40:9.56	14996P	3	15.402	33.3	7	13	
3:40:9.59	14997P	3	15.402	33.3	7	13	

Table B8 - Telemetry Frames and Camera Parameters (Cont.'d)

UMT	Telemetry Frame	Filter	Tracker Exp. Time (ms)	Plume Exp. Time (ms)	Tracker Gain Step	Plume Gain Step	Comments
3:40:9.63	14998P	3	15.402	33.3	7	13	
3:40:9.66	14999P	3	15.402	33.3	7	13	
3:40:9.69	15000P	3	15.402	33.3	7	13	
3:40:9.73	15001T	0	15.402	33.3	7	13	
3:40:9.76	15002T	0	15.402	33.3	7	13	
3:40:9.79	15003P	3	15.402	33.3	7	13	
3:40:9.83	15004P	3	15.402	33.3	7	13	
3:40:9.86	15005P	3	15.402	33.3	7	13	
3:40:9.89	15006P	3	15.402	33.3	7	13	
3:40:9.93	15007P	3	15.402	33.3	7	13	
3:40:9.96	15008P	3	15.402	33.3	7	13	
3:40:9.99	15009P	3	15.402	33.3	7	13	
3:40:10.03	15010P	3	15.402	33.3	7	13	
3:40:10.13	15013P	3	15.402	33.3	7	13	
3:40:10.16	15014P	3	15.402	33.3	7	13	
3:40:10.19	15015P	3	15.402	33.3	7	13	
3:40:10.23	15016P	3	15.402	33.3	7	13	
3:40:10.26	15017P	3	15.402	33.3	7	13	
3:40:10.29	15018P	3	15.402	33.3	7	13	
3:40:10.33	15019P	3	15.402	33.3	7	13	
3:40:10.36	15020P	3	15.402	33.3	7	13	
3:40:10.39	15021T	0	15.402	33.3	7	13	
3:40:10.43	15022T	0	15.402	33.3	?	13	
3:40:10.46	15023P	3	15.402	33.3	7	13	
3:40:10.49	15024P	3	15.402	33.3	7	13	
3:40:10.53	15025P	3	15.402	33.3	7	13	
3:40:10.56	15026P	3	15.402	33.3	7	13	
3:40:10.59	15027P	3	15.402	33.3	7	13	
3:40:10.63	15028P	3	15.402	33.3	7	13	
3:40:10.66	15029P	3	15.402	33.3	7	13	
3:40:10.69	15030P	3	15.402	33.3	7	13	
3:40:10.73	15031T	0	15.402	33.3	7	13	
3:40:10.76	15032T	0	15.402	33.3	7	13	
3:40:10.79	15033P	3	15.402	33.3	7	13	
3:40:10.83	15034P	3	15.402	33.3	7	13	
3:40:10.86	15035P	3	15.402	33.3	7	13	
3:40:10.89	15036P	3	15.402	33.3	7	13	
3:40:10.93	15037P	3	15.402	33.3	7	13	
3:40:10.96	15038P	3	15.402	33.3	7	13	
3:40:10.99	15039P	3	15.402	33.3	7	13	
3:40:11.03	15040P	3	15.402	33.3	7	13	

Table B8 - Telemetry Frames and Camera Parameters (Cont.'d)

UMT	Telemetry Frame	Filter	Tracker Exp. Time (ms)	Plume Exp. Time (ms)	Tracker Gain Step	Plume Gain Step	Comments
3:40:11.06	15041T	0	15.402	33.3	7	13	
3:40:11.09	15042T	0	15.402	33.3	7	13	
3:40:11.13	15043P	3	15.402	33.3	7	13	
3:40:11.16	15044P	3	15.402	33.3	7	13	
3:40:11.19	15045P	3	15.402	33.3	7	13	
3:40:11.23	15046P	3	15.402	33.3	7	13	
3:40:11.26	15047P	3	15.402	33.3	7	13	
3:40:11.29	15048P	3	15.402	33.3	7	13	
3:40:11.33	15049P	3	15.402	33.3	7	13	
3:40:11.36	15050P	3	15.402	33.3	7	13	
3:40:11.39	15051T	0	15.402	33.3	7	13	
3:40:11.43	15052T	0	15.402	33.3	7	13	
3:40:11.46	15053P	3	15.402	33.3	7	13	
3:40:11.49	15054P	3	15.402	33.3	7	13	
3:40:11.53	15055P	3	15.402	33.3	7	13	
3:40:11.56	15056P	3	15.402	33.3	7	13	
3:40:11.59	15057P	3	15.402	33.3	7	13	
3:40:11.63	15058P	3	15.402	33.3	7	13	
3:40:11.66	15059P	3	15.402	33.3	7	13	
3:40:11.69	15060P	3	15.402	33.3	7	13	
3:40:11.73	15061T	0	15.402	33.3	7	13	
3:40:11.76	15062T	0	15.402	33.3	7	13	
3:40:11.79	15063P	3	15.402	33.3	7	13	
3:40:11.83	15064P	3	15.402	33.3	7	13	
3:40:11.86	15065P	3	15.402	33.3	7	13	
3:40:11.89	15066P	3	15.402	33.3	7	13	
3:40:11.93	15067P	3	15.402	33.3	7	13	
3:40:11.96	15068P	3	15.402	33.3	7	13	
3:40:12.00	15069P	3	15.402	33.3	7	13	
3:40:12.03	15070P	3	15.402	33.3	7	13	
3:40:12.06	15071T	0	15.402	33.3	7	13	
3:40:12.10	15072T	0	15.402	33.3	7	13	
3:40:12.13	15073P	3	15.402	33.3	7	13	
3:40:12.16	15074P	3	15.402	33.3	7	13	
3:40:12.20	15075P	3	15.402	33.3	7	13	
3:40:12.23	15076P	3	15.402	33.3	7	13	
3:40:12.26	15077P	3	15.402	33.3	7	13	
3:40:12.30	15078P	3	15.402	33.3	7	13	
3:40:12.33	15079P	3	15.402	33.3	7	13	
3:40:12.36	15080P	3	15.402	33.3	7	13	
3:40:12.40	15081T	0	15.402	33.3	7	13	

Table B8 - Telemetry Frames and Camera Parameters (Cont.'d)

UMT	Telemetry Frame	Filter	Tracker Exp. Time (ms)	Plume Exp. Time (ms)	Tracker Gain Step	Plume Gain Step	Comments
3:40:12.43	15082T	0	15.402	33.3	7	13	
3:40:12.46	15083P	3	15.402	33.3	7	13	
3:40:12.50	15084P	3	15.402	33.3	7	13	
3:40:12.53	15085P	3	15.402	33.3	7	13	
3:40:12.56	15086P	3	15.402	33.3	7	13	
3:40:12.60	15087P	3	15.402	33.3	7	13	
3:40:12.63	15088P	3	15.402	33.3	7	13	
3:40:12.66	15089P	3	15.402	33.3	7	13	
3:40:12.70	15090P	3	15.402	33.3	7	13	
3:40:12.73	15091T	0	15.402	33.3	7	13	
3:40:12.76	15092T	0	15.402	33.3	7	13	
3:40:12.80	15093P	3	15.402	33.3	7	13	
3:40:12.83	15094P	3	15.402	33.3	7	13	
3:40:12.86	15095P	3	15.402	33.3	7	13	
3:40:12.90	15096P	3	15.402	33.3	7	13	
3:40:12.93	15097P	3	15.402	33.3	7	13	
3:40:12.96	15098P	3	15.402	33.3	7	13	
3:40:13.00	15099P	3	15.402	33.3	7	13	
3:40:13.03	15100P	3	15.402	33.3	7	13	
3:40:13.06	15101T	0	15.402	33.3	7	13	
3:40:13.10	15102T	0	15.402	33.3	7	13	
3:40:13.13	15103P	3	15.402	33.3	7	13	
3:40:13.16	15104P	3	15.402	33.3	7	13	
3:40:13.20	15105P	3	15.402	33.3	7	13	
3:40:13.23	15106P	3	15.402	33.3	7	13	
3:40:13.26	15107P	3	15.402	33.3	7	13	
3:40:13.30	15108P	3	15.402	33.3	7	13	
3:40:13.33	15109P	3	15.402	33.3	7	13	
3:40:13.36	15110P	3	15.402	33.3	7	13	
3:40:13.40	15111T	0	15.402	33.3	7	13	
3:40:13.43	15112T	0	15.402	33.3	7	13	
3:40:13.46	15113P	3	15.402	33.3	7	13	
3:40:13.50	15114P	3	15.402	33.3	7	13	
3:40:13.53	15115P	3	15.402	33.3	7	13	
3:40:13.56	15116P	3	15.402	33.3	7	13	
3:40:13.60	15117P	3	15.402	33.3	7	13	
3:40:13.63	15118P	3	15.402	33.3	7	13	
3:40:13.66	15119P	3	15.402	33.3	7	13	
3:40:13.70	15120P	3	15.402	33.3	7	13	
3:40:13.73	15121T	0	15.402	33.3	7	13	
3:40:13.76	15122T	0	15.402	33.3	7	13	

Table B8 - Telemetry Frames and Camera Parameters (Cont.'d)

UMT	Telemetry Frame	Filter	Tracker Exp. Time (ms)	Plume Exp. Time (ms)	Tracker Gain Step	Plume Gain Step	Comments
3:40:13.80	15123P	3	15.402	33.3	7	13	
3:40:13.83	15124P	3	15.402	33.3	7	13	
3:40:13.86	15125P	3	15.402	33.3	7	13	
3:40:13.90	15126P	3	15.402	33.3	7	13	
3:40:13.93	15127P	3	15.402	33.3	7	13	
3:40:13.96	15128P	3	15.402	33.3	7	13	
3:40:14.00	15129P	3	15.402	33.3	7	13	
3:40:14.03	15130P	3	15.402	33.3	7	13	
3:40:14.06	15131T	0	15.402	33.3	7	13	
3:40:14.10	15132T	0	15.402	33.3	7	13	
3:40:14.13	15133P	3	15.402	33.3	7	13	
3:40:14.16	15134P	3	15.402	33.3	7	13	
3:40:14.20	15135P	3	15.402	33.3	7	13	
3:40:14.23	15136P	3	15.402	33.3	7	13	
3:40:14.26	15137P	3	15.402	33.3	7	13	
3:40:14.30	15138P	3	15.402	33.3	7	13	
3:40:14.33	15139P	3	15.402	33.3	7	13	
3:40:14.36	15140P	3	15.402	33.3	7	13	
3:40:14.40	15141T	0	15.402	33.3	7	13	
3:40:14.43	15142T	0	15.402	33.3	7	13	
3:40:14.46	15143P	3	15.402	33.3	7	13	
3:40:14.50	15144P	3	15.402	33.3	7	13	
3:40:14.53	15145P	3	15.402	33.3	7	13	
3:40:14.56	15146P	3	15.402	33.3	7	13	
3:40:14.60	15147P	3	15.402	33.3	7	13	
3:40:14.63	15148P	3	15.402	33.3	7	13	
3:40:14.66	15149P	3	15.402	33.3	7	13	
3:40:14.70	15150P	3	15.402	33.3	7	13	
3:40:14.73	15151T	0	15.402	33.3	7	13	
3:40:14.76	15152T	0	15.402	33.3	7	13	
3:40:14.80	15153P	3	15.402	33.3	7	13	
3:40:14.83	15154P	3	15.402	33.3	7	13	
3:40:14.86	15155P	3	15.402	33.3	7	13	
3:40:14.90	15156P	3	15.402	33.3	7	13	
3:40:14.93	15157P	3	15.402	33.3	7	13	
3:40:14.96	15158P	3	15.402	33.3	7	13	
3:40:15.00	15159P	3	15.402	33.3	7	13	
3:40:15.03	15160P	3	15.402	33.3	7	13	
3:40:15.07	15161T	0	15.402	33.3	7	13	
3:40:15.10	15162T	0	15.402	33.3	7	13	
3:40:15.13	15163P	3	15.402	33.3	7	13	

Table B8 - Telemetry Frames and Camera Parameters (Cont.'d)

UMT	Telemetry Frame	Filter	Tracker Exp. Time (ms)	Plume Exp. Time (ms)	Tracker Gain Step	Plume Gain Step	Comments
3:40:15.17	15164P	3	15.402	33.3	7	13	
3:40:15.20	15165P	3	15.402	33.3	7	13	End interval 7, PC-3

GLOSSARY

AOS	acquisition of signal
ARI	average radiant intensity
ARSI	average radiant spectral intensity
CCD	charge-coupled device
CFC	camera frame controller
CHARM	Composite High Altitude Radiation Model
CMOS	complementary metal oxide semiconductor
CPU	Central processing unit
DN	digital number
DN/PE	digital number per photoevent
EIA	electronics interface assembly
ERD	experiment requirements document
FOR	field of regard
FOV	field of view
FPA	focal plane array
FWHM	full-width-half-maximum
GMT	Greenwich Mean Time
Hz	Hertz
ICC	instrument control computer
ICCD	intensified charge-coupled device
IDA	Institute for Defense Analyses
IR	infrared
ITT	International Telephone and Telegraph
IUE	International Ultraviolet Explorer
K	degrees Kelvin
KTF	Kauai Test Facility
LACE	Low-power Atmospheric Compensation Experiment
LOS	loss of signal; line of sight
LOTB	LACE Operational Test Bed
Mbps	megabits per second
MCP	microchannel plate
MHz	megahertz
NER	noise equivalent radiance
NQE	net quantum efficiency
NRL	Naval Research Laboratory
OAO	Orbiting Astrophysical Observatory
PC-N	plume-camera filter, $N = 1, 2, 3, 4$
PE	photoevent
PMRF	Pacific Missile Range Facility
PSAG	Phenomenology Steering and Analysis Group
PSF	point spread function
RMS	root mean square
s	seconds
SDIO	Strategic Defense Initiative Organization
SIRRM	Standardized Infra Red Radiation Model
SNR	signal-to-noise ratio
sr	steradian
TALO	time after liftoff
TGS	transportable ground station
ULTRASEEK	ultraviolet seeker
UMT	UVPI mission time
UV	ultraviolet
UVPI	Ultraviolet Plume Instrument
VAFB	Vandenberg Air Force Base
W	watt